SAKARYA UNIVERSITY
INSTITUTE OF SCIENCE AND TECHNOLOGY

ENHANCED MICROCHANNEL EVAPORATOR WITH INTEGRATED NANOSTRUCTURES IN SPACE APPLICATION

Ph.D. THESIS

Murat BULUT

Department	**:**	**MECHANICAL ENGINEERING**
Field of Science	**:**	**ENERGY**
Supervisor	**:**	**Assoc. Prof. Dr. Nedim SÖZBİR**
Co-Advisor	**:**	**Prof. Dr. Satish G. KANDLIKAR**

December 2016

SAKARYA UNIVERSITY
INSTITUTE OF SCIENCE AND TECHNOLOGY

ENHANCED MICROCHANNEL EVAPORATOR WITH INTEGRATED NANOSTRUCTURES IN SPACE APPLICATION

Ph.D. THESIS

Murat BULUT

Department : MECHANICAL ENGINEERING

This thesis has been accepted unanimously / with majority of votes by the examination committee on 16.12.2016

Assoc. Prof. Dr. **Nedim SÖZBİR** **Head of Jury**	**Prof. Dr.** **H. Rıza GÜVEN** **Jury Member**	**Prof. Dr.** **Zafer GÜL** **Jury Member**
Prof. Dr. **Yaşar İSLAMOĞLU** **Jury Member**		**Assist. Prof. Dr.** **Ünal UYSAL** **Jury Member**

DECLERATION

I declare that all the data in this thesis was obtained by myself in academic rules, all visual and written information and results were presented in accordance with academic and ethical rules, there is no distortion in the presented data, in case of utilizing other people's works they were refereed properly to scientific norms, the data presented in this thesis has not been used in any other thesis in this university or in any other university.

Murat BULUT

16.12.2016

ACKNOWLEDGEMENTS

I am very grateful to my advisor Assoc. Prof. Dr. Nedim Sozbir for his generous support in my research and academic life. I am also thankful to Prof. Dr. H. Riza Guven and Assist. Prof. Dr. Unal Uysal for being a member of my thesis committee. I would like to express my sincere gratitude to Prof. Dr. Satish G. Kandlikar for providing me the opportunity to pursue research in Thermal Analysis. Microfluidics and Fuel Cell laboratory at RIT in Rochester, NY USA. His support and quidance enable me to understand the subject and also convinced me to pursue my PhD. Without his quidance and persistent help this dissertation would not have been possible. I would like to thank the following by name, but there are countless many who equally deserve to be named here. Thank you all!

My wife; Gul, My parents; Ali Seydi and Elif, My mother in law and father in law and brother in law; Unal, Nebahat and Ahmet Can, My sisters; Handan and Aysun, My nephews and nieces; Yavuz Selim, Hilal Rabia, Dilek Selin, Hamza, My friends; Hüseyin and Sema Yılmaz, The people signed the contract with TUBITAK and TURKSAT for me; Ali Seydi and Hülya Agçelik, Faruk and Gönül Koray, Samet and Handan Yardim, The faculty at RIT; Prof.Dr. Ferat Şahin, Prof.Dr. Hany Ghoneim, Prof.Dr. Erhan Mergen, Prof.Dr. Tarık Kaya at Carleton University, Dr. Şenol Gülgönül and Hakkı Coşkun. I am thankful to all the past and present members of the Thermal Analysis, Microfludics and Fuel Cell lab. I would like to thank the Scientific and Research Council of Turkey (TUBITAK) for TUBITAK-BIDEB 2214/A International Research Fellowship Program Grant. I also would like to thank you TÜRKSAT AŞ to give me an oppurtunity to pursue my study in USA.

TABLE OF CONTENTS

LIST OF SYMBOLS AND ABBREVIATIONS

A	: Surface area (m^2)
A_c	: Cross sectional area (m^2)
ASME	: American society of mechanical engineering
B	: Bias error
CHF	: Critical heat flux (W/m^2)
CPL	: Capillary pumped loop
C_{pl}	: Specific heat of the liquid ($J/kg.^oC$)
C_{sf}	: Experimental constant that depends on surface-fluid combination
D	: The channel (hydraulic) diameter (m)
d_v	: The vapor escape channel width (m)
g	: Gravitational acceleration (m/s^2)
HP	: Heat pipe
HTC	: Heat transfer coefficient ($W/m^{2o}C$)
h	: Heat transfer coefficient ($W/m^{2o}C$)
h_{fg}	: Enthalpy of vaporization
IPA	: Isopropyl alcohol
JHT	: Journal of heat transfer
K	: Kutateladze number
k_{Cu}	: Thermal conductivity of copper (W/m^oC)
LHP	: Loop heat pipe
MLI	: Multilayer insulation
NBHT	: Nucleate boiling heat transfer
NRFC	: Nucleating region feeder microchannel
OSR	: Optical solar reflector
n	: Experimental constant that depends on the fluid

P	: Precision error
P	: Wetted perimeter (m)
P_l	: Pressure of liquid (Pa)
Pr	: Prandtl number of the liquid
P_v	: Vapor pressure inside the bubble
q"	: Heat flux (W/m^2)
$q"_{nucleate}$	: Nucleate boiling heat flux (W/m^2)
R	: The radius of the bubble (m)
TSC	: Thermal control systems
T_B	: Bottom thermocouple temperature (^oC)
T_M	: Middle thermocouple temperature (^oC)
T_S	: Saturation temperature (^oC)
T_T	: Top thermocouple temperature (^oC)
T_w	: Wall temperature (^oC)
U	: Uncertainty
VC	: Vapor chamber
θ	: Contact angle (^{o})
θ_a	: Receding contact angle (^{o})
θ_r	: Receding contact angle (^{o})
$\Delta\theta$	: Contact angle hysteresis (^{o})
ρ_g	: Vapor density of water (kg/m^3)
ρ_l	: Liquid density of water (kg/m^3)
μ_l	: Viscosity of the liquid (kg/m.s)
Δh_{lg}	: latent heat of evaporation (kJ/kg)
ΔT_{sat}	: Wall superheat (^oC)
Δx_1	: Distance between thermocouples (mm)
Δx_2	: Distance between top thermocouple and surface (mm)
δ_s	: The wall thickness of the grid (m)
θ_r	: Receding contact angle (^{o})
θ_r	: Receding contact angle (^{o})
σ	: Liquid-vapor surface tension (N/m)

γ_L : Liquid-vapor interfacial tension (N/m)

γ_S : Solid-vapor interfacial tension (N/m)

γ_{SL} : Solid-liquid interfacial tension (N/m)

LIST OF FIGURES

LIST OF TABLES

SUMMARY

Keywords: Pool boiling, microchannel, sintered surface, pin fins

Increasing processing capacity within the size of electronic device has made thermal management a key factor to electronic industries. Commercialized thermal management such as conventional air cooling system will not suffice the future requirements due to effects of increasing heat dissipation and miniaturization. In order to increase performance of electronic devices with high heat flux needs to be dissipated and electronic devices must operate reliably within safe temperature ranges. Heat transfer improvement will result in lower size of equipment and increased efficency. Compared to other conventional methods of heat transfer, pool boiling offers a much attractive option, as it is able to dissipate large amount of heat at low wall superheats. Evaporators play a crucial role in the design of vapor chambers and heat pipes. Reducing the temperature difference during evaporation and increasing heat flux are two important areas that directly affect the performance of the heat transfer systems. Therefore, special surfaces have been developed to further enhance the heat transfer using pool boiling. These special surfaces are microchannel, sintered and pin-fins.

The present study deals with enhancement of heat transfer using combination of multiple passive techniques, namely nanostructures and microporous sintered surfaces over open microchannel surfaces and microchannels with pin-fins. Seven structures were studied as individual. Experiments were conducted to study the effects of microchannel, sintered, and pin fins (micropillar) on the boiling heat transfer from a copper chip in a pool of degassed water. Boiling performance was measured in terms of critical heat flux (CHF) and heat transfer coefficient (HTC). Both HTC and CHF have been greatly improved on all modified surfaces compared to the plain copper chip baseline.

UZAY UYGULAMASI İÇİN NANOYAPI İLAVELİ ISI TRANSFER ALANI ARTIRILMIŞ MİKROKANALLI BUHARLAŞTIRICI

ÖZET

Anahtar kelimeler: Havuz kaynama, mikrokanal, sinterlenmiş yüzey, pin fin

Elektronik cihazların işletim kapasitesinin artması ve elektronik ekipmanların boyutunun değişimi ile birlikte elektronik sanayinde ısıl yönetim önemli bir faktör haline gelmiştir. Elektronik ekipmanların gelecekte ısı yükünün artması ve elektronik ekipmanların boyutların küçülmesi ile birlikte günümüzde kullanılan ticari ısıl yönetim sistemlerinden hava ile soğutma sistemleri yeterli olmayacaktır. Yüksek ısı akılı elektronik ekipmanların performansının artırılması için ve elektronik ekipmanların güvenilir sıcaklık aralığında çalışabilmesi için ısının transfer edilmesi gerekmektedir. Isı tranferinde iyileştirme ekipman boyutlarının küçülmesine ve veriminin artmasına sebep olacaktır. Diğer ısı transfer yöntemleri ile karşılaştırıldığında havuz kaynamanın yüksek ısı akısını düşük duvar sıcaklığı ile transferi nedeni ile en iyi seçenek olmuştur. Buharlaştırıcılar buhar odası ve ısı boru tasarımlarında önemli rol oynamaktadır. Buharlaşma sırasında sıcaklık farkının azaltılması ve ısı akısının artırılması ısı transfer sistemlerine etki eden iki önemli alandır. Bu yüzden havuz kaynama kullanılarak ısı transferini artırmak için özel yüzeyler geliştirilmiştir. Bu özel yüzeyler mikrokanal, sinterlenmiş yüzey ve pin finlerdir.

Bu çalışma ile ısı transferinin geliştirilmesi için mikrokanallar üzerinde birden fazla pasif teknik olarak kullanılan nanoyapılar, sinterlenmiş yüzeyler ve pin fin ile sağlanmıştır. Yedi yapı bireysel olarak incelenmiştir. Deneyler bakır malzeme ve gazı alınmış su kullanılarak mikrokanal, sinterlenmiş yüzey ve pin fin (mikro sütunlar) yapıların etkilerini incelemek için yapılmıştır. Kaynama performansı kritik ısı akısı ve ısı transferi katsayısı cinsinden ölçülmüştür. Kritik ısı akısı ve ısı transfer katsayısının bütün değiştirilmiş yüzeyler için düz bakır yüzeye oranla geliştiği görülmüştür.

CHAPTER 1. INTRODUCTION

The modern electronics has brought about a stream of equipment dealing with extremely high heat flux needing more and more cooling efficiency. The recent advances in the electronic industry and quick development of the integrated circuits technology significantly reduces the size of the electronic devices and increases the density of the power dissipation in the equipment. Thermal management system becomes a key factor to the continued development and progress of electronic devices for not only terrestial applications but also future space applications. Typical commercialized thermal management has not been able to dissipate high heat fluxes due to effects of increasing heat dissipation and miniaturization. Therefore, the conventional cooling systems for electronic devices are not suitable anymore considering the the small size of elecronic devices. In order to increase performance of electronic devices with high heat flux needs to be dissipated and electronic devices must operate reliably within safe operational temperature ranges. To improve the desired performance of future electronic devices, heat transfer improvement need to be developed with using new enhancement techniques such as microchannels, sintered, pin-fins etc.

Temperature is a key factor in operation of any electronic equipment. For most integrated circuit, most mainframe memory and logic chips, a cooling system is needed to maintain a relatively constant component temperature below the junction temperature approximately 85 ^{o}C. Thus, primary issues related to the chip cooling with pool boiling are the enhancement of nucleate boiling, increasing the critical heat flux (CHF) and heat transfer coefficient.

The development and the miniaturization of electronic components lead increasing power densities. The increase of heat dissipation of electronic devices, thermal

management problem becomes more challenging not only terrestrial applications but also space applications. Electronic systems in future will involve small size, lighweight and compact components to release high heat waste heat. A key design issue is a fast charge so as not to overheat the electronic device. The increasing heat dissipation from electronic devices on board spacecraft makes it necessary to find new solutions for their cooling. Developments in many applications becomes dependant on the ability to dissipate large amounts of heat from small surface areas. In order to achieve the heat dissipation requirements, boiling can be implemented in a variety of configurations including pool boiling, channel flow boiling, jet and spray, as well as with enhanced surfaces. Of the different boiling schems, microchannel boiling has gained unprecedented popularity because of both outstanding heat transfer performance and system advantages, including compact and lightweight design and small coolant inventory [1].

Microchannels and minichannels are preffered in diverse energy and process system including compact heat exchangers, refrigeration and cryogenic systems, power electronics, automotive and aerospace industries, catalytic reactors, fuel cells, and space applications etc., Boiling is the primary two modes of two-phase heat transports, which exhibit promising perspectives for micro/nanoscale thermal management. Incorporate microporous surfaces in microchannels provide liquid transport along the heat transfer surfaces while nanostructrues and microporous surfaces promote evaporation at low wall superheats-critical heat flux is also increased. Microporous surfaces and pin-fins in microchannels will be studied in pool boiling. Work will involve experimental work as well as theoretical work.

1.1. Heat Generation Trends in Electronic Industry

Since the first working transistor was invented in 1947 and the integrated circuit in 1958, the main focus was to reduce the size of the transistors. Reducing the size of the transistors not only improves the performance but also reduces the cost of the electronic device. On the other hand, decreasing a electronic device’s temperature increases its performance and reliability. Gordon Moore was the first to identify a trend in size reduction in 1965 [2]. The trend is known as Moore’s law in the

literature. Moore statement states that the number of transistors on integrated circuits doubles every years. Figure 1.1. shows microproccesor transistor count against date of introduction. In Figure 1.1. the blue line shows Moore's law applied, staring from the first microprocessor on the graph. The red line shown the least square fit of the entire set.

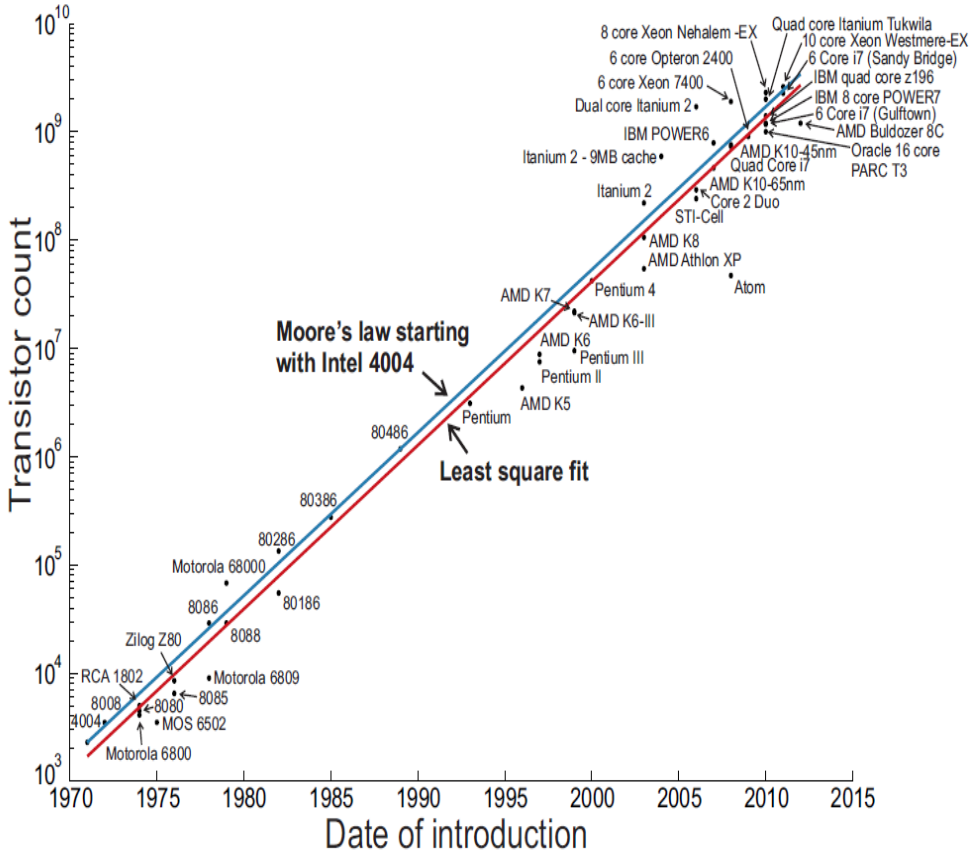

Figure 1.1. Microprocessor transistor count against date of the introduction [3]

Figure 1.1. shows heat flux at die for some widely used commercieal microprocessors of the recent past. It is seen from Figure 1.1. that it is actually the number of transistors per die that determines which cooling method is adequate to cool the electronic device.

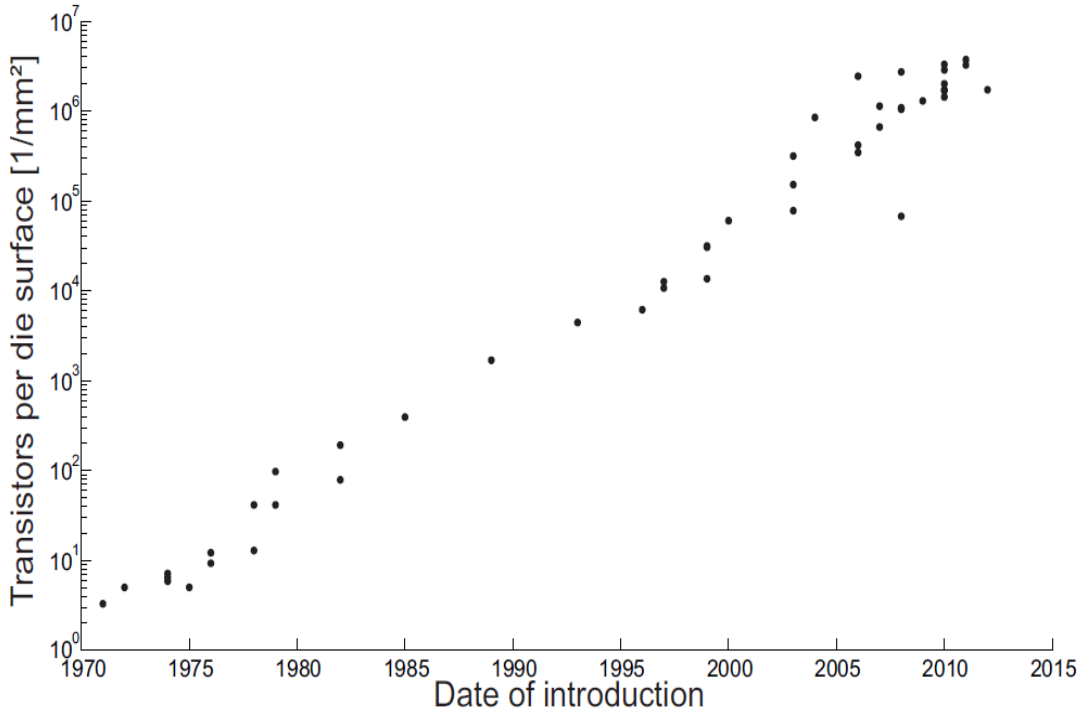

Figure 1.2. Microprocessor transistor count per die area against date of introduction [3]

While the number of transistor count per diea area as shown in Figure 1.2., it is important for the total power dissipation of the electronic device which is shown in Figure 1.3. The heat flux was about 10-15 W/cm^2 in the year 2000 and had reached 100 W/cm^2 in 2006 and it continous to increase significantly each year while the size of die on the procosser has been reduced and heat flux is high.

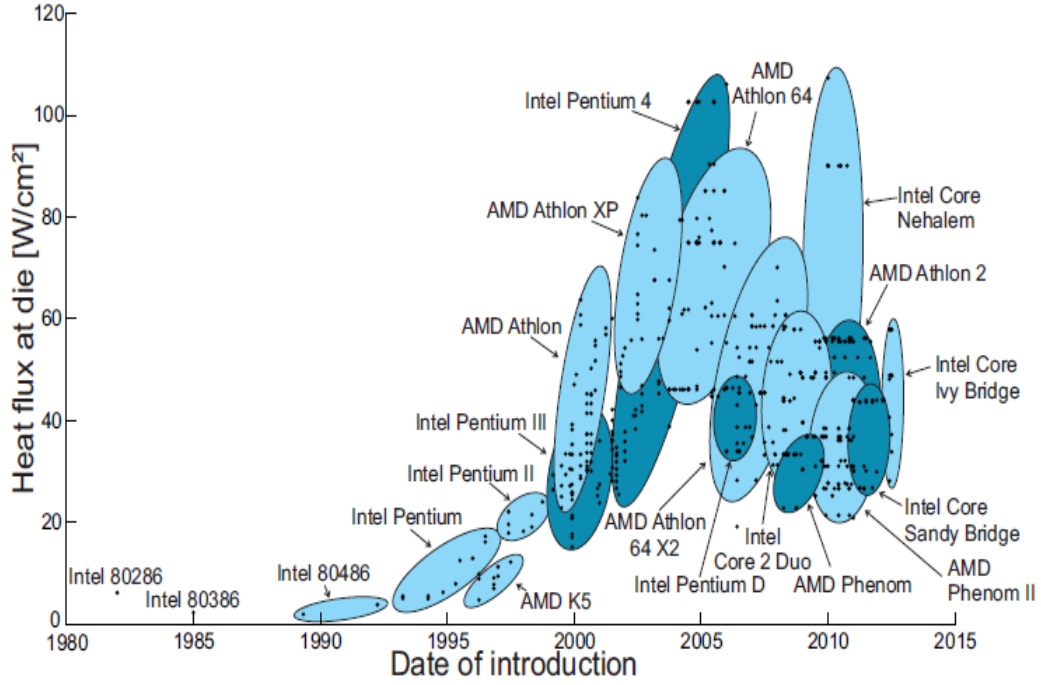

Figure 1.3. Heat flux at die for some widely used commercial microprocessors of the recent past [3]

1.2. Thermal Management in Space Applications

The space environment is unforgivingly harsh on spacecraft with surrounding the Earth and Sun. Spacecrafts are subjected to extremes of hot and cold temperatures in space. These temperatures can range from the extremely cold (below freezing) to the extremely hot if the spacecraft is close to the Sun. Although there is no air in space, energy is carried by radiation. The Sun, planets, or other celestrial bodies causes heating when it is absorbed by spacecraft.

Spacecraft relies on the efficiency of their heat removal systems in order to keep the electronic device within safe operational temperature ranges during its mission. When the outer surface of the spacecraft receives the heat flux from the outer space (Sun, Albedo, Earth IR, etc), the internal temperature would rise to unacceptably high values. Therefore, the heat needs to be removed from internal utilities such as electronic devices, payloads, and so on to outer heat sink.

The main purpose of the thermal management of a spacecraft is to maintain all the components within the allowable temperature ranges under all operational conditions. Thermal management is achieved by both active (external power is required such as heaters, Loop Heat Pipe (LHP), Capillary Pumped Loop (CPL)) and passive methods (no external power is required such as optical solar reflector (OSR), Multilayer Insulation (MLI), heat pipe (HP), vapor chamber (VC), paintings, etc.).

Heat removal in a spacecraft is generally pursued via a heat pipe or loop which a fluid transports the rejected from the internal utilities to the external radiators where power is radiated to outer space. At present, a spacecrafts generally uses a mechanically-pumped ones, in which a single-phase fluid is operated, hence their heat removal capability is based on the so-called sensible heat of the fluid, i.e. in its capacity of absorbing energy by rising its own temperature. However, as well known, a fluid exchange energy in a different way as latent heat, i.e. changing its aggregation state from liquid to vapor and vice versa (boiling and condensation, respectively). The main advantages of boiling systems are that they are nearly isothermal, require smaller heat exchange surface, have high power density removal and consequently require lower pumping power. As a result, boiling is recognized as a very effective technique to exchange high heat fluxes from heated bodies and is widely applied in on-earth technology in component heating and cooling. The adaption of boiling systems may yield substantial savings of weight, space and power aboard spacecraft in order to work out the crucial problem of heat rejection to space.

Two-phase passive systems have been serving the thermal management industry, in general, and space missions in particular, for quite some time now because two-phase heat transfer utilizes latent heat of vaporization of liquid and is capable of dissipating high heat fluxes while maintaining lower surface temperatures. This makes it a promising candidate for cooling high heat dissipation systems in earth-based and microgravity environments alike.

For space applications boiling is the heat-transfer mode of choice because the size of the components can be significantly reduced for a given power rating. The size and

in turn the weight of the component plays an important role for any spacecraft mission in the economics mission. Applications of boiling heat transfer in space can be found in such areas as thermal management, fluid handling and control, and power systems.

1.3. Boiling

Boiling is considered as one of the most important phase change phenomena and is widely used as a liquid-vapor phase mechanism in Terrestrial and Space applications. Boiling phenomena involves nucleation, growth and departure of vapor bubbles. Boiling heat transfer is of great interest to many researchers as efficent way to dissipate high heat flux through the use of latent heat. The first boiling curve was defined by Nukiyama [4] in 1934. He was able to develop the boiling curve by plotting the heat flux versus wall superheat by using a power controlled nichrome wire. He also identified the boiling regime as free convection, nucleate, transition and film region.

Boiling is a phase change process in which vapor bubbles are formed either on a heated surface and/or in a superheated liquid layer adjacent to the heated surface. It can be further classified into pool boiling and forced flow boiling. Pool boiling refers to boiling under natural convection conditions, whereas in forced flow boiling, liquid flow over the heater surface imposed by external forces such as pumps. The noticeably high HTC observed in the boiling process is due to the addition of the latent heat vaporization associated with the phase change from liquid to vapor. The heat transfer during the boiling process is highly advantageous in systems that generate large amount of heat over a relatively small area.

1.4. Pool Boiling

Boiling is the process which evaporation occurs at a solid-liquid interface. In order to boil to be occurred, the surface temperature T_s must be exceed the saturation temperature of the liquid T_{sat} at a given pressure. Boiling is characterized by bubble formation at the surface, these bubbles nuclete, grow and detach from the surface in a

complex manner dependent on many variables such as superheat temperature, surface tensions, surface geometries, surface materials, etc. Newton's Law of cooling describes the process in the form of

$$\frac{Q}{A} = q'' = h(T_s - T_{sat}) = h\Delta T \tag{1.1}$$

where Q is the total heat transfer, A is the surface area over which the heat is transerred, q" is the heat flux (heat transfer per unit area), h is the heat transfer coefficeint and $\Delta T=T_s-T_{sat}$ is defined as the wall superheat temperature which is the difference between the temparature of the surface and a convenent reference one taken in the fluid. Both the heat transfer area and the temperature difference should be kept as small as possible, the former to minimize weight and investment costs, and to avoid surface overheating, which in turn may lead to equipment failure. Consequently, the heat transfer coefficient has to be as high as possible to accommodate large heat fluxes. Boiling heat transfer coefficients are order of magnitude higher than in single-phase flow. This makes it a very suitable technique for space applications, in which very efficient, compact and lighweight devices are required.

It is important to understand a pool boiling curve to understand heat dissipation using boiling. A classical pool boiling curve is shown in Figure 1.4. The curve shows a plot of heat flux againt wall superheat. The wall superheat is defined as the difference between the wall temperature and the saturation temperature of the liquid at the system pressure. The curve is divided 4 regions whic are natural convection boiling (region I), nucleate boiling (region II), transition boiling (region III), and film boiling (region IV).

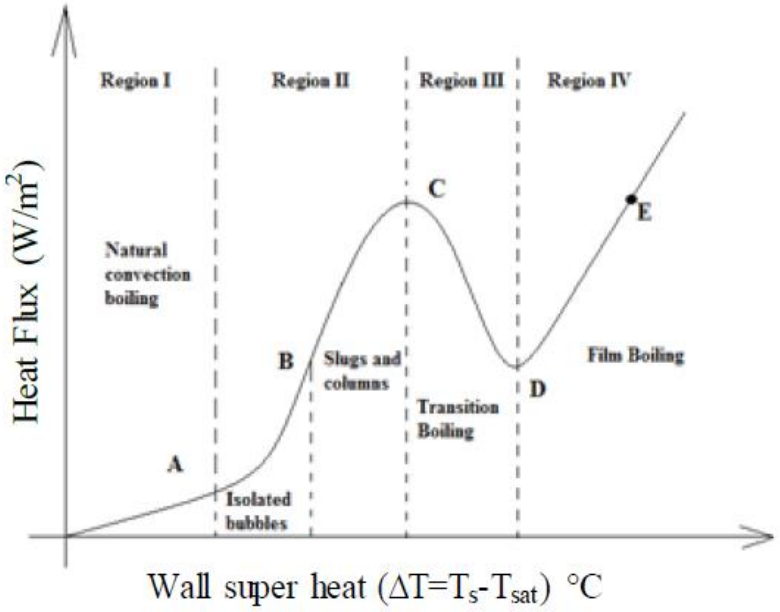

Figure 1.4. Pool boiling curve [5]

Natural Convection Boiling (region I) : At very low superheat levels, no bubble nucleation is observed and heat is transferred from the surface to the liquid by natural convection.

Nucleate Boiling (region II) : When wall superheat difference rises to a certain value corresponding to point ‘A’, small vapor bubbles are observed on the heater surface. This is the onset of nucleate boiling. Once nucleation is initiated, under right conditions, the bubble grows and nucleates from the heater surface and rises to free surface of liquid. As the wall superheat rises beyond point ‘B’, additional nucleation sites become active and the rate of generation of bubbles increases. This increases the heat dissipation rate till point ‘C’, where heat flux reaches maximum value, referred to as the critical heat flux (CHF). It is the point where maximum amount of heat can be dissipated with the liquid still re-wetting the surface. The CHF sets the upper limit of fully developed nucleate boiling.

Transition Boiling (region III) : If the wall superheat increased beyond the critical heat flux condition, overall heat flux continues to be reduced. This regime is referred

to as the transition boiling regime. Beyond point ‘D’, the bulk liquid and heating surface are completely separated by vapor film. The boiling process occurs at vapor-liquid boundary.

Film Boiling (region IV) : In film boiling, the surface flux becomes a function of temperature because of heat transfer from surface to liquid is by means of radiation. This continues till the surface reaches the maximum allowable temperature, which is melting temperature of the heated surface, indicated by point ‘E’. From the curve it can be seen that for a relatively small wall superheat, pool boiling has capacity to dissipate large amounts of heat.

Cooling methods can be achieved by natural convection and forced convection. Table 1.1. shows the typical range of heat transfer coefficients for single phase and two phase cooling regimes for air and water. It can be seen from Table 1.1. that high heat transfer coefficient is achieved by boiling.

Table 1.1. Standard heat transfer coefficient ranges for convective heat transfer method [6]

Cooling method	Heat transfer coefficient (W/m^2K)
Natural convection with gas	2-25
Forced convection with gas	25-250
Natural convection with liquid	50-1000
Forced convection with liquid	100-20,000
Boiling (convection with phase change)	2500-100,000

1.5. Critical Heat Flux

The critical heat flux (CHF) is the maximum value of the heat flux which a boiling surface can reach safely, once wall heat flux is the controlled variable. After this point, the wall temperature suddenly rise and cause the physical burnout of the heater surface. Therefore, it is important limit to the boiling performances of any devices. In order to understand the mechanisms leading to CHF and find appropriate means for improving its value constitute fundamental issues for enhancing the effectiveness of any heat exchange equipment.

1.6. Bubble Nucleation Criteria

When the temperature of the heated surface is higher than the saturation temperature of the fluid, bubble nucleation starts to occur. On the surface, their exist cavities with vapor entrapped in it. For the vapor bubble to grow, the temperature of the fluid surrounding it should be greater that saturation its temperature. Figure 1.5. shows bubble nucleation mechanism.

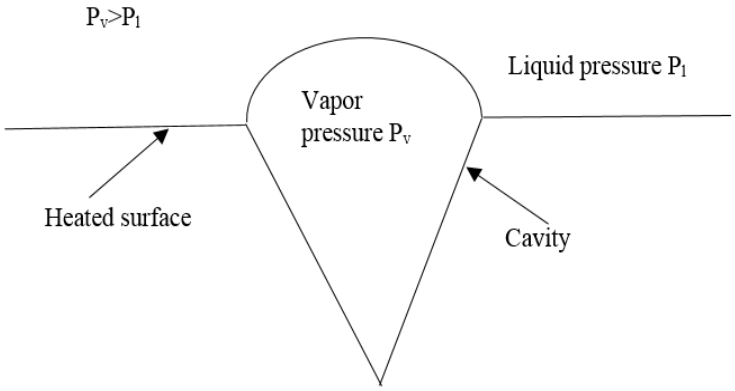

Figure 1.5. Bubble nucleation mechanism

The force balance is as shown as follows.

$$\pi R^2 \left(P_v - P_l\right) - 2\pi R\sigma = 0 \tag{1.2}$$

From equation (1.2), vapor pressure can be presented as,

$$P_v = P_l + \frac{2\sigma}{R} \tag{1.3}$$

where, P_v is vapor pressure inside the bubble, P_l is pressure of liquid, σ is the surface tension and R is the radius of the bubble.

1.7. Pool Boiling Enhancement

Boiling is one of the great cooling method which use to remove the high heat dissipation from the high dissipative electronic device. Taking the advantage of the

boiling phenomenan, surface enhancement technique has been widely used as passive method. The main idea of all studies was to dissipate high heat flux at low wall superheats. Heat transfer coefficient can be reached at considerably low wall superheat with removing the heat flux from the surface. By delaying CHF and lowering wall superheat can be achieved which improves the efectiveness of the surface. Figure 1.6. shows a representation of pool boiling enhancement. The main goal are to reduce wall super heat and to increase CHF to prove the effectiveness of the surfaces.

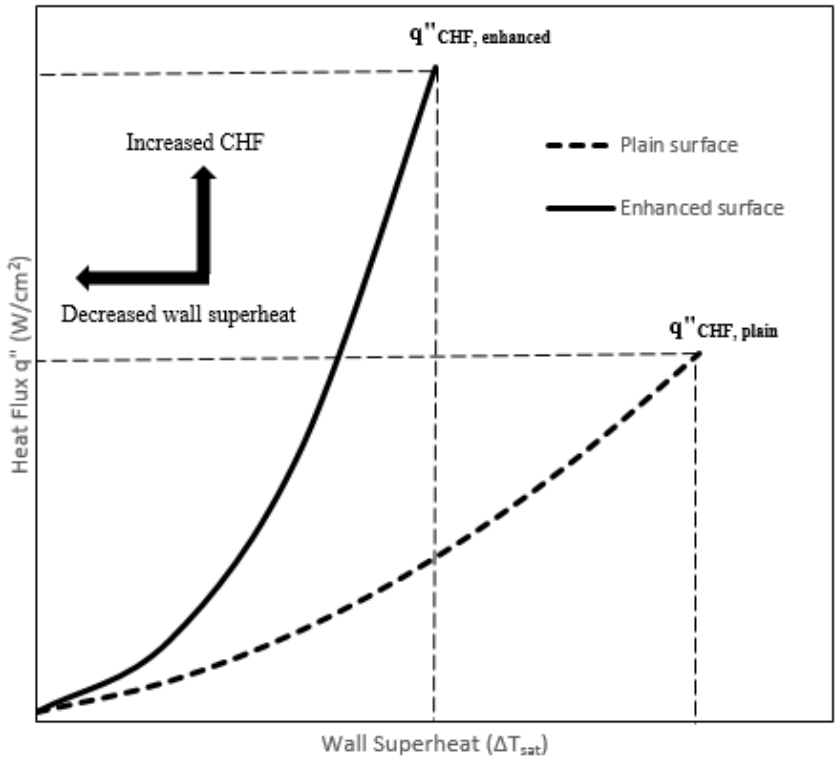

Figure 1.6. Pool boiling enhancement

1.8. Heat Transfer Performance Enhancement Parameters

The generated high heat flux from electronic devices must be removed from the system as quick as possible. Heat removel can be done from electronic devices in various ways. One of them is pool boiling. Pool boiling heat performance are influenced by many parameters that are the working fluid, surface area, surface characteristics and surface material. Efficient heat dissipation lies to enhance the heat transfer coefficient and critical heat flux through the manipulation of these

parameters. In this work, the surface area modifications are studied as the enhancement.

1.9. Enhancements of Pool Boiling Heat Transfer

Several technique were used to enhance the performance of pool boiling. Bergles [7] summarized that enhancement methods could be divided into passive, active and compound technique in Table 1.2.

Table 1.2. Classification of enhancement techniques [7]

Passive techniques		**Active techniques**
Treated surfaces		Mechanical aids
Rough surfaces		Surface vibration
Extended surfaces		Fluid vibration
Displaced enhancement devices		Electrostatic fields
Swirl flow devices		Suction or injection
Coiled tubes	**Compound enhancement**	Jet impingement
Surface tension devices	Condensation on a rough, rotating surface, for example	
Additives for fluids		

The passive techniques do not require any external power, whereas the active techniques require an external power to bring about the enhancement.

Surface roughness and material modifications, geometrical or area are some of the enchancement technique used in order to enhance the surface without increasing the footprint of the surface. Mini channels, microchannels and pin-fins are the area or geometrical modifications. These structures consists of machined channels with reentrant cavities, mini and microchannels and pin-fins. This type of modification on the surface increase surface area without increasing the footprint of the surface.

Nano and porous coating structures modify nucleation site size and density on a surface have the ability to alter the surface energy, resulting in a change in the wettability of the surface. The wettability change can be implemented by surface material changes or fluid type. Nucleation site and density are affected by nano and porous coating structures.

Nanoparticles, nanochannels, and nanotubes are employed to create the nano and porous coating structures. These nano and porous coating structures have a high thermal conductivity to reduce the thermal resistance. Due to the high thermal conductivity of carbon based materials such as graphen and carbon nanotubes (CNTs), these metarials have considerable interest for boiling applications.

1.10. Channel Classification and Microchannel Surfaces

Channel classification based on hydraulic diameter is intended to serve as a simple guide for conveying the dimensional range under consideration. One of the several criteria proposed in the literature is an easy-to-use criterion suggested by Kandlikar and Grande [8] which the authors suggested for single phase gas, liquid flows and two-phase flows as well and given as follows. Table 1.3. shows channel classification scheme.

Table 1.3. Channel classification scheme [9]

Channel classification scheme	
Conventional channels	> 3 mm
Minichannels	$3\text{ mm} \geq D > 200\ \mu\text{m}$
Microchannels	$200\ \mu\text{m} \geq D > 10\ \mu\text{m}$
Transitional Microchannels	$10\ \mu\text{m} \geq D > 1\ \mu\text{m}$
Transitional Nanochannels	$1\ \mu\text{m} \geq D > 0.1\ \mu\text{m}$
Nanochannels	$0.1\ \mu\text{m} \geq D$
D: smallest channel dimension	

In Table 1.3., D is the channel (hydraulic) diameter. Equation 1.4 gives the channel diameter.

$$D = \frac{4A_c}{P} \tag{1.4}$$

where, A_c is the cross sectional area and P is the wetted perimeter.

The critera in Table 1.3. is not based on any physical laws but was supported by testing it with different studies present in the literature.

Rapid increases in the density and speed of functional components in microproccesors have led to a significian rise in the rate of heat generation in electronic chips, as well as in the heat fluxes that need to be dissipated for maintaining chip temperatures below allowable maximum levels. Conventional heat sinks are fast reaching their limits for handling the increased cooling needs for electronic equipments. Hence, several efforts have been made to find a suitable alternative technology capable of dissipating high heat flux per unit area. Liquid-cooled microchannel heat sinks are recognized as being among the most effective solutions and hence thermal characteristics and fluid flow in microchannels have been extensively studied. The microchannels provide a combination of small flow passage, large heat transfer area, and efficient boiling heat transfer. Heat transfer with liquid-vapor phase change over microchannel offers extremely high heat fluxes. Therefore, it attracts great attention in thermal management of microelectronics, as continuous minimization in microelectronic component requires superior heat dissipation ability in small and confined spaces.

1.11. Nano Structures and Microporous Surfaces

Surface modification by nanostructures for boiling enhancement has attracted great attentions recently due to some unique properties they possessed. The nanostructure modified surface has higher wettability, which causes an increased CHF through the enhanced liquid spreading over the heated area. In addition, the modified surface contains more microscale activities, which serve as the starting sites for nucleation of liquid for bubble formation.

As the surface modification at nano-scale has proven to be an effective approach to improve boiling heat transfer, the enhancement due to combination of microporous surfaces with nano structures on boiling heat transfer is an area of current interest. Most of the surface nanostructures were effective in decreasing the wall superheat at boiling incipience, and enhancing the nucleate boiling heat transfer and critical heat flux. The factors leading to enhanced boiling surfaces, however is not fully understood, therefore, it is of great interest to investigate the enhancement mechanism behind those phenomena.

The present study deals with enhancement of heat transfer using combination of multiple passive techniques, namely nanostructures and microporous sintered surfaces and pin-fins over open microchannel surfaces in space application.

1.12. Contact Angle and Surface Wettability

The theoretical description of the contact angle is the consideration of thermodynamic equilibrium between the three phase system with a solid surface, a fluid and a vapor. The behavior of liquids in contact with solid surface varies with the different type of surfaces. It also depends on the type of fluids. The wettability of the liquid is quantified by contact angle θ which is defined as the vapor interface and the solid surface. It is measured through the liquid at O where a liquid/vapor interface meets a solid surface as shown in Figure 1.7. As θ decreases, liquid spreads more on the surface and as θ tends to form a thin liquid film on the solid surface.

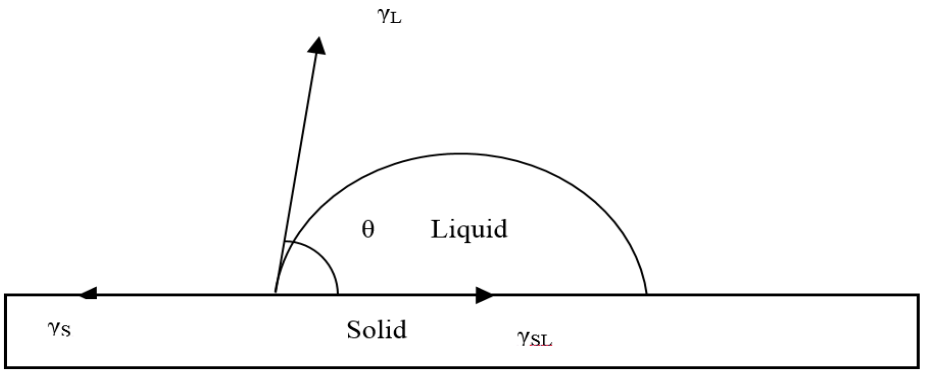

Figure 1.7. Schematic diagram showing contact angle of a liquid on a surface

As first described by Thomas Young [10] in 1805, the contact angle of a liquid drop on an ideal solid surface is defined by mechanical equilibrium of the drop under the action of three interfacial tensions in Figure 1.7:

$$\gamma_L \cos\theta = \gamma_S - \gamma_{SL} \tag{1.5}$$

where $\gamma_L, \gamma_S, and \gamma_{SL}$ represent the liquid-vapor, solid-vapor, and solid-liquid interfacial tensions, respectively, and θ is the contact angle. Equation 1.5. is usually

referred to as Young's equation, and θ is Young's contact angle. A surface is called hydrophilic when the contact angle of water is θ <90°, and hydrophobic when θ >90°. When the contact angle is larger than 150°, it is called superhydrophobic and when the contact angle is almost 0°, it is called superhydrophilic [11]. Low values of the contact angle correspond to high surface wettability.

It is difficult to prepare a solid surface with homogeneity and smoothness at molecular level. Nearly all surfaces are heterogeous and rough to an appreciable extent [12]. Therefore, a liquid in contact with the solid surface shows more than a contact angle. Advancing and receding contact angles are of practical significance in the characerization of the solid surface. The contact angle measured for the liquid tending to advance is called the advancing contact angle (θ_a) and it is larger than the contact angle measured for the liquid tending to reced which is known as the receding contact angle (θ_r). Advancing and receding contact angles are shown in Figure 1.8.

The difference between advancing and receding contact angles, θ_a and θ_r, is referred to as contact angle hysteresis. To calculate contact angle hysteresis: the arithmetic difference,

$$\Delta\theta = \theta_a - \theta_r \tag{1.6}$$

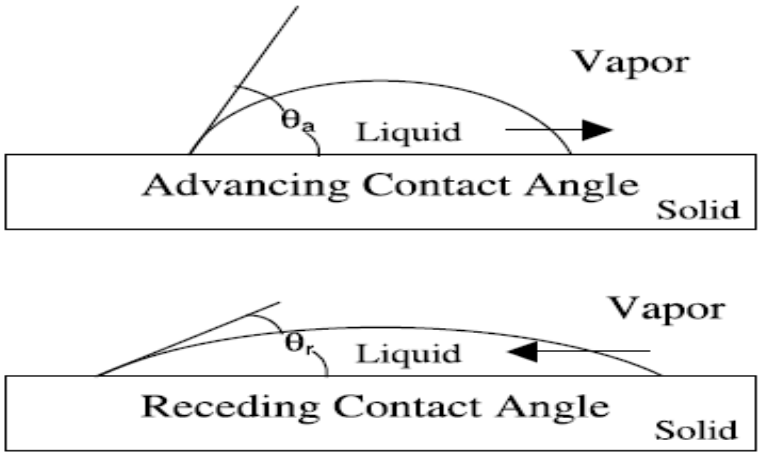

Figure 1.8. Advancing and receding contact angles [13]

CHAPTER 2. LITERATURE REVIEW

In order to manage large amounts of heat dissipation and provide adaquate cooling is not new topic to be discussed and dissipating high heat flux is also gained importance. Researchers have studied different enhancement techniques to improve pool boiling performance. Microchannels have been in use since the beginning of the early 1960's. The first pioneering work demonstrating the potential of small passages for heat transfer enhancement was performed by Bergles [14]. The first successful application in electronics cooling was used by Tuckerman and Pease [15]. They were able to dissipate a heat flux up to 790 W/cm^2 with a temperature rise of 71 ^oC between inlet and outlet. It was a force convective system and single phase cooling.

Boiling and condensation are being considered for operation of the thermal control systems (TCSs) in future space applications to increase their high heat transfer coefficients and reduce weight and volume in TCS [1]. In space applications, the use of passive thermal components, such as heat pipes (HP), vapor chambers (VC), loop heat pipes (LHP) and future pulsating heat pipes, and active components such as miniaturized pumped systems, makes very important the thorough understanding of the boiling mechanism, in order to simulate precisely the heat transfer conditions in satellites and in thermal components for extraplanetary exploration [16].

2.1. A Review of Pool Boiling in Microchannels

There are many papers that address the topic of heat transfer enhancement in conventional passages. Many researchers and companies have focused their efforts on a new heat management technology called a microchannel heat sink.

The first concept on a pore and tunnel surface had been developed by Nakayama et al. [17]. They tested water, R-11 and liquid mitrogen as working fluids with a copper surface. Open microchannels have been shown to be extremely efficient in boiling

heat transfer. Incorporating microporous surfaces on the microchannel surfaces has been shown to further increase the performance. Dr. Kandlikar has been involved in the advanced study involving open microchannels and nanostructures [18-23]. Recently Dr. Kandlikar has been involved on developing microporous surfaces for enhanced boiling surfaces [24]. The mechanism of heat transfer in through capillary transport coupled with evaporation at the interfaces.

Microstructures have been studied extensively for pool boiling enhancement [24]. Open microchannels were also investigated by Cooke and Kandlikar [25] for pool boiling on 10 mm x 10 mm square copper chips with water at atmospheric pressure. Nucleation at low heat fluxes was observed and it was noted that the nucleation occured on the top surfaces of the microchannel fins. Figure 2.1 shows schematic of bubble dynamics as observed by the authors. However, at higher heat fluxes, nucleation appeared to occur in microchannels as well.

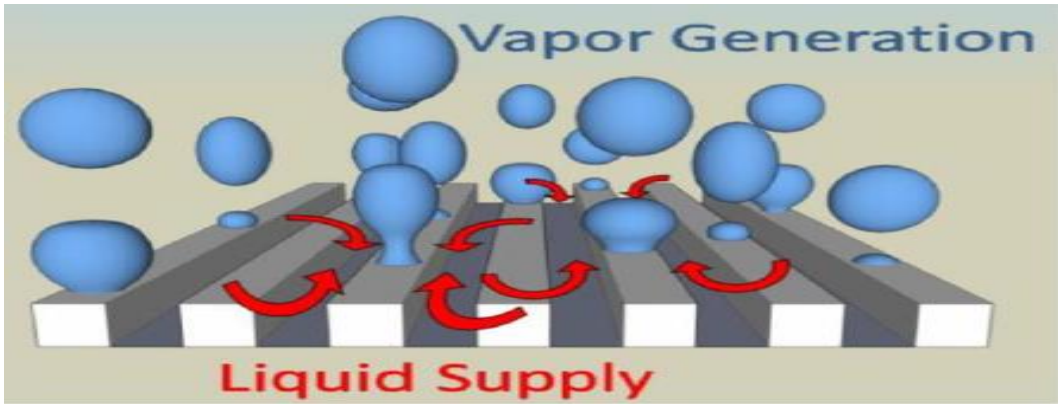

Figure 2.1. Mechanism of bubble dynamics proposed by Cooke and Kandlikar [25]

Kim et al. [26] reviewed the boiling heat transfer enhancement on micro/nanostructured surfaces. In the review paper, micro/nanostructured surface, which have been designed to enhance boiling heat transfer, are introduced and the charcteristics of these surfaces are explained in view of nucleate boiling heat transfer (NBHT) and critical heat flux (CHF). Based on the review, a well-established boiling heat transfer model and comprehensive understanding of the NBHT and CHF enhancement mechanism are necessary for designing and fabricating an optimized surface for boiling heat transfer. Moita et al. [27] addresses the qualitative and

quantitative analysis of the pool boiling heat transfer over micro-structured surfaces. The results show a significant increase of the heat transfer coefficient of about 10 times for water and 8 times for the dielectric fluid, in comparison to the smooth surface, when the micro-patterning based on pillars is used. Shojaeian and Kosar [28] studied reviews recent experimental investigations performed on pool and flow boiling over nano-and micro engineered structures for enhancements in boiling heat transfer, namely heat transfer coefficient (HTC) and critical heat flux (CHF). More enhancements were generally reported for microstructured surfaces compared to the nanostructured surfaces, and their performance enhancements were comparable to the existing commercially avaliable enhnaced surfaces. However, further enhancements are possible with future optimization studies using important nanostructure parameters and configurations, and there is much room for improvement in boiling heat transfer with nanostructured surfaces.

2.2. A Review of Pool Boiling in Pin Fins

Pin-Fins have been studied and provided enchanced boiling preformance. Microstructures such as pin-fins have been studied extensively for pool boiling enhancement by Patil and Kandlikar [24]. Mudawar and Anderson [29] used a pin fin design to enhance the heat transfer from high power electronic chips. Surface enhancement resulted in CHF of 105.4 W/cm^2 for saturation and 159.3 W/cm^2 for 35 ^{o}C subcooled FC-72. Hubner and Kunstler [30] investigated the heat transfer enhancement of trapezoid-shaped, T-shaped and Y-shaped. They also increased the surface roughness of the pins. Surface roughness was found to increase the bubble formation for trapezoidal fins while T-Y- shaped fins increase the *h.* Mitrovic and Hartmann [31] used micropins or fins to enhance the boiling surface and reported improved heat fluxes. Wei and Honda [32] conducted to study the effects of height and thickness of square micro-pin-fin on boiling heat transfer from silicon chips immersed in a pool of degassed or gas-dissolved FC-72. Micropin fins were fabricated on a 10 x 10 x 0.5 mm^3 square silicon chip by using the dry etching technique. They conducted the experiment under subcooled and atmospheric conditions. The micro-pin-finned chips showed a considerable heat transfer

enhancement in the nucleate boiling region and increase in the critical heat flux compared to the smooth chip. Honda et al. [33] studied the effects of square micro-pin-fins (50 x 60 μm^2 in thickness x height and 100 μm in fin pitch) and submicron scale roughness (about 30 nm in r.m.s roughness) on boiling FC-72. The micro-pin-finned chips showed a sharp increase in the heat flux with increasing wall superheat in the nucleate region and the wall temperature at the CHF point was lower than 85 ^oC. CHF was 1.8-2.3 times large as that for a smooth surface. Honda et al. [34] further studied the effect of the thickness of square micro-pin-fin on boiling of FC-72. The fin dimensions were 10 x 60, 10 x 60 and 50 x 60 μm^2 (thickness x height) and the fin pitch was twice the fin thickness. The heighest CHF obtained by these chips was close to that obtained by the micro-pin-finned chip with submicron-scale roughness on it [34]. Guglielmini et al. [35] tested twelve extended surfaces with different geometrical configurations from copper surfaces immersed in a saturated dielectric fluid (Flurinert FC-72) at three different saturation pressures which are 0.5, 1.0 and 2.0 bar. Fins were 3 and 6 mm long and their width varied 0.4 to 1.0 mm. Fins were uniformly or non-uniformly spaced on the base surface. If pressure is increased, the boiling curves of finned surfaces move towards lower wall superheats and raises maximum heat flux. In the case of extended surfaces composed of uniformly spaced fins, longer fins appear to work slightly better, particularly in proximity to the maximum heat flux. When fin width and spacing decrease, the heat transfer rate increase, but, at high heat fluxes, the overall heat transfer coefficient diminishes.

2.3. A Review of Pool Boiling in Sintered Coatings

In addition to surface enhancements such as pin fins, or channels, sintered is another technique to improve heat transfer. Patil and Kandlikar [24] presented a comprehensive review on the different manufacturing technique to develop porous heat transfer surfaces for boiling. In the survey, they summarized the porous enhancement into sintering, electrodeposition and advanced manufacturing technique. They suggested that sintering coatings is easy and effective technique from manufacturing perspective. Li and Peterson [36] examined the effects of the geometric dimensions (i.e., coating thickness, volumetric porosity, and pore size, as

well as the surface conditiosn of the porous coatings) on the pool boiling performance and characteristics using distilled water at atmospheric pressure (101 kPa). They studied on pore sizes, 119.2 μm, 140 μm and 232.2 μm. The experimental results showed that smaller porse size was better for heat transfer performance. A thicker coating increased the CHF. On the other hand, the low wall superheats achived with a thin coating. Web [37] studied the effects of particle diameter, coating thickness and pore size of copper porous coatings. The performance of seven porous coatings tested with R-11 was compared and the effect of the geometric variables on the boiling were examined. The test results showed for coatings with copper (high-conductivity particles), the particle diameter was a negligible effect on performance, but maximum boiling coefficient occured for a coating thickness of roughly three to four times particle diameters. For lower thermal conductivity particles (bronze) the performance was not sensitive to coating thickness for $2 < \delta/d_p < 6$. Furthermore he suggested that pore size has a significiant effect than particle size. Bergles and Chyu [14] conducted a study of pool boiling form a commercial porous metallic matrix surface. They observed that nucleation takes place within the porous matrix and these reentrant cavities are not subjected to flooding.

It was seen from the literature reviews that surface enhancement techniques have significantly improved the pool boiling performance by providing additional surface area and/or nucleation sites. Enhanced surfaces such as open microchannels, microporous surfaces (sintering, nanowires, electrodeposition, surfactant, electrochemistry, carbon nanotubes, etc), pin-fins, micropillars, nanostructures and nanofluids have significantly improved by increasing the heat transfer area or by affecting the liquid wettability on the surface.

2.4. Pool Boiling Enhancement Technique

Wick structures are one of the key parameters that needs to be considered during a design phase of vapor chamber especially evaporator section. In order to apply the optimized wick structures, recent studies on pool boiling enhancement technique also summarized. The critical heat flux (CHF) and heat transfer coefficient (HTC) pool

boiling have been experimentally studied on different type of structures by using de-ionized water. Pool boiling enhancement is achieved by delaying critical heat flux and increasing heat transfer coefficient. Most recent research summarized in Figure 2.2. and Figure 2.3.

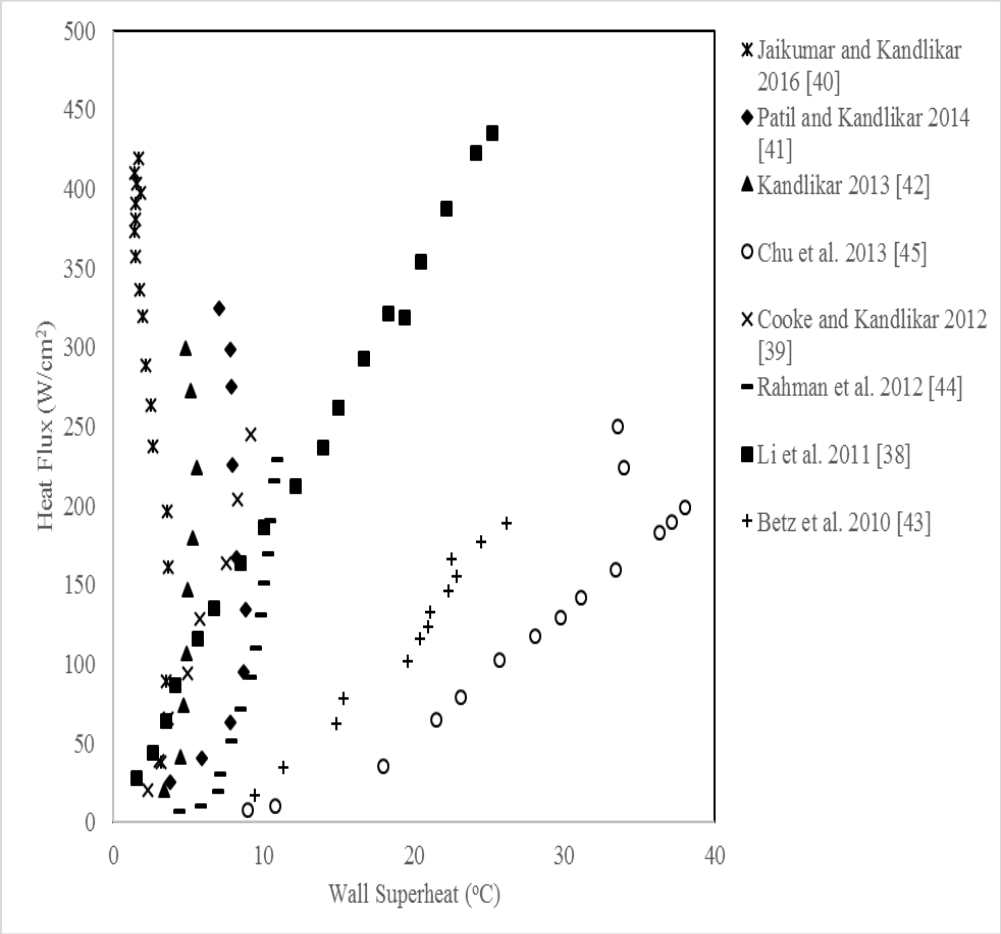

Figure 2.2. Pool boiling performance comparison with different structures [38-45] reported in the literature with water at atmospheric pressure

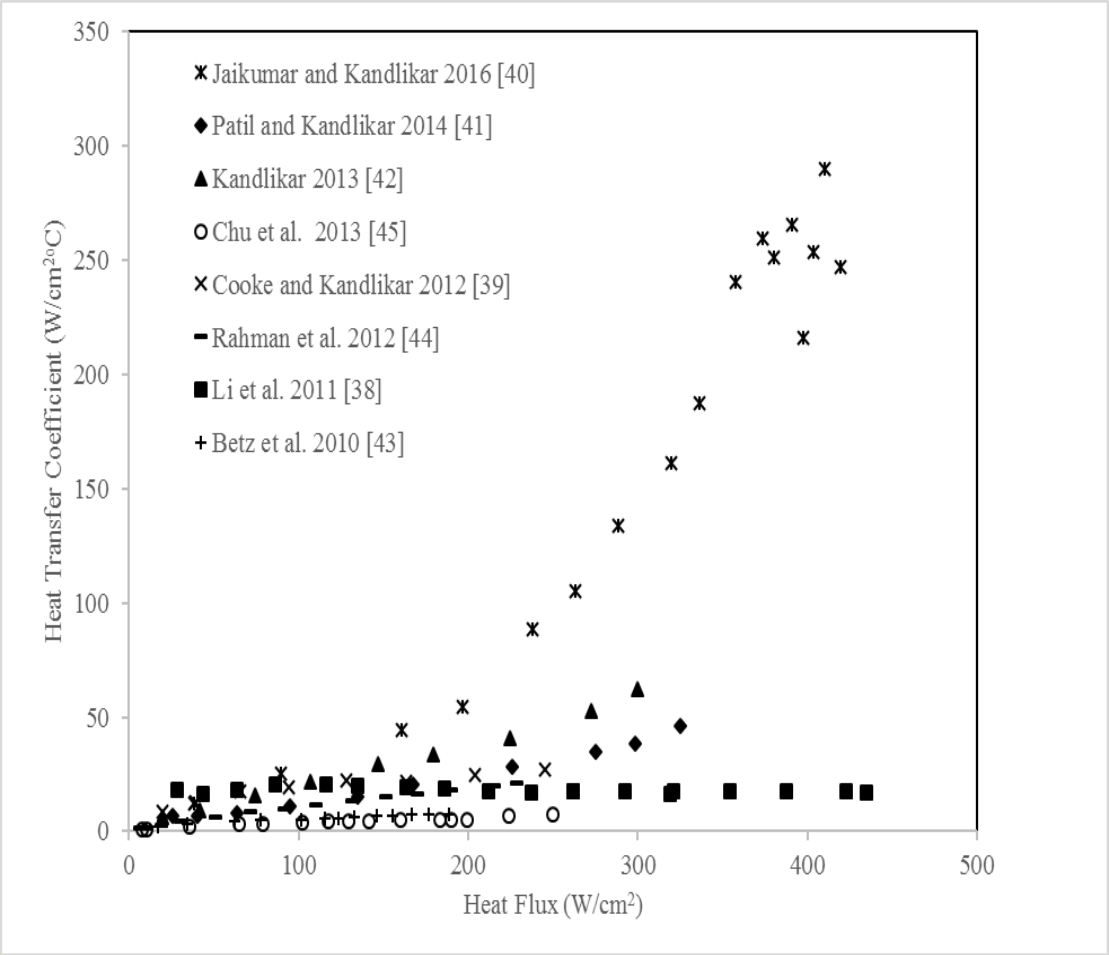

Figure 2.3. Heat transfer coefficient comparison with different structure [38-45] reported in the literature with water at atmospheric pressure

Li et al. [38] studied the modulated porous structure which has a porous base of 0.55 mm thick with four 3 mm diameter porous pillars of 3.6 mm high on the top of the base. The highest heat flux and the highest heat transfer coefficient on the modulated porous structures reached 450 W/cm^2 and a value of 20 W/cm^{2}K, respectively. Cooke and Kandlikar [39] used different microchanneled surface to enhance heat transfer performance. They found that the best heat transfer results were reached by using the wider and deeper channels and thinner finned surfaces. The best performing chip dissipated a heat flux of 244 W/cm^2 corresponding to a record heat transfer coefficient of 269 kW/m^{2}K. Jaikumar and Kandlikar [40] focused on the effect of channel width on the heat transfer performance and heat transfer mechanism on open microchannel surface with sintered-throughout, sintered-fin-tops, and sintered channels. A record of 420 W/cm^2 at a wall superheat of 1.7 ^{o}C was observed

for the 300 μm channel width test surface. Patil and Kandlikar [41] reported a maximum CHF of 325 W/cm^2 at a wall superheat of 7.3 ^{o}C with fin width= 200 μm, channel width=500 μm and channel depth=400 μm with electrodeposition of microporous surface on fin top. The thickness of deposit is 73.3 μm. Kandlikar [42] used the depth of groove= 200 μm and the corner angle= 60 ^{o}. He reported a record of heat transfer coefficient 629 kW/m^{2o}C at a CHF of 300 W/cm^2 at a wall superheat of 4.8 ^{o}C.

Betz et al. [43] tested a combination of hydrophilic and hydrophobic patterns with changing the wetting angle. The best enhancement of the CHF and HTC was achieved with hydrophilic networks featuring hydrophobic islands which had the best performance, with a maximum CHF of approximately 180 W/cm^2 and a heat transfer coefficient 85 kW/m^{2}K. Rahman et al. [44] studied the effect of low-conductivity materials at the interface between the surface and fluid. Replacing ~18% of the surface with non-conductive epoxy results in a greater than 5 times increase in heat transfer rate a given superheat temperature. Chu et al. [45] studied hiearchically structured surfaces by using electrophoretic deposition of silica nanoparticles on microstructured silicon and electroplated copper microstructures covered with copper oxide (CuO) nanostructures. The CHF of ~ 250 W/cm^2 was reached with a CuO hiearchical surface with a roughness factor of 13.3.

Based on the studies mentioned above, the mechanism of CHF enhancement can be explained by the capillary suction effect, the extended surface area effect, the liquid supply caused by the hydrodynamic effect, and the wettabilty of the heated surface.

CHAPTER 3. CRITICAL HEAT FLUX CORRELATIONS IN POOL BOILING

Heat transfer in nucleate boiling has been predicted by many researchers. The most widely used correlation for the rate of heat transfer in the nucleate boiling region was proposed in 1952 by Rohsenow [46]. He developed a model to predict the relation between heat transfer and the wall superheat. The expression for heat transfer and wall superheat during pool boiling is given by Rohsenow as follows.

$$q''_{nucleate} = \mu_l h_{fg} \left[\frac{g(\rho_l - \rho_v)}{\sigma} \right]^{1/2} \left[\frac{C_{pl}(T_w - T_s)}{C_{sf} h_{fg} \, \mathrm{Pr}_l^n} \right]^3 \tag{3.1}$$

where, $q''_{nucleate}$ is nucleate boiling heat transfer, μ_l is viscosity of the liquid, h_{fg} is enthalpy of vaporization, g is gravitational of acceleration, ρ_l is density of the liquid, ρ_v is the density of vapor, σ is surface tension, C_{pl} is specifif heat of the liquid, T_w is surface temperature of the heater, T_s is saturation temperature of the fluid, and Pr_l is Prandtl number of the liquid. He used a surface-fluid coefficient, C_{sf} for various combinations. C_{sf} is called the experimental constant that depends on surface-fluid combination. n is the experimental constant that depends on the fluid. Values of coefficient C_{sf} and n are 0.0130 and 1.0 for water-copper (polished) respectively. Values of coefficient C_{sf} and n are 0.0068 and 1.0 for water-copper (scored) respectively.

The interpretation of the critical heat flux correlations in pool boiling is still controversial. Over the years, many researches have attempted to predict CHF with various models and equations. The critical heat flux represents the maximum heat dissipation that can endure in the nucleate boiling region. Therefore, it sets an upper limit for safe operation of the maximum power generation of given boiling systems.

It is unclear if one mechanism determines the occurence of the critical heat flux (CHF) in any geometrical and thermodynamics condition. After Drew and Muller [47] completed Nukiyama's [4] boiling curve, a number of studies were done to explain the maximum and minimum heat fluxes. Among these, the most successful models for the maximum heat flux were those by Kutateladze [48], Zuber [49] and Kandlikar [50]. Kutateladze and Zuber models were based on the hydrodynamics of vapor outflow. Kandlikar [50] modified the Zuber hydrodynamic instability model to include effects of the heater surface. Zuber's model employed stability of vapor jets whereas Kutateladze developed dimensionless groups from the equations governing the flow of vapor and liquid. Kutateladze and Zuber models resulted in a nearly identical expression for the maximum heat flux on flat plates as. Regardless of modeling, critical heat flux data on flat plates have been correlated by Kutateladze as follows.

$$q''_{CHF} = K\rho_g^{0.5} h_{fg} \left[\sigma g(\rho_l - \rho_g)\right]^{0.25} \tag{3.2}$$

The value of K (often referred to as Kutateladze number) was found to be 0.16 in the experimental, and 0.131 in Zuber's [49] correlation from the experimental data. The Lienhard and Dhir [51] modification of Kutateladze-Zuber [48-49-52], the value of K was found 0.149. The Zuber-Kutateladze do not include the contact angle as a parameter.

Very few researchers have studied the effects of the liquid surface contact angle on CHF even though it is considered to be very crucial parameter. Kirishenko and Cherniakov [53] developed a model based on dynamic receding contact angle. Dynamic receding contact angle (β) is chosen because as the bubble grows along the surface the contact angle between the surface and the receding liquid/vapor interface characterizes the wettability of the surface.

$$q''_{CHF} = 0.171 h_{fg} \rho_v^{1/2} \left[\sigma g(\rho_l - \rho_v)\right]^{1/4} \frac{\left(1 + .000324\beta^2\right)^{1/4}}{\left(0.018\beta\right)^{1/2}} \tag{3.3}$$

Diesselhorst [54] found that this model overestimates CHF for large contact angles and found it to overestimate CHF values for water, but the trend on increasing CHF with decreased contact angle was correct.

Kandlikar [50] developed a model for predicting the critical heat flux for pool boiling based on the contact angle and the orientation was included in his model. He developed a model considering a force balance on a bubble and the presence of a thin liquid micro layer under the bubble. It was proposed that near CHF the momentum created by the evapoartion on the sides of the bubble exceeded gravity and the surface tension forces causing the bubble to grow along the heated surface. Critical heat flux developed by Kandlikar based on the contact angle as follows.

$$q''_{CHF} = h_{fg}\rho_g^{1/2}\left(\frac{1+\cos\beta}{16}\right)\left[\frac{2}{\pi}+\frac{\pi}{4}(1+\cos\beta)\cos\phi\right]^{1/2}\left[\sigma g(\rho_l-\rho_g\right]^{1/4} \qquad (3.4)$$

Equation (3.4) predicts the CHF for saturated pool boiling of pure liquids. In general, for a heater surface inclined at an angle ϕ to the horizontal (ϕ = 0 deg for a horizontal upward facing surface, ϕ = 90 deg for a vertical surface). β is the dynamic receding contact angle. An experimental work reporting the dynamic receding contact angles for water droplets impinging on hot surfaces is presented by Kandlikar and Steinke [55] For water/copper system, β is 45 deg. Zuber-Kutateladze [52] and Kandlikar [50] correlations are the most well known to calculated the critical heat flux for saturated pool boiling. The critical heat flux prediction by using Kandlikar correlation is quite good and consistently better than the Kutatelazde prediction.

CHAPTER 4. OBJECTIVES OF RESEARCH

The main objective of this work was to study the effect of microporous coating on open microchannels using screen printing and sintering and the effect of pin-fins over microchannels. This study focuses on pool boiling of varies surface structures (plain surface, microchannel, sintered surface and pin fins (or micropillar)) to enhance heat transfer surface with water as the working fluid at atmospheric pressure. The present studies, in order to succeed in heat removal from a a heat surface with high heat flux, various surface enhancements were tested. The literature showed that surface enhancement has resulted in improvement in the heat transfer rate. The surface enhancement also enhanced CHF and reduced wall superheats. The major objectives of this research were listed as follows.

1. Developed a test setup to test the developed surfaces for their heat transfer performance and obtain their boiling curves.

2. Developed a process to obtain different type of surfaces of a variety of morphologies on the top a plain chip and study the effects morphologies on boiling heat transfer.

3. Developed a process to selectively deposit the best performing morphology of different type of surfaces on top of the test the surfaces for boiling heat transfer.

4. Obtain high speed camera images to understand the heat transfer mechanism and bubble dynamics.

5. Analyze high speed camera images and the experimental data results to understand the heat transfer mechanism.

Work involved experimental work as well as theoretical work. This was mainly a two-phase study.

CHAPTER 5. MATERIAL AND EXPERIMENTAL TEST SET UP

The pool boiling test facility used for the present study is shown in Figure 5.1. The experimental facility with distilled water was working fluid was designed and constructed to investigate the pool boiling phenomenon and the heat transfer performance. The experimental set up was also designed and built to allow testing of different surfaces.

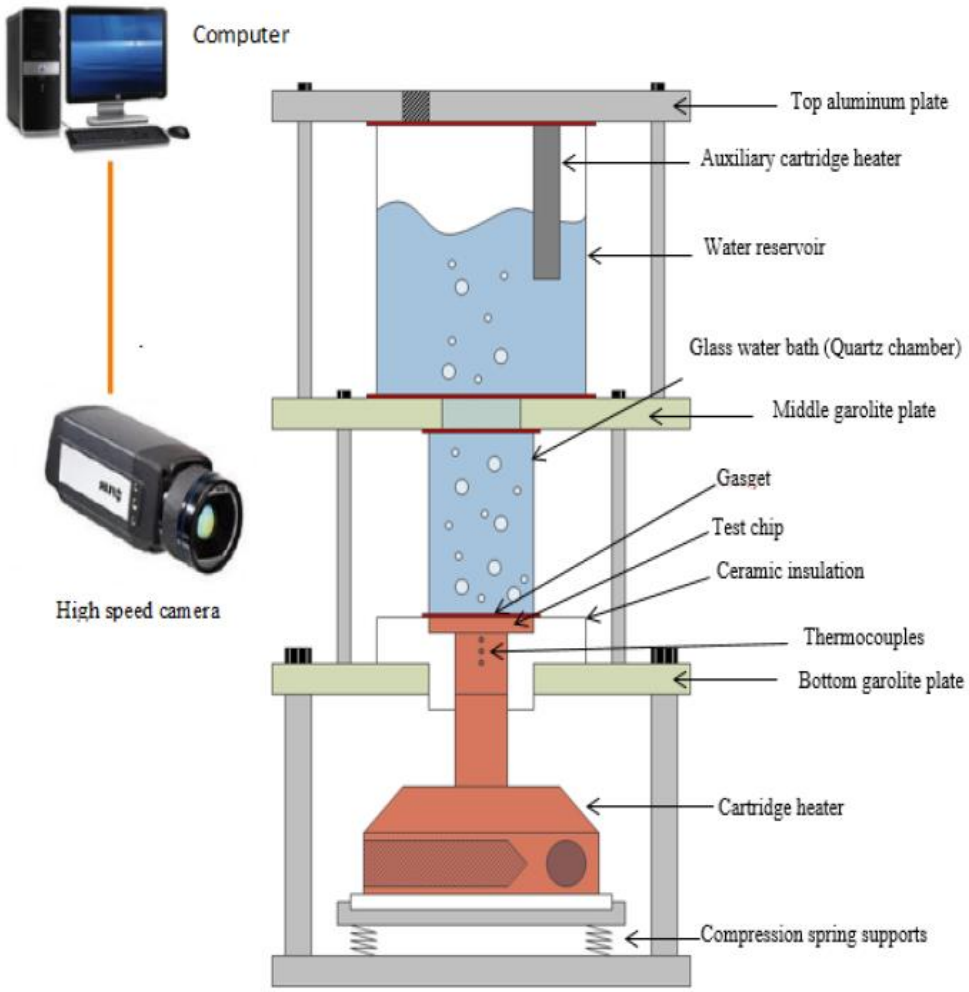

Figure 5.1a. Experimental set up of the pool boiling

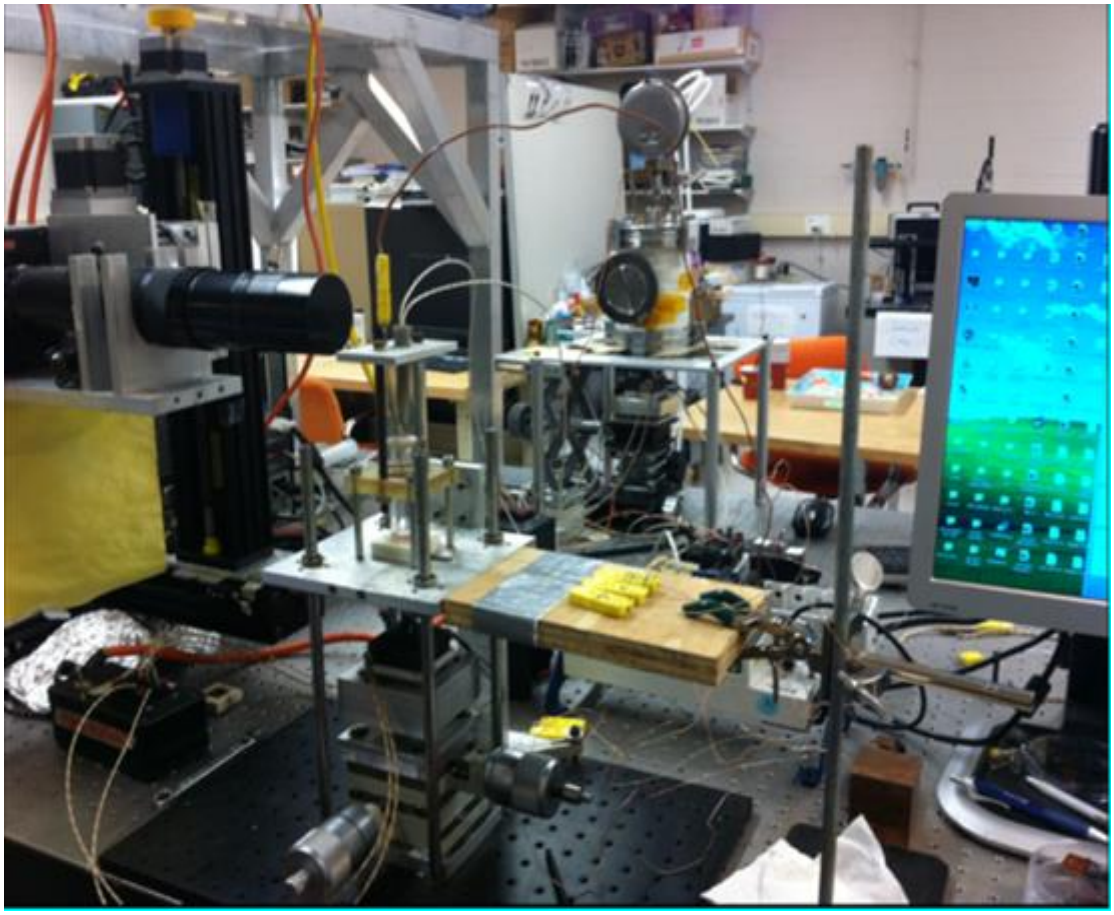

Figure 5.1b. Experimental set up of the pool boiling view

The test set up consists of five major parts as follows:

1. Test section
2. Heating module
3. Measurement and data acquisition system
4. A water bath and degas system
5. Environmental system (high speed camera, computer, illuminating lamp, etc.,)

For the material selection, copper was chosen because of compability with water as the working fluid and copper has also high thermal conductivity value.

5.1. Test section

All test sections are made of copper. 10 mm x 10 mm area of the copper test section was machined by using a CNC machine. The copper test section was located inside a ceramic insulation to minimize heat losses.

5.2. Heating Module

For heat dissipation, the heater was a 1 square cm copper heating block. The copper heater was made of a copper 101 alloy block with 200 W cartridge heaters (primary) inserted on each of four sides. Auxiliary cartridge is located into water reservoir to maintain the water reservoir at saturation temperature and reducing any heat losses to the environment. All cartridge heaters main function are to serve as the heating element to apply heat flux to the test section. The primary and the auxiliary cartridge heaters were powered by DC power sources. A TCR power supply was used to provide to the joule heating system. The voltage of the current provided was changed to regulate the power input the heaters. The heater block is shown in Figure 5.2.

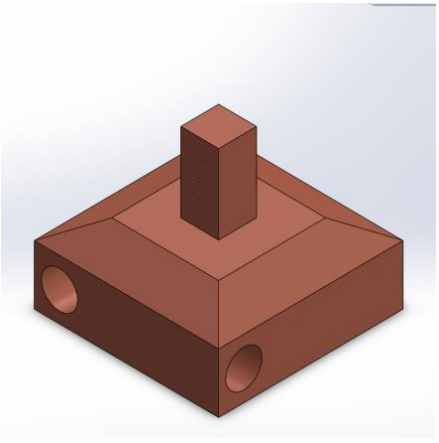

Figure 5.2. Heater block

The voltage of the power supply was adjusted to set the heat input to the test section. Heat flux q" was calculated from voltage V_{heater} supplied to the test sample heater, the evaluated current $I_{circuit}$ from the known reference resistance and loaded voltage to the resistance, and heating area A_{heater}:

$$q'' = \frac{\left(V_{heater} * I_{circuit}\right)}{A_{heater}} \tag{5.1}$$

5.3. Data Acquisition System

Three holes for thermocouples was drilled to measure inlet temperatures for calculation of input heat flux on the test setup. Three K-type thermocouples ($T_{1(top)}$, $T_{2(middle)}$ and $T_{3(bottom)}$) were used to measure the temperature gradient through the block. A National Instruments cDaq-9172 data acquisition system with NI-9211 temperature module was used to record the temperatures during testing. A LABVIEWVR virtual instrument was created to display and calculate the surface temperatures and heat fluxes. The test sample voltage load was directly monitored with a power-measuring line. The test data were collected using a data logger, interface card, and personel computer. The system recorded voltage data from the test sample heater and reference resistor, and temperature data for the bulk fluid from type-K thermocouple. A super Omega K type thermocouple used to measure the fluid saturation temperature was placed inside the water bath. The temperature of the water was monitored by a K-type thermocouple (T_4).

5.4. A Water Bath and Degas System

The liquid on top of the copper chip is contained using a quartz glass bath casing which is 14 mm (width) x 14 mm (lenght) x 38 mm (height). A clear fused Quartz square tube was placed on the top of the copper test chip to form the fluid bath.

5.5. Environmental System

The top of the copper heat block is in contact with the bottom of the copper chip. A graphoil $^{(R)}$ paper was inserted as a thermal interface material between the heater's top pin surface and the chip's bottom surface to reduce the thermal contact resistance between them. The copper test chip is located in a ceramic chip holder. The

schematic of the test copper chip and the ceramic chip holder assembly is seen in Figure 5.3. The ceramic chip holder dimension is 30.4 mm x 30.4 mm.

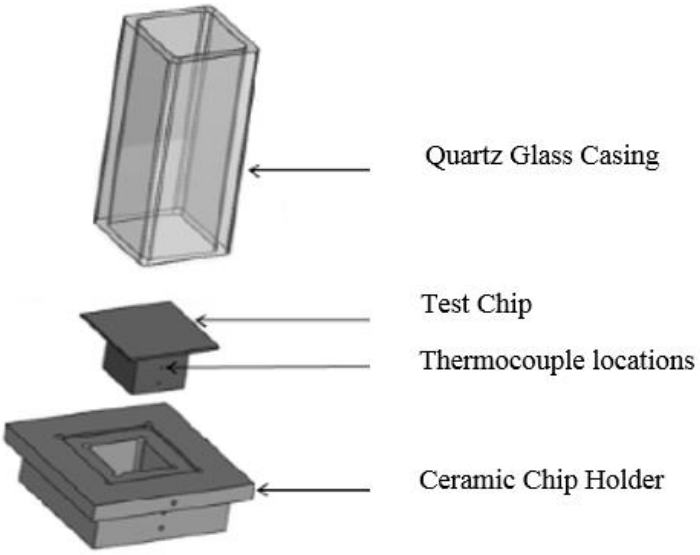

Figure 5.3. The copper test section with the ceramic chip holder assembly

The aluminum plate located at the top was provided with two circular holes for the saturation thermocouple probe and a 60-VDC, 200 W auxiliary cartridge heater to maintain water in the reservoir at saturation (100 ^{o}C) by boiling continuously. A rubber gasket was used to seal the two contacting surfaces and it is covered the area outside the 100 mm^2 boiling surface. Additionally, this area was further covered with a Kapton $^{(R)}$ tape to prevent it from participationg in heat transfer. To ensure the surface does not dry out during experimental, a liquid reservoir is located on the top of the glass casing. In order to let the bulk liquid at saturation temperature, an auxiliary heater is added.

The ceramic chip and the copper test section was located on the base aluminum plate, which was attached to a fine adjustment stage that allowed the plate to be moved up and down. The middle and bottom garolite plate were connected with a shaft pin to ensure stability of the test set up. Four compression springs were used to support the bottom aluminum plate which provides the required degree of movement in order to

make te contact beween the copper test setup and the heater and these compression springs also accommadate for any expansion during test duration.

In order to see the bubble dynamic during the pool boiling process, a Keyence high speed camera was used which is shown in Figure 5.4. The camera was inclined at the proper angle so that nucleation at the heated surface could be clearly viewed. The frame rates of 4000 fps was employed at resolution of 256 x 256 in order to keep resolution. The camera was placed as close as possible without losing the sharp focus required. An illuminating lap was installed at the opposite side of the test section, so that the heating surface looked shining bright. Figure 5.4. shows the images which were taken during the low heat fluxes.

Figure 5.4. The images of bubbles at low heat fluxes

5.6. Working Fluid

Water was used as the working fluid. Water was chosen to be the working fluid because of its high latent heat, large surface tension and nontoxicity. Selection of the working fluid for heat transfer applications also depends on a number of considerations regarding: (1) operating temperature range, (2) the compability with the metarials and (3) the fluid thermophysical properties. Distilled water was used in this research as the working fluid; relevant thermophysical properties of the distilled water is shown in Table 5.1.

Table 5.1. Distilled water properties

Boiling point	^{o}C	100
Liquid density	kg/m^3	950
vapor density	kg/m^3	0.5
Latent heat	KJ/kg	2260
Surface tension	N/m	5.88 x 10-2

5.7. Test Chip

A 3-D representation and the dimension of the test chip which were shown in Figure 5.5. and Figure 5.6., respectively. The outer dimensions of the chip was 17 mm x 17 mm x 9.2 mm. The heater section of the copper test chip was a 10 mm x 10 mm x 9.2 mm protrusion with three 0.64 mm holes drilled 3 mm apart to accommodate the thermocouples as shown in Figure 5.6. After machining the chip surfaces, they were cleaned with isopropyl alcohol (IPA) and distilled water, and further dried using pressurized air. The effect of contact resistance in the heat flux calculation was eliminated by placing thermocouples in holes drilled in the copper test section. Three K-type thermocouples were inserted into these holes to read the temperature at different locations on the copper test chip.

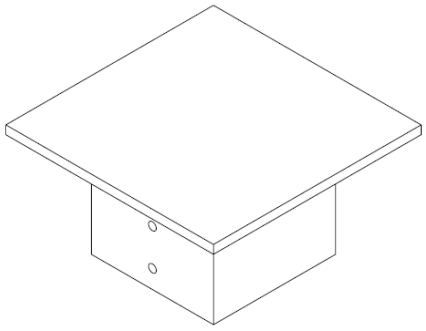

Figure 5.5. A 3-D representation of the test chip

In this study, seven different copper chips were used. Table 5.2. describes the seven copper chips matrix were tested using the pool boiling test setup. This selection of chip designs has been used to evaluate the effects of sintering, microchannel and pin-fins during the boiling process.

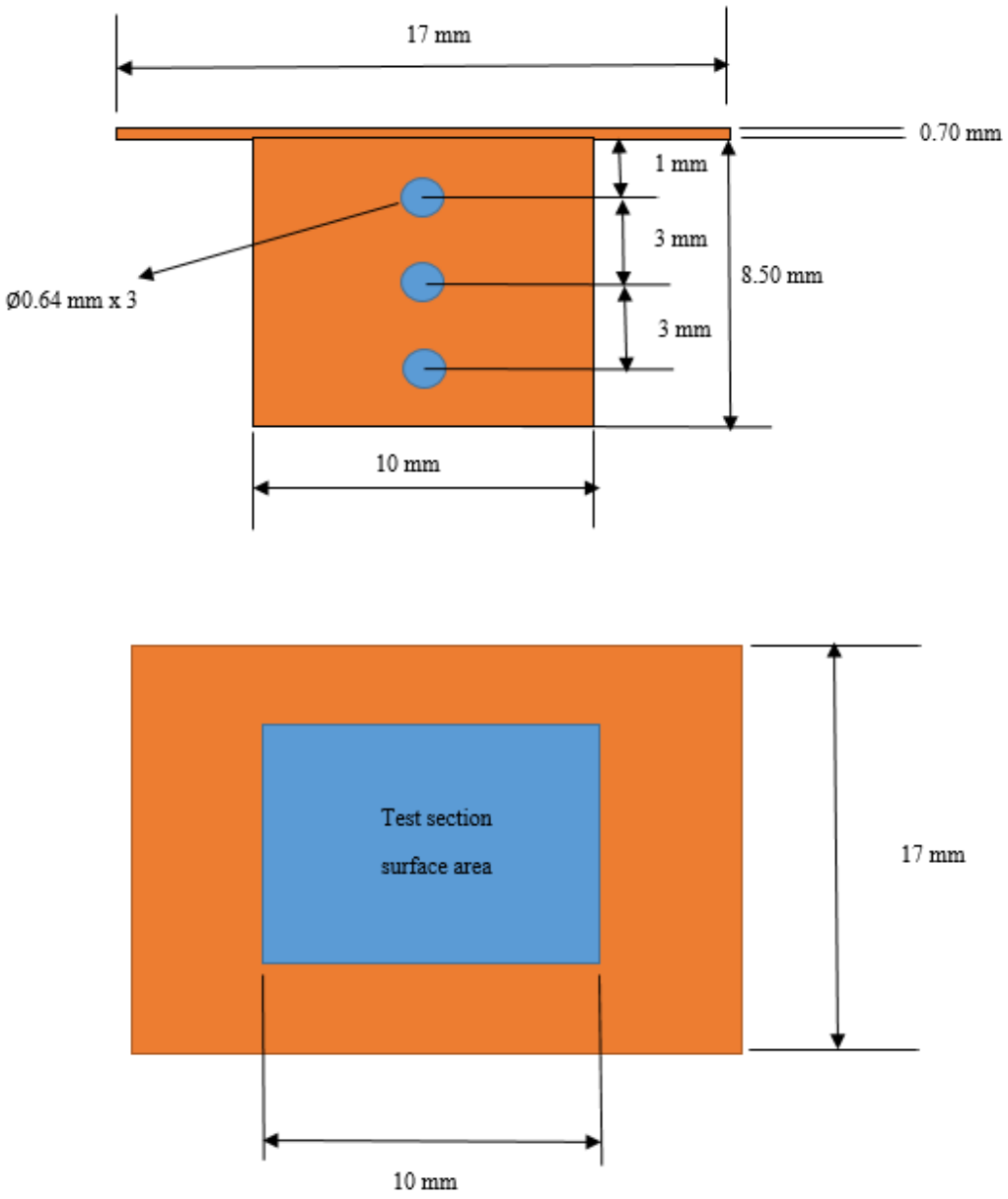

Figure 5.6. Test section with the dimensions

Table 5.2. The copper test chip matrix

				Channel Dimension			Pin-Fin Dimension		
Sample	Name	Type of surface	Sintered Thickness	Width	Depth	Fin	Width	Depth	Fin
			(μm)	(μm)	(μm)	(μm)	(μm)	(μm)	(μm)
1	P	Plain	N/A	N/A	N/A	N/A	N/A	N/A	N/A
2	P_S	Plain with sintering	60-70	N/A	N/A	N/A	N/A	N/A	N/A
3	MC	Microchannel	N/A	500	400	200	N/A	N/A	N/A
4	MC_SFT	Microchannel with sintered top fins	60-70	500	400	200	N/A	N/A	N/A
5	PF	Pin-Fins	N/A	N/A	N/A	N/A	500	400	200
6	MC_SPF	Microchannel with Single Pin-Fins	N/A	500	250	200	100	125	100
7	MC_DPF	Microchannel with Double Pin-Fins	N/A	800	200	100	200	200	100

A measurement was done by using a laser confocal microscopy for surface morphology. Using a Keyence (R) laser confocal microscope, the copper test chip dimensions and parameters were quantified. Figure 5.7. shows the test chips.

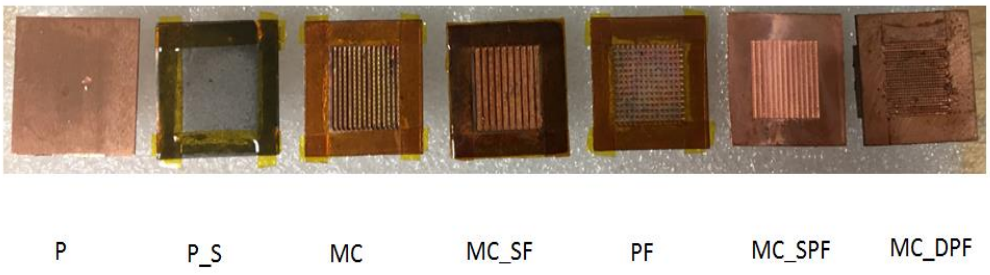

Figure 5.7. Test chips

5.8. Plain Copper with Sintering and Microchannel with Sintering Process

Sintering is the most common technique to produce a metallic microporous surface. Plain copper chip and microchannel chip were sintered. The plain copper chip was shown in Figure 5.5. A copper powder from 3M^{TM} with a particle size of 10-20 μm was used. Porous coating was prepared as a powder to ink composition of 2:1 and then screen printing technique was applied the plain surface to deposit on porous coating. When porous coatings were deposited on the plain chip surface, the test chips were subject to sintering in an inert atmosphere. Figure 5.8. shows the sintering process. Temperature is raised to 500 ^{o}C and held for 30 minutes to remove the sintering oil. Temperature is then raised to 850 ^{o}C and held for 1 hour. The test chip

is then allowed to cool gradually to room temperature. The process involved ramp up, hold and ramp down to ensure that substrate was bonded to the test chip surface. Figure 5.8 shows the furnace of the sintering. Figure 5.9. shows the sintering details used in this study. A coating thickness was measured roughly 60-70 µm by using a laser confocal microscope.

Figure 5.8.The furnace of sintering.

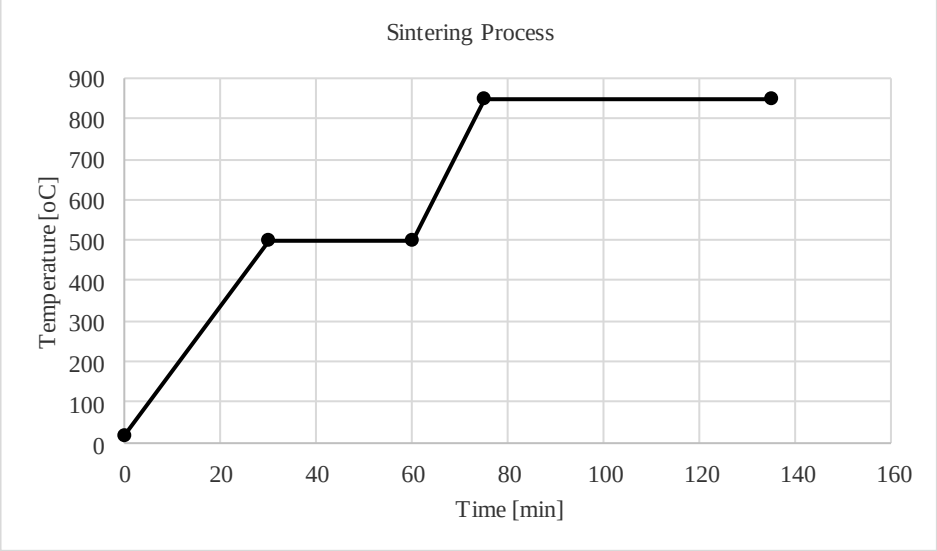

Figure 5.9. Sintering cycle process

Table 5.3. Sintering details

Parameter	Value
Sintering temperature	850 ^{o}C
Sintering duration	1 hours
Sintering atmosphere	Helium

For microchannel with sintered surface (porous deposit) was fabricated in two-step process. First, porous deposits are screen printed (mesh size= 230 count) on a plain copper chip. Second, microchannels are machined. A coating thickness was measured roughly 60-70 μm by using a laser confocal microscope.

5.9. Surface Roughness Measurements

Roughness is commonly accepted as one of the most important parameters in surface characteristics for enhancing the heat transfer coefficient due to an increase in the number of the nucleation sites. It is also well known that the surface roughness is effective in enhancing nucleate boiling. The arithmetic average roughness R_a is used as the roughness parameter. Surface roughness of the chips was determined with Keyence $^{(R)}$ laser confocal microscope. Test chips were manufactured with a polished surface for use in the water experiments. The polishing was achieved using a polishing machine. The surfaces were first cut by a CNC machine and measured surface roughness by a Keyence $^{(R)}$ laser confocal microscope. If the surface rougness average value (R_a) is more than 9 μm, the finer grits of sandpaper used to decrease the surface rougness until 9 μm. If the surface rougness value is less than 9 μm, the polishing machine used to decrease the surface roughness less than 1 μm. In the polishing machine process, the machine parameters can be controlled to produce surfaces with different roughness. Enough surface material was removed with the polishing machine so that the final roughness was due to the polishing machine process rather than the original machining operation.

Several scans were performed in different locations on each surface using a Keyence $^{(R)}$ laser confocal microscope. The roughness average (R_a), RMS roughness (R_q), the maximum profile peak height (R_p), and five-point average maximum height (R_z) were

evaluated according to ASME B46.1-1995 standards and were reported in Table 5.4. R_a is the average deviation of the peaks and valleys from the mean elavation. R_q is the root-mean-square devaition from the mean elavation.

Table 5.4. Surface roughness parameters

	Surface roughness parameters			
Surface preparation	R_a (µm)	R_q (µm)	R_p (µm)	R_z (µm)
Plain	2,428	3,49	31,154	75,148
Plain with Sintering	7,807	16,71	377,982	608,261
Microchannel (Top Fin)	4,496	6,067	27,085	84,188
Microchannel (Channel)	4,716	6,298	34,556	86,566
Pin-Fins (Top Fin)	3,669	5,131	32,859	66,161
Pin-Fins (Channel)	2,023	3,224	43,181	94,649
Microchannel with fin top sintering (Microchannel_Top_Fin)	33,692	49,115	129,787	422,113
Microchannel with fin top sintering (Channel)	5,5	6,72	87,083	182,489
Microchannel with Single Pin-Fins (Micro Channel_Channel_Top_Fin)	3,892	4,649	14,016	24,357
Microchannel with Single Pin-Fins (Pin_Fins_Top_Fin)	12,147	22,301	88,174	347,306
Microchannel with Single Pin-Fins (Channel)	4,009	5,274	31,367	60,198
Microchannel with Double Pin-Fins (Micro Channel_Channel_Fin_Top)	3,155	4,466	31,499	61,952
Microchannel with Double Pin-Fins (Pin_Fins_Top_Fin)	2,781	3,706	33,861	73,499
Microchannel with Double Pin-Fins (Channel)	2,254	3,085	20,057	62,728

3D image of test chips, as measured with a Keyence (R) laser confocal microscope, are shown in Figure 5.10.-5.16.

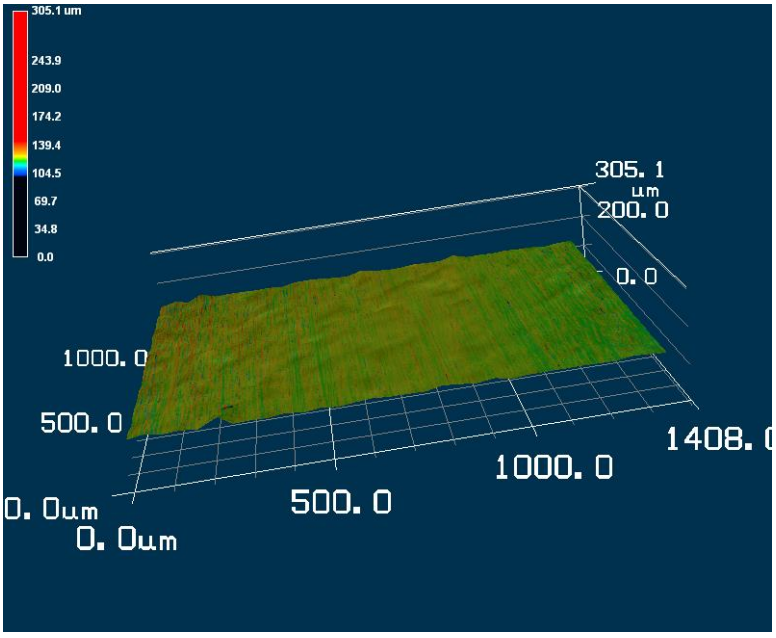

Figure 5.10. A 3D image of the plain test chip

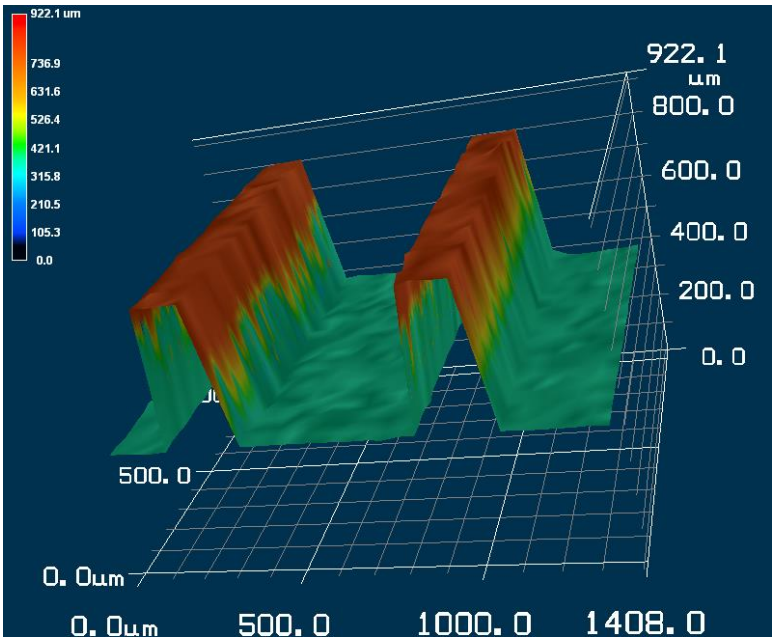

Figure 5.11. A 3D image of the microchannel test chip

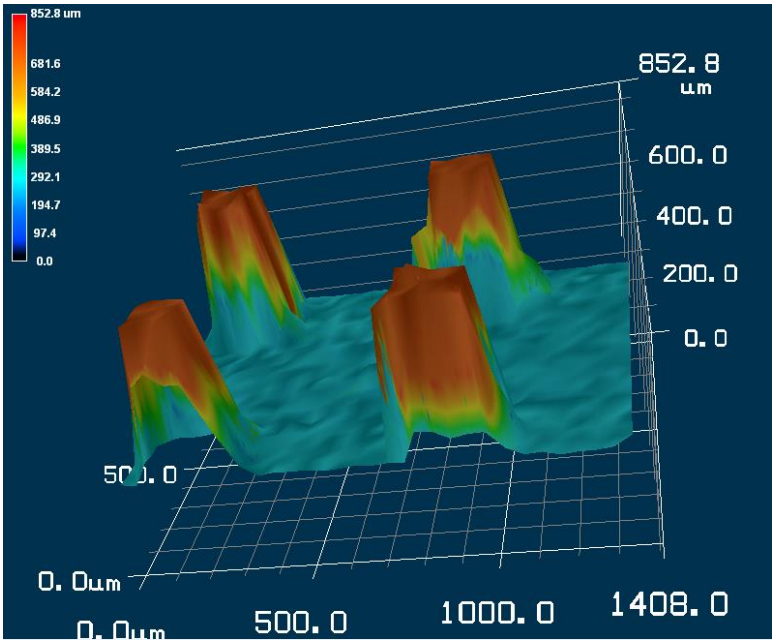

Figure 5.12. A 3D image of the pin-fins test chip

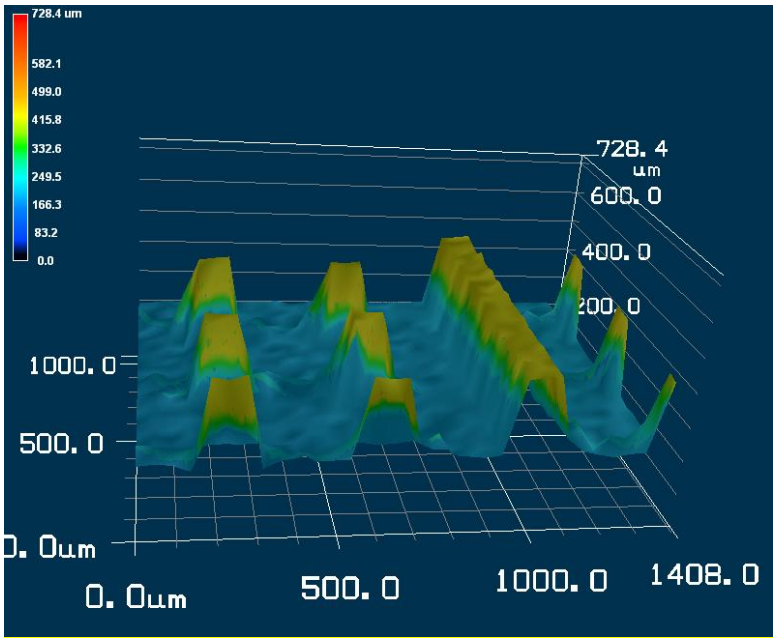

Figure 5.13. A 3D image of the microchannel with double pin-fins test chip

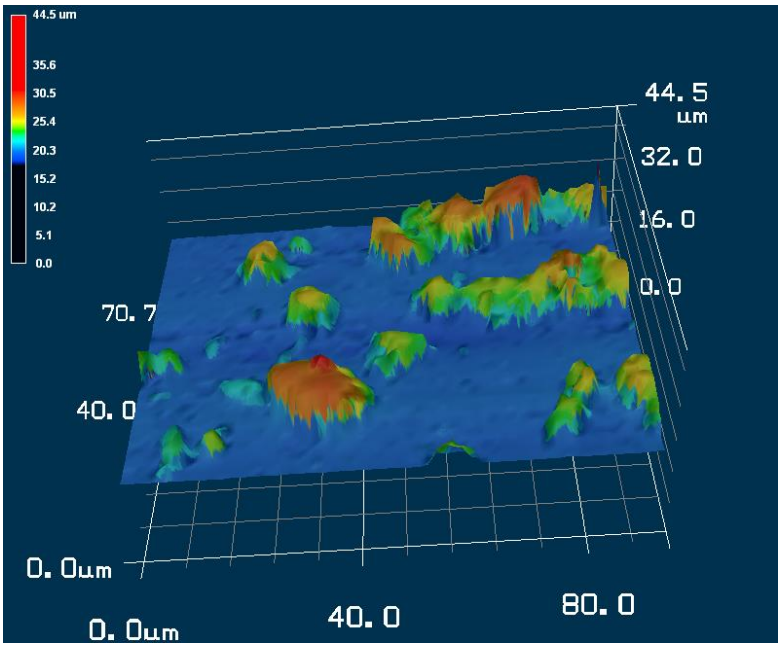

Figure 5.14. A 3D image of sintered test chip

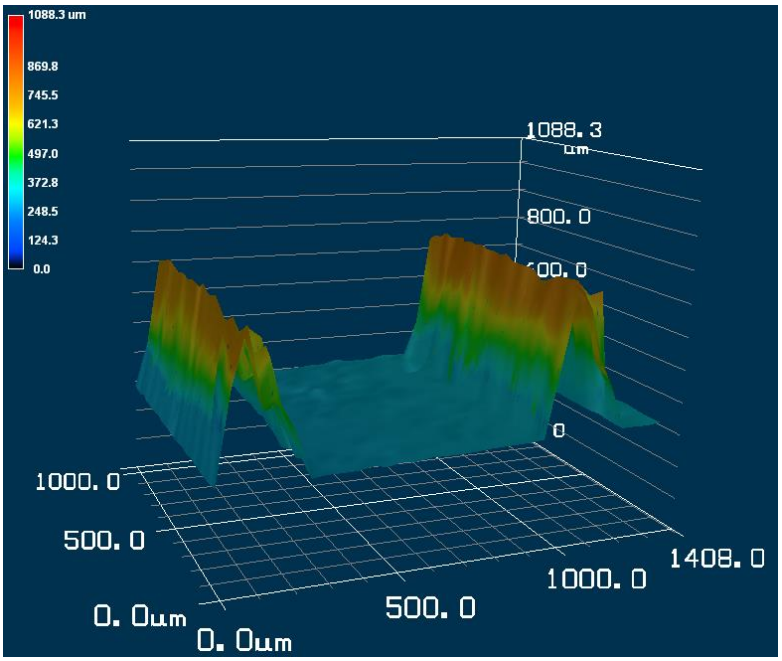

Figure 5.15. 3D image of microchannels with sintered top fins

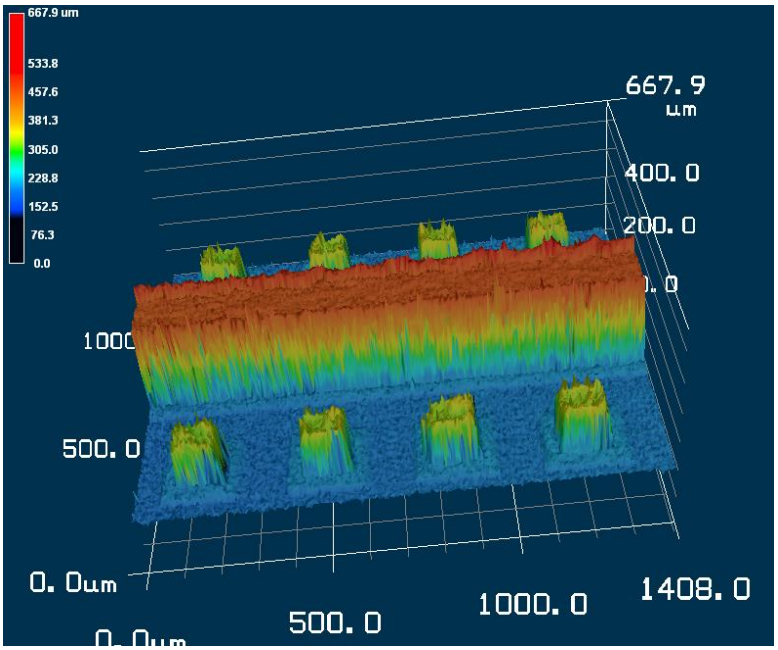

Figure 5.16. A 3D image of microchannels with single pin-fins

5.10. Data Acquisition System and Instrumentation

4 K-type thermocouples are used to measure the temperatures during the pool boiling. The thermocouple readings were recorded with a data acquisition system.

Three thermocouples $T_{1(top)}$, $T_{2(middle)}$, and $T_{3(bottom)}$ are inserted at the bottom of the copper chip and are spaced 3 mm apart. The fourth thermocouple is inserted from the top of the test setup and is used to measure the temperature of the liquid. A data acquisition unit was connected to a personel computer that automatically converted the thermocouples' output voltages into temperatures. All reported values of the surface temperature represent the average over an interval of at least 1 min, after the surface temperature reached equilibrium. In order to log data, a LABVIEW virtual instrument was generated. The temperatures of the thermocouples were recorded as the key data. 5 samples/sec was the sampling rate. The data was taken during 10 seconds. Figure 5.17. shows a screen shot of the LABVIEW 2012. All data was recorded at steady state condition.

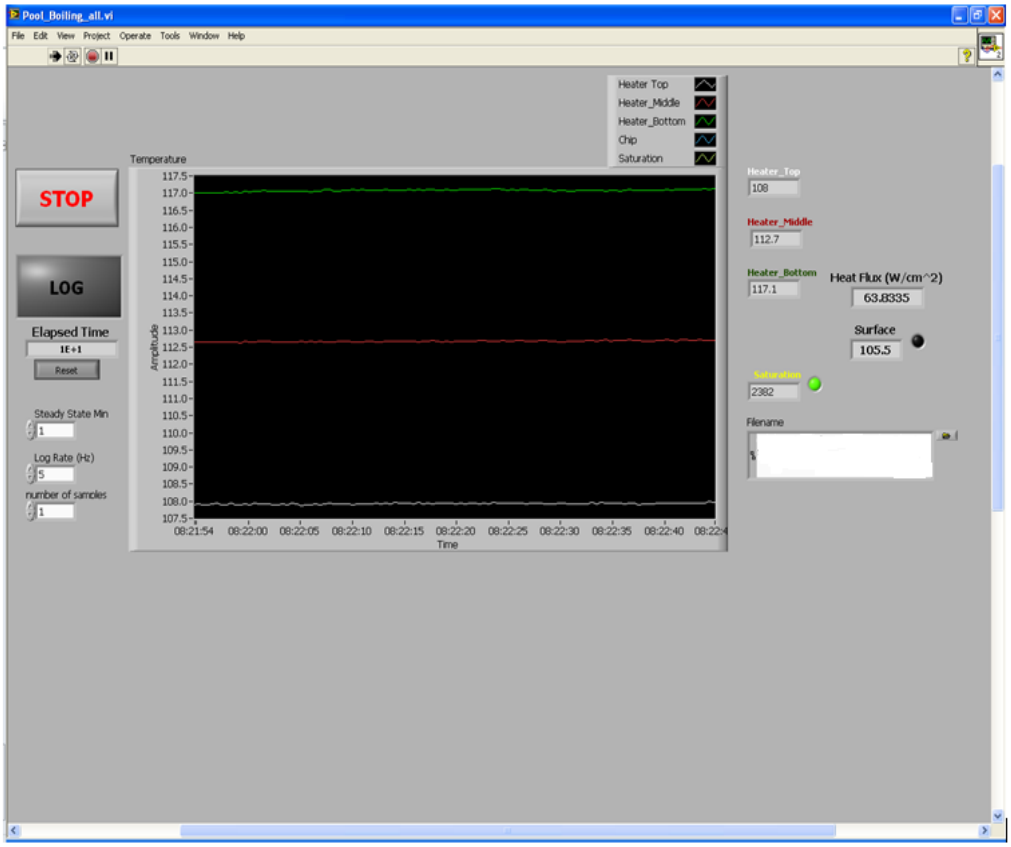

Figure 5.17. LabVIEW virtual instrument

In order to evaluate the boiling data, the heat flux was calculated. The heat flux to the test section computed using the Fourier's 1-D conduction equation

$$q'' = -k_{Cu}\frac{dT}{dx} \tag{5.2}$$

The temperature gradient, dT/dx, was calculated using a three-point backward-difference Taylor series approximation as given below,

$$\frac{dT}{dx} = \frac{3T_1 - 4T_2 + T_3}{2\Delta x} \tag{5.3}$$

Where $T_{1(top)}$, $T_{2(middle)}$ and $T_{3(bottom)}$ were the temperatures measured by thermocouples located at distances Δx=3 mm. The surface temperature of a testing sample, Ts obtained by calculating the heat flux through the copper block. Figure 5.18. shows the locations of the thermocouples on the copper test chip.

The boiling wall temperature was obtained by using Equation (5.4) and is given by,

$$T_{wall} = T_1 - q''(\frac{x_1}{k_{Cu}}) \tag{5.4}$$

The *h* was calculated by dividing the q" by the change in the saturation temperature (ΔT_{sat}), as seen in Equation (5.5)

$$h = \frac{q''}{\Delta T_{sat}} \tag{5.5}$$

The contact resistance has been minimized with the use of grafoil $^{(R)}$ paper between the heater and the chip. Since the heat flux is measured through the heater and the surface temperature is calculated from the thermocouple with the chip, the contact resistance is not used in calculating the heat transfer coefficients.

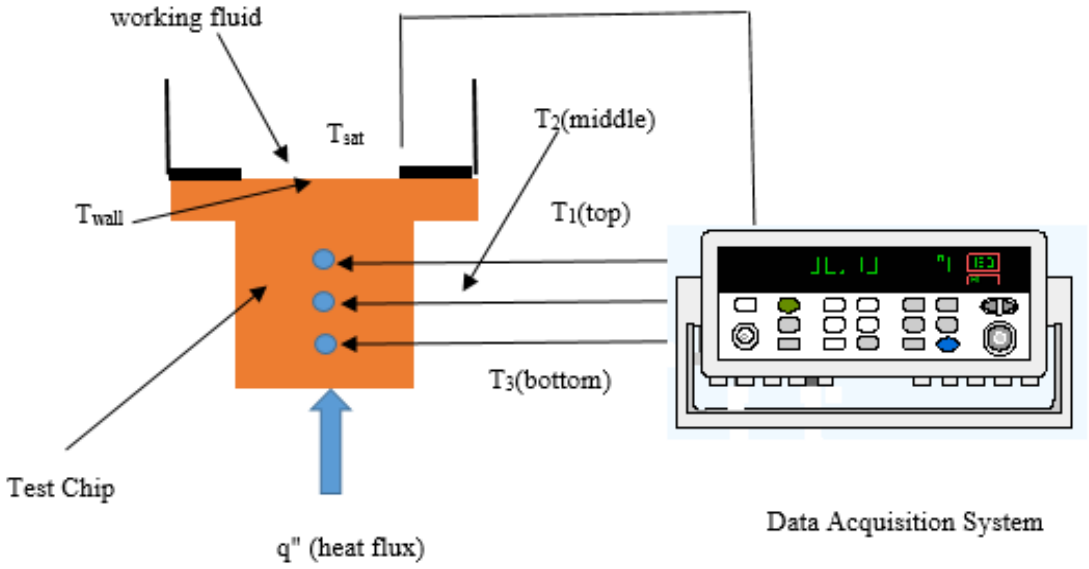

Figure 5.18. Schematic of heater assembly and data acquisition

5.11. An Uncertainity Analysis

An uncertainty analysis is critical to an experimental study in order to have the recorded data closest to its fullest value. In this work, experimental uncertainties were determined by using the Journal of Heat Transfer (JHT)-ASME standard.

The major uncertainties originated as follows; 1) thermocouple calibration accuracy and precision resolution; 2) thermal conductivity of materials being altered under temperature changes and 3) lenght measurements, spacing between thermocouples, and thickness of materials.

There is a certain amount of error that occurs in any experiment studies. Two main errors that arise during experimantation are the bias and precision errors. Bias error (B) is a systematic error that repeatedly occurs as a result system accuracy and it can be obtained by calculating the variation of the equipment calibration. Bias errors are due to errors from calibration. Precision error (P) is the result of the inherent variability of the measurement equipment and it is calculated using a statical analysis of the recorded data with 95% confidence (2 standard deviations). Precision errors are due to sensivity of the testing devices. An uncertainty analysis was conducted

and cumulatively, the bias and precison errors will be calculated using the following equation,

$$U_y = \sqrt{\left(B_y^2 + P_y^2\right)} \tag{5.6}$$

where the U_y is the uncertainity of parameter y. The uncertainties are shown in Table 5.5. q", h, ΔT_{sat} values are calculated using the parameters in Table 5.5.

Table 5.5. The uncertainties in various parameters

Parameter	Value	Units	Precision Uncertainty (U_p)	% Uncertainty
k_{Cu}	391	$W/m^{2o}C$	9	2%
Δx_1	3,00E-03	m	1,00E-04	3%
Δx_2	1,70E-03	m	1,00E-04	6%
$T_{1(Top)}$	Varies	^oC	0,08	Varies
$T_{2(Middle)}$	Varies	^oC	0,11	Varies
$T_{3(Bottom)}$	Varies	^oC	0,08	Varies

Temperature uncertainty was determined through termocouple calibration and 2 times standard deviation of a large sample (100 readings for a given temperature) for precision uncertainty. JHT is not specific about the number of sample readings and mention only a large sample readings (>30) to be taken for precision error measurement. The uncertainties in measurment of temperature and distance between thermocouples propagate an error in evaluation of heat flux.

Uncertainties for calculated values such as heat flux, surface temperature and heat transfer coefficient were determined using the error propagation through partial sums in the equation below:

$$U_p = \sqrt{\sum_{i=1}^{n} \left(\frac{\partial p}{\partial a_i} u_{a_i}\right)^2} \tag{5.7}$$

Where U_p is the uncertainty in the calculated paramater, u_{ai} is the uncertainty of the measured parameter a_i. The uncertainty in the heat flux is expressed as follows.

$$\frac{U_{q''}}{q''} = \sqrt{\left[\left(\frac{U_k}{k_{Cu}}\right)^2 + \left(\frac{3U_{T_1} * k_{Cu}}{\Delta x * q''}\right)^2 + \left(\frac{4U_{T_2} * k_{Cu}}{\Delta x * q''}\right) + \left(\frac{U_{T_3} * k_{Cu}}{\Delta x * q''}\right) + \left(\frac{U_{\Delta x}}{\Delta x}\right)^2\right]} \quad (5.8)$$

The variation of uncertainty with the heat flux for a plain polished copper chip is shown in Figure 5.19. by using Equation (5.8).

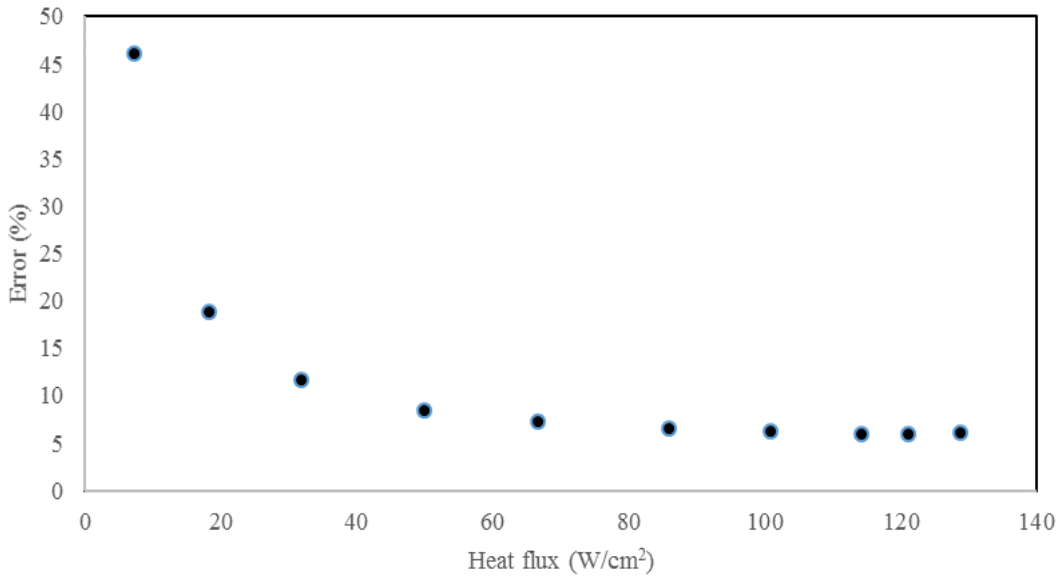

Figure 5.19. Variation of uncertainty with heat flux for plain surface

It is seen from Figure 5.19. at at low heat flux an error of %46 is observed, while at higher heat flux an error of % 6 is observed. At CHF, the main region of interest this value is %6. This is considered to acceptable because the sample performance is evaluated mainly at elevated heat fluxes.

5.12. Heat Loss Study

To ensure that the heat generated from the heater which was transferred to the copper test chip section through 1D conduction, a heat loss study was conducted. According to Fourier's law of conduction, the temperature profile across the copper test chip section is expected to be linear. A heat loss study is shown in Figure 5.20. Figure 5.20. shows a plot of temperature distribution 32 W/cm^2, 86 W/cm^2 and 129 W/cm^2.

It was seen from Figure 5.20. that the profile of the line progression as R^2 was close to 1 at all heat fluxes. This indicated that the test section has a minimal heat loss during the experimental process.

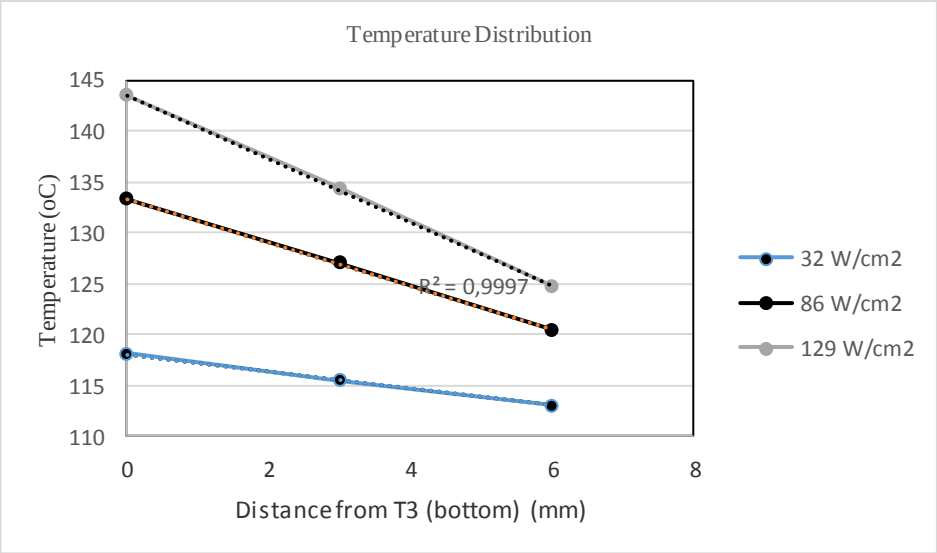

Figure 5.20. Heat loss study showing variation of temperature over the distance for a plain chip

5.13. Contact Angle Measurement

The contact angle measurement was carried out by goniometer (VCA Optima) that takes and analyzes the image of a sessile droplet on a surface. Contact angles have been measured for sessile droplets of water at room temperatures (22 +/- 2 ^{o}C). A droplet with small volume (2-7 µl) was deposited on the surface to ensure that a Cassie drop is formed. In order to have a good reproducibility of the measurements a standard procedure for the experiments has been defined: the volume of the injected drop is chosen as 2µl droplets of DI water by using syringe and the measurements are carried out five seconds after the drop injection in order to reduce evaporation effects. The static contact angle of the fluid of plain copper chip is shown in Figure 5.21. Several measurements are performed for each case and the results are averaged over a large number of the tests.

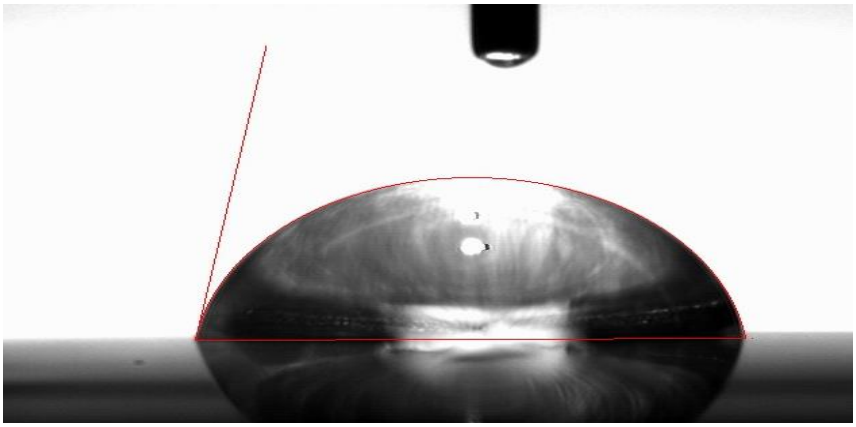

Figure 5.21. Static contact angle of a water droplet on a plain copper surface

The three-phase contact line of the liquid drop was made to advance or retreat by adding or withdrawing a small volume of liquid. The values of the advancing and receding contact angles were measured at room temperature (22 +/- 2 ^{o}C) using a horizontal surface. After test chip was located to the plane, a liquid drop was deposited using a variable syringe. Side-view images of the drops were recorded with a lens and video camera. The event was replayed. At the instant the drop began to move, the image recording was stopped. The advancing contact angle was measured after each volume increment. Receding contact angle measurements were conducted by removing fixed amount water from the droplet in steps. The apparent contact angle was measured after each volume reduction. Advancing and receding contact angles, θa and θr, were measured from these images which are showin in Figure 5.22. and Figure 5.23.

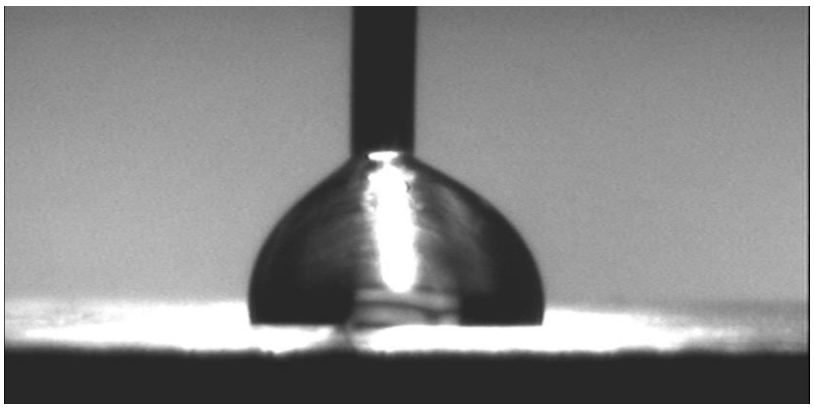

Figure 5.22. Advancing contact angle on a plain copper surface

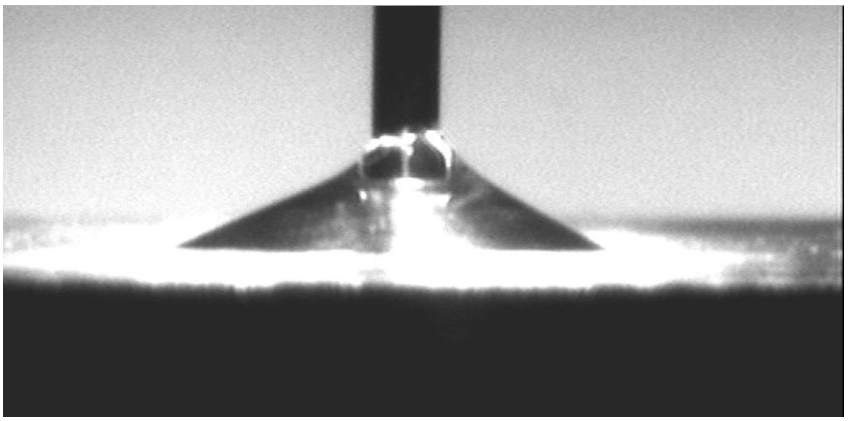

Figure 5.23. Receding contact angle on a plain copper surface

The contact angle measurement list is shown in Table 5.6. Five to eight measurements were done for each volume.

Table 5.6. Contact angle measurement list for the plain copper surface

Surface type	Static contact angle	Advancing contact angle	Receding contact angle	Contact angle hysteresis
	θ (^{o})	θ_a (^{o})	θ_r (^{o})	$\Delta\theta$ (^{o})
Plain	87	80	35	45

5.14. Pool Boiling Experimental Procedure

In order to start the pool boiling experiments, the test chip was mounted into the pool boiling test setup. Distilled water was placed into the water bath and reservoir. When the test chip was mounted, K type thermocouples were placed in the three holes the test chip. In order to degass the distilled water, the auxiliary cartridge heater in the reservoir was turned on and the power supply set up 50V to heat up. When the distilled water was degased and reached the saturation temperature, the chip cartridge heaters were turned on. The voltage and the current were recorded. When the saturation temperature is reached, the auxiliary heater is turned off. The system was allowed to reach stedy state after 15 minutes, then data was recorded for 10 seconds at a rate of 5 data points per second. The temperatures were recorded when the thermocouple fluctutation was not greater than +/- 0.1^o C over a duration of 10 minutes. Then the power supply voltage was increased by 5 V and let the system was reached again steady state condition. The process continued until the system reached at CHF. When the CHF was occurred, the chip cartridge heaters were cut off. Once

the surface reached CHF, the temperature of the test section rises by 200-300 ^{o}C in a matter of few seconds which may result in permanent damage to the test setup.

5.15. Thermocouple Calibration

K-type thermocouples were used. The thermocouples were calibrated over range of operating temperature (25-200 ^{o}C at intervals of 25 ^{o}C). An Omega CL950 hot point$^{(R)}$ Dry Block Calibrator was used to calibrate the thermocouples with an accuracy of +/- 1.5 ^{o}F (0.83 ^{o}C) +/- 1LSD of displayed value. The thermocouples were placed inside the cell at 25 ^{o}C and allowed to reach at steady state condition. The input value and measured temperature were recorded. After the cells temperature was increased by 25 ^{o}C and allowed to reach at steady state condition again. This process was repeated three times up to 200 ^{o}C.

CHAPTER 6. RESULTS AND DISCUSSION

Pool boiling experiments were conducted with distilled water at atmospheric pressure. As a baseline comparison, distilled water was boiled over a plain surface. The seven surfaces fabricated and performed the pool boiling performance. The objective of this study was to observed the effect of porous coating on plain, open microchannels with sintered surface, and open microchannels with pin-fins.

6.1. Plain Chip Test Result as Baseline

A plain chip was first tested in order to provide the baseline and compared the result with the enhanced chip surfaces. The boiling performance of the plain chip was investigated and characterized by a CHF of 128.71 W/cm^2 at a wall superheat of 19.64 ^{o}C, resulting in a heat transfer coefficient (h) 65.53 kW/m^{2o}C.

6.2. Comparison to Literature with the Correlations on Plain Surfaces

Figure 6.1. shows the results comparison between the existing correlations (Zuber, Kutateladze, Kirishenko and Cherniakov, Lienhard-Dhir and Kandlikar correlations) and the experimental result. Kutateladze, Zuber and Lienhard-Dhir correlation predicts a CHF of about 123.69 W/cm^2, 101.27 W/cm^2, and 115.19 W/cm^2, respectively. These predictions overestimates the measured results for the plain test chip in the present experiment. This discrepancy can be attributed to the fact that these correlations does not take into account the surface wettability which has significiant effects on the CHF. Using Kandlikar's correletion, the CHF was predicted to be 126.32 W/cm^2 and agreed extremely well with the experimental result. For Kandlikar correlation, the dynamic receding contact angle of water/copper system were taken as 35 deg. It can be seen from Figure 6.1. that the correlations

results are quite good compare with the experimental result except Kirishenko and Cherniakov which predict the CHF as 86.00 W/cm^2.

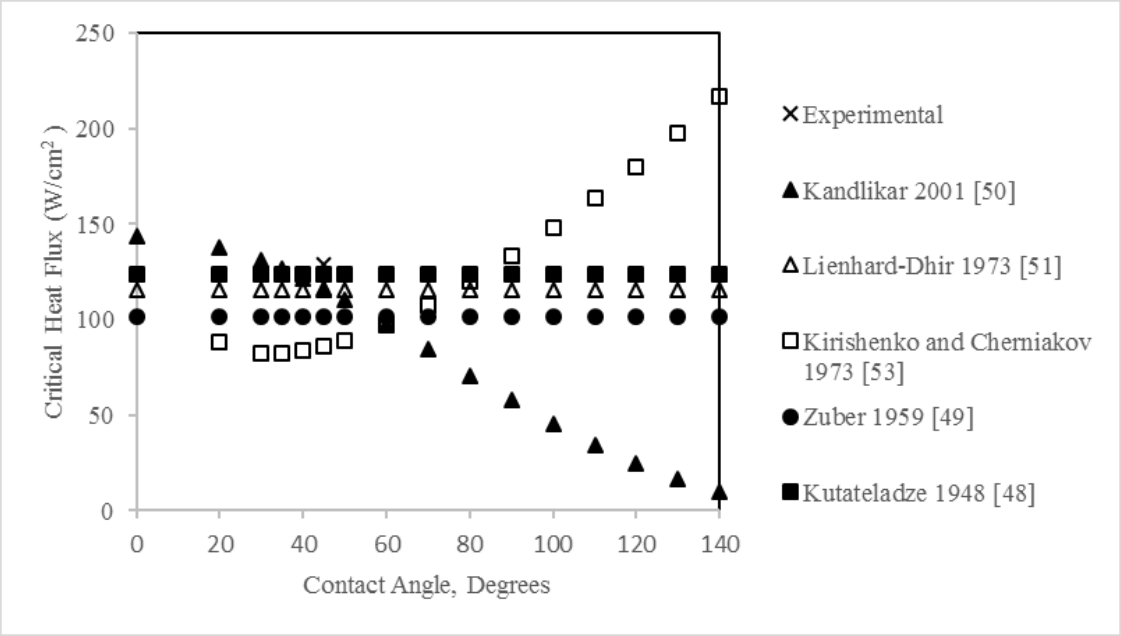

Figure 6.1. Comparison of critical heat flux result with existing correlations on a plain surface.

6.3. Comparison to Literature with the Test Results on Plain Surfaces

Figure 6.2. shows the plain copper chip data which was compared the experimental results which were taken from the literature [24, 36, 56-59, 61-63].The plain copper chip has a boiling curve that shows an early onset of nucleation, has a higher heat transfer than the plain surfaces for most surface temperatures. The plain chip used for this study has an average of roughness of 2.42 μm, which could be the contributing factor to the higher heat transfer coefficients. A CHF occurred on the plain copper chip at 128.71 W/cm^2 at a wall superheat of 19.64 ^{o}C. The maxiumum heat transfer coefficient of 65.51 kW/m^{2o}C occured at CHF. The results obtained were in good agreement with both theoretical and previous experimental results [24, 36, 56-59, 61-63].

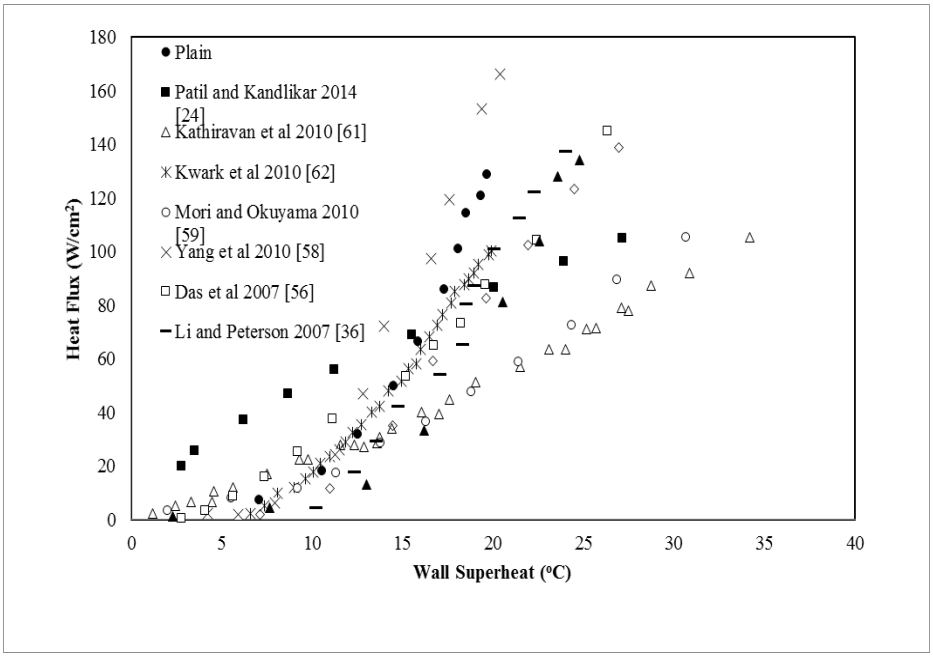

Figure 6.2. Plain surface data compared to data from literature [24, 36, 56-59, 61-63]

6.4. Comparison between Plain Surface and Plain with Sintering

Figure 6.3 shows heat flux comparison between plain surface and plain with sintering. A CHF of 128.71 W/cm^2 at a wall superheat of 19.64 ºC was reached with the plain test chip. The plain with sintered chip reached a CHF of 179.73 W/cm^2 at 13.25 ºC. Plain with sintering represents an enhancement of %39.63 compared to a plain copper test chip.

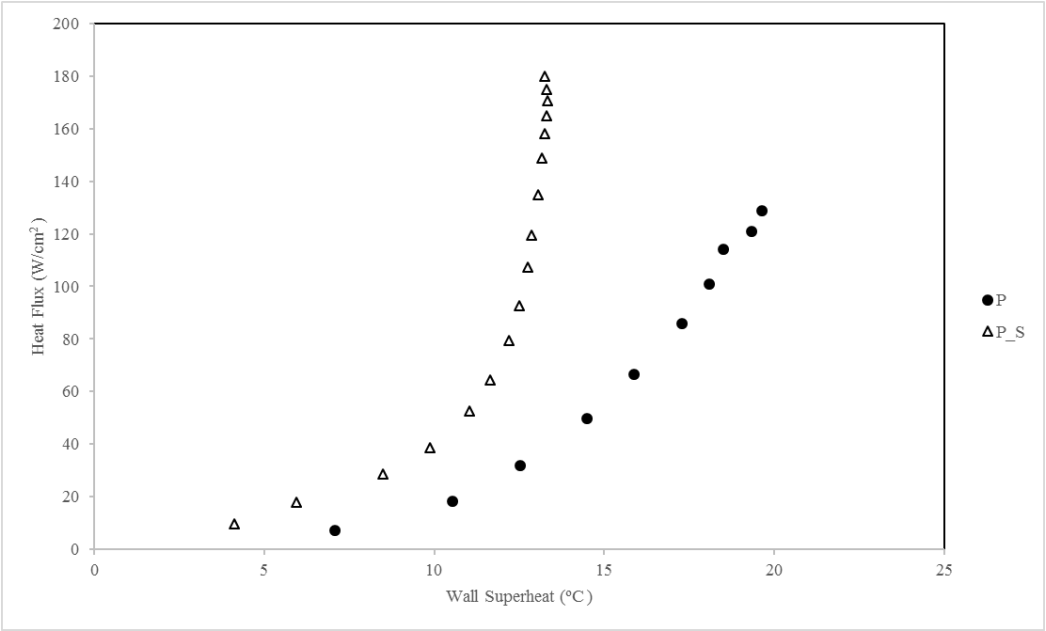

Figure 6.3. Heat flux comparison between plain surface and plain with sintering

Figure 6.4 shows heat transfer coefficent vs. heat flux comparison between plain surface and plain with sintering. The HTC reported in this study was 65.514 $kW/m^{2o}C$ for a plain copper test chip. The HTC reported for plain with sintering was 135.64 $kW/m^{2o}C$ at a heat flux of 179.73 W/cm^2. Plain with sintering represents an enhancement of %107.04 compared to a plain copper test chip.

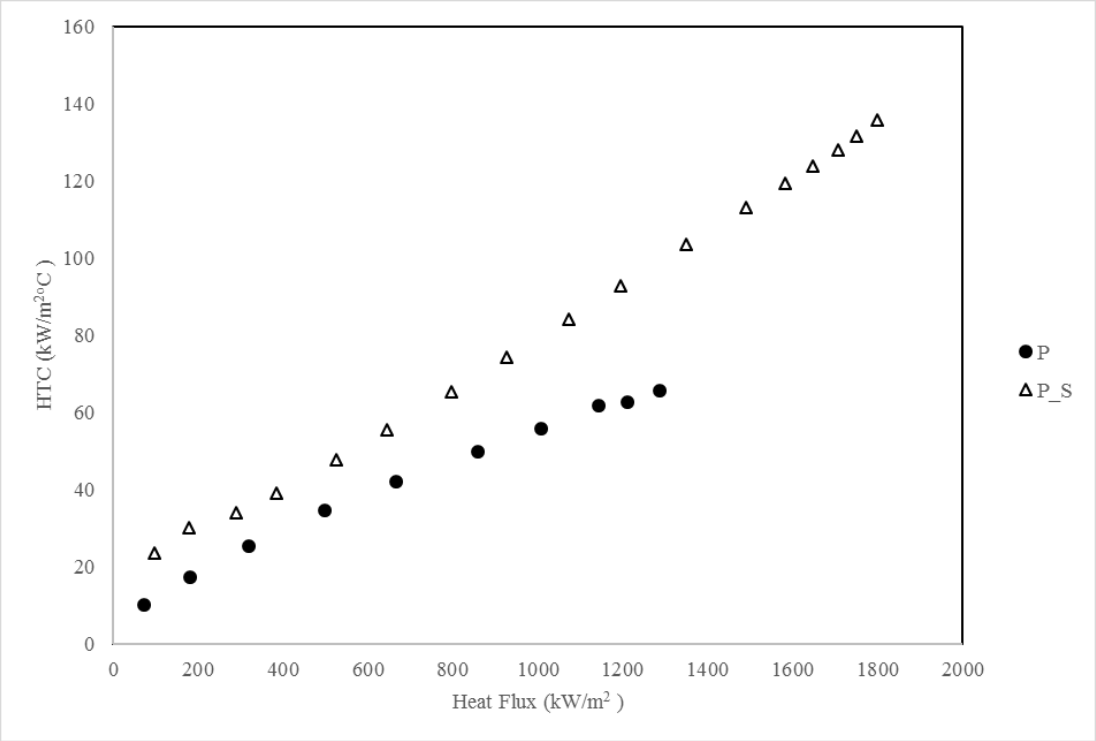

Figure 6.4. Heat transfer coefficent vs. heat flux comparison between plain surface and plain with sintering

6.5. Comparison between Plain Surface and Microchannel

Figure 6.5 shows heat flux comparison between plain surface and plain with sintering. A CHF of 128.71 W/cm^2 at a wall superheat of 19.64 ^{o}C was reached with the plain test chip. Microchannel reached a CHF of 203.03 W/cm^2 at 15.66 ^{o}C. Microchannel represents an enhancement of %57.73 compared to a plain copper test chip.

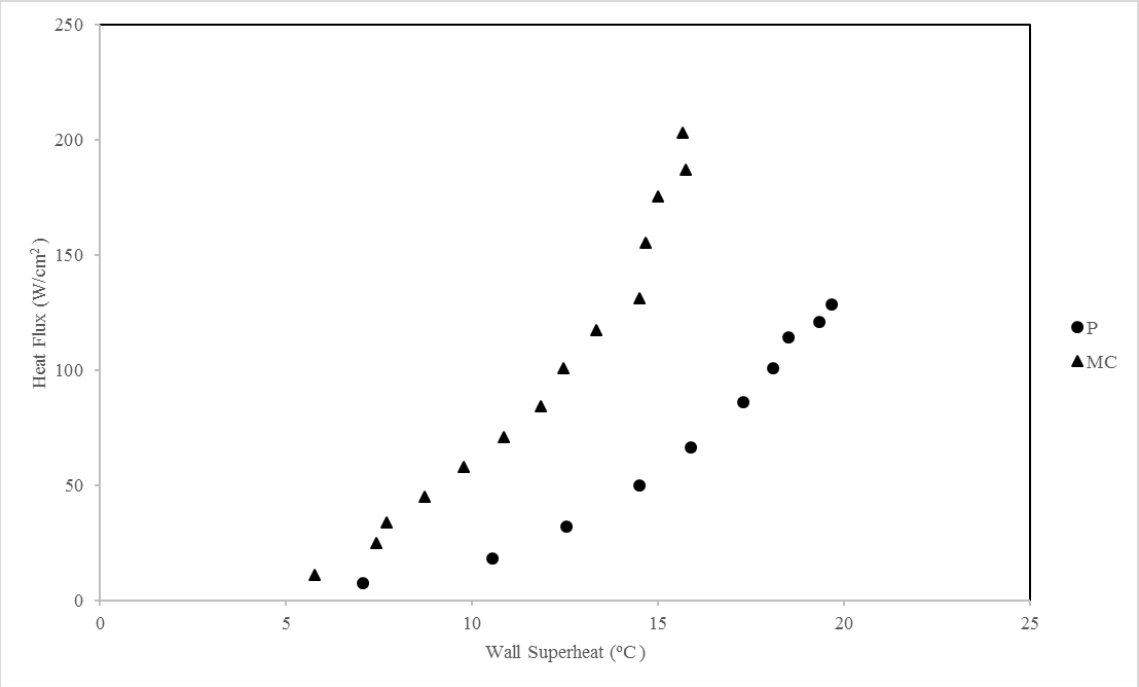

Figure 6.5. Heat flux comparison between plain surface and microchannel

Figure 6.6 shows heat transfer coefficent vs. heat flux comparison between plain surface and plain with sintering. The HTC reported in this study was 65.514 kW/m^{2o}C for a plain copper test chip. The HTC reported for microchannel was 129.61 kW/m^{2o}C at a heat flux of 203.03 W/cm^2. Microchannel represents an enhancement of %97.84 compared to a plain copper test chip.

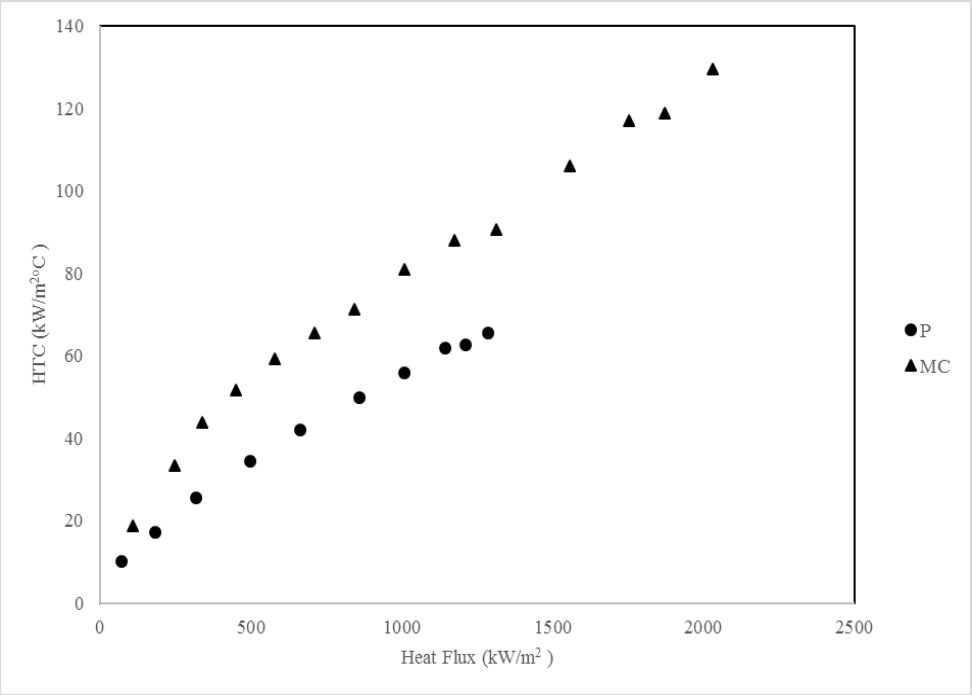

Figure 6.6. Heat transfer coefficent vs. heat flux comparison between plain surface and microchannel

6.6. Comparison Between Plain surface and Pin Fins

Figure 6.7. shows heat flux comparison between plain surface and plain with sintering. A CHF of 128.71 W/cm^2 at a wall superheat of 19.64 ºC was reached with the plain test chip. Pin fins reached a CHF of 243.75 W/cm^2 at 15.46 ºC. Pin fins represents an enhancement of %89.37 compared to a plain copper test chip.

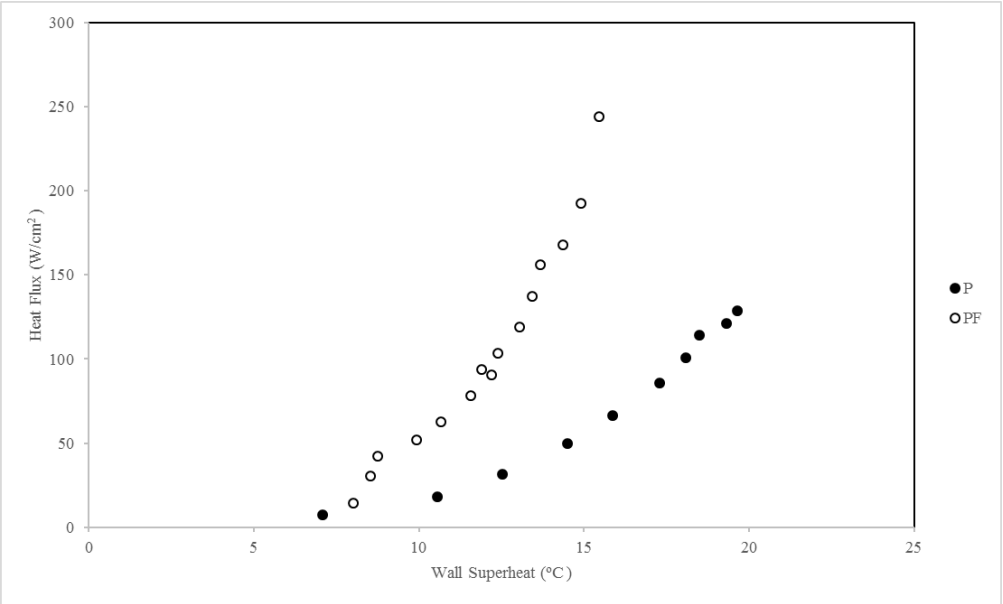

Figure 6.7. Heat flux comparison between plain surface and pin fins

Figure 6.8. shows heat transfer coefficent vs. heat flux comparison between plain surface and plain with sintering. The HTC reported in this study was 65.514 kW/m^{2o}C for a plain copper test chip. The HTC reported for pin fins was 157.67 kW/m^{2o}C at a heat flux of 243.75 W/cm^2. Pin fins represents an enhancement of %140.67 compared to a plain copper test chip.

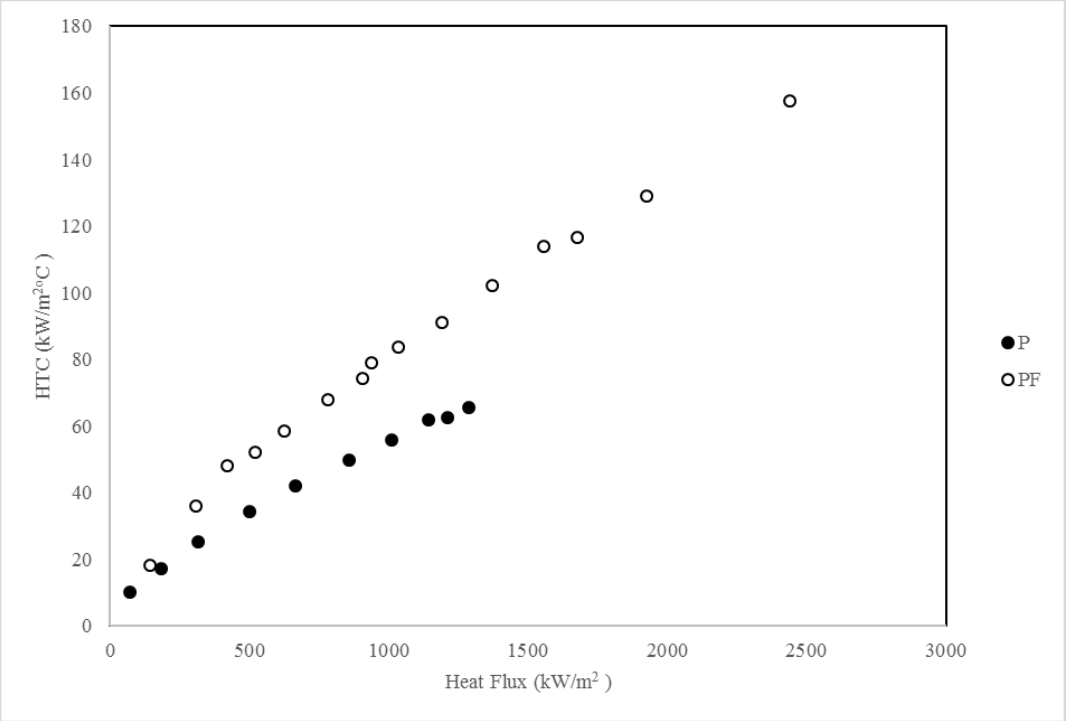

Figure 6.8. Heat transfer coefficent vs. heat flux comparison between plain surface and pin fins

6.7. Comparison between Plain Surface and Microchannel with Sintered Fin Tops

Figure 6.9. shows heat flux comparison between plain surface and plain with sintering. A CHF of 128.71 W/cm^2 at a wall superheat of 19.64 ^{o}C was reached with the plain test chip. Microchannel with sintered fin tops reached a CHF of 214.19 W/cm^2 at 14.30 ^{o}C. Microchannel with sintered fin tops represents an enhancement of % 66.40 compared to a plain copper test chip.

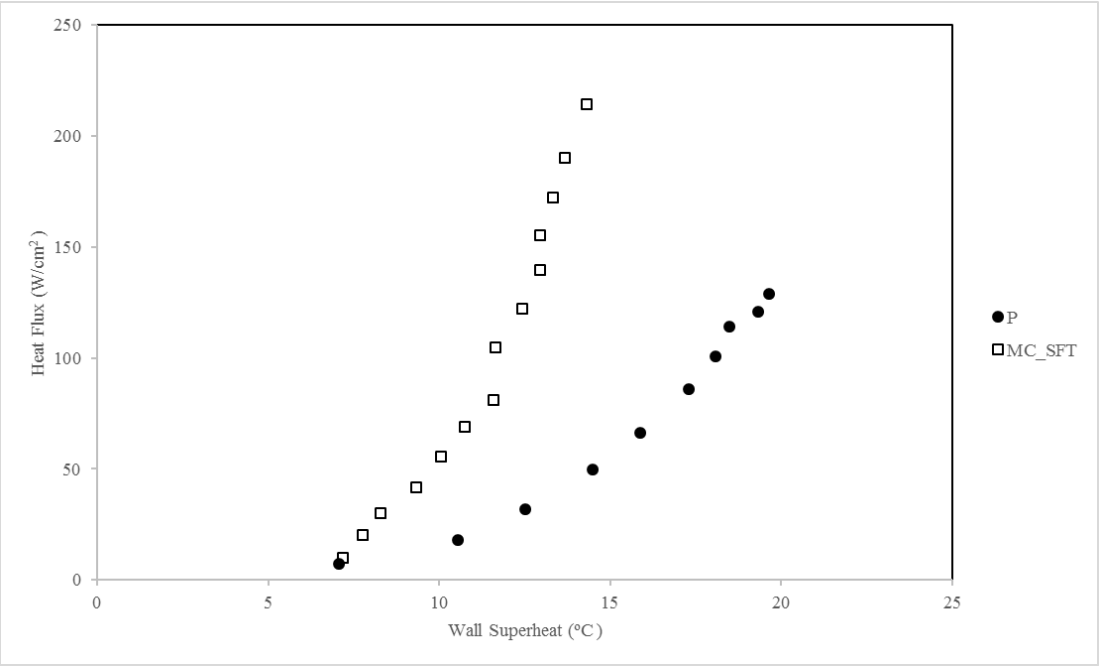

Figure 6.9. Heat flux comparison between plain surface and microchannel with sintered fin tops

Figure 6.10. shows heat transfer coefficent vs. heat flux comparison between plain surface and plain with sintering. The HTC reported in this study was 65.514 kW/m^{2o}C for a plain copper test chip. The HTC reported for microchannel with sintered fin tops was 149.80 kW/m^{2o}C at a heat flux of 214.19 W/cm^2. Microchannel with sintered fin tops represents an enhancement of %128.65 compared to a plain copper test chip.

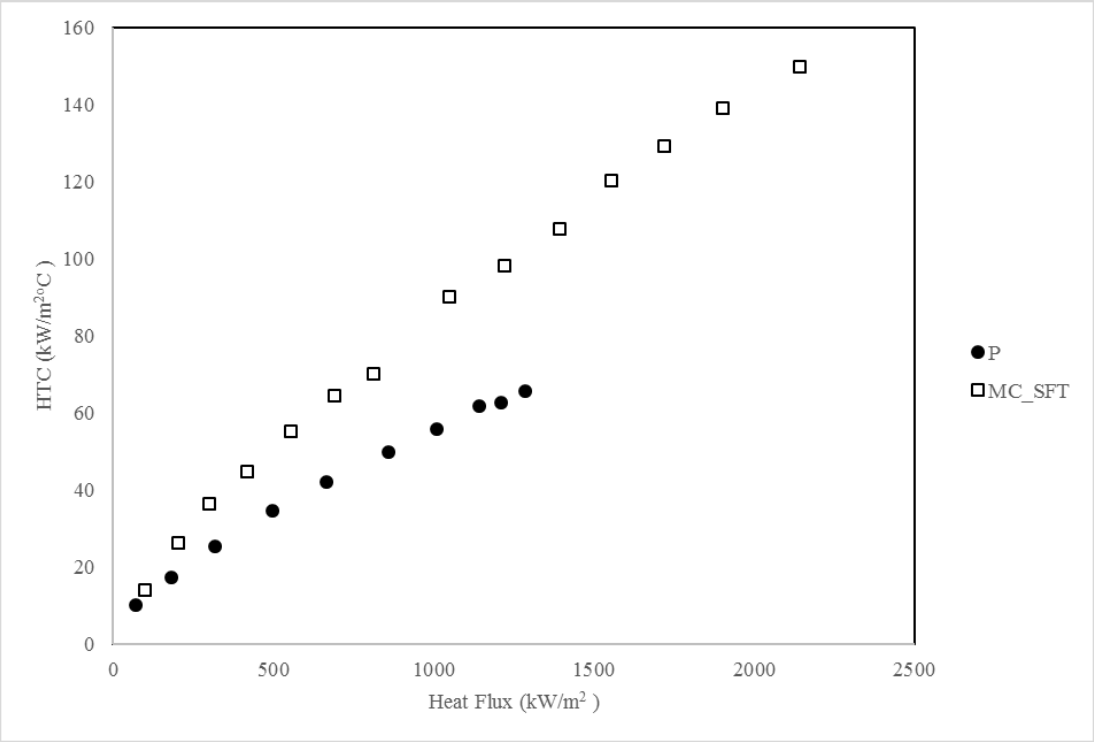

Figure 6.10. Heat transfer coefficent vs. heat flux comparison between plain surface and microchannel with sintered pin tops

6.8. Comparison between Plain Surface and Microchannel with Single Pin-Fins

Figure 6.11. shows heat flux comparison between plain surface and plain with sintering. A CHF of 128.71 W/cm^2 at a wall superheat of 19.64 ^{o}C was reached with the plain test chip. Microchannel with single pin fins reached a CHF of 220.91 W/cm^2 at 13.78 ^{o}C. Microchannel with single pin fins represents an enhancement of % 71.62 compared to a plain copper test chip.

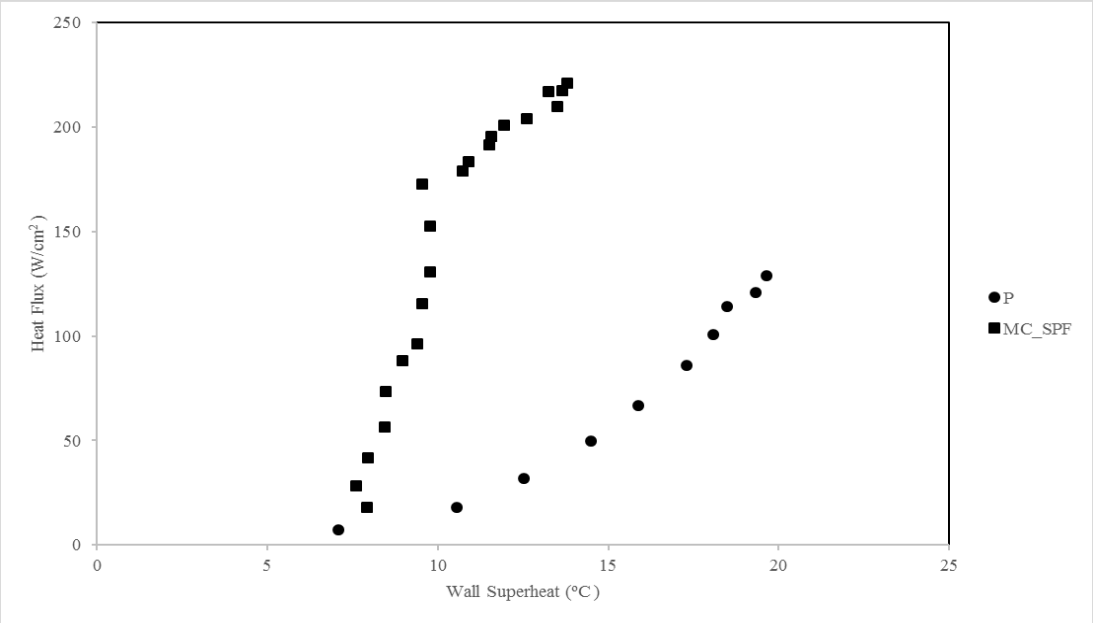

Figure 6.11. Heat flux comparison between plain surface and microchannel with single pin fins

Figure 6.12. shows heat transfer coefficent vs. heat flux comparison between plain surface and plain with sintering. The HTC reported in this study was 65.514 kW/m^{2o}C for a plain copper test chip. The HTC reported for microchannel with single pin fins was 181.03 kW/m^{2o}C at a heat flux of 220.91 W/cm^2. Microchannel with single pin fins represents an enhancement of %176.32 compared to a plain copper test chip.

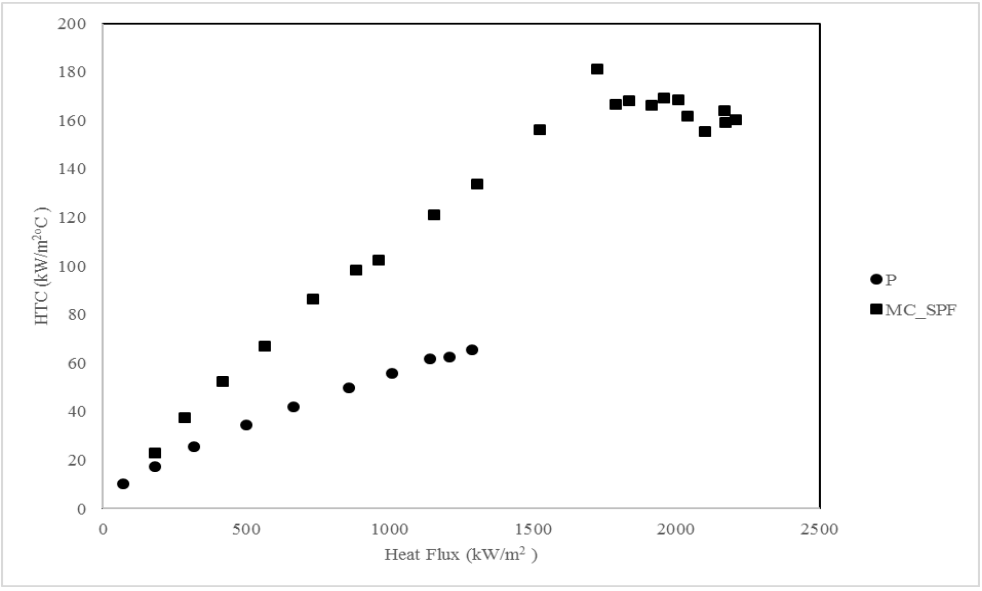

Figure 6.12. Heat transfer coefficent vs. heat flux comparison between plain surface and microchannel with single pin fins
.

6.9. Comparison between Plain Surface and Microchannel with Double Pin Fins

Figure 6.13. shows heat flux comparison between plain surface and plain with sintering. A CHF of 128.71 W/cm^2 at a wall superheat of 19.64 ^{o}C was reached with the plain test chip. Microchannel with double pin fins reached a CHF of 204.34 W/cm^2 at 13.49 ^{o}C. Microchannel with double pin fins represents an enhancement of % 58.75 compared to a plain copper test chip.

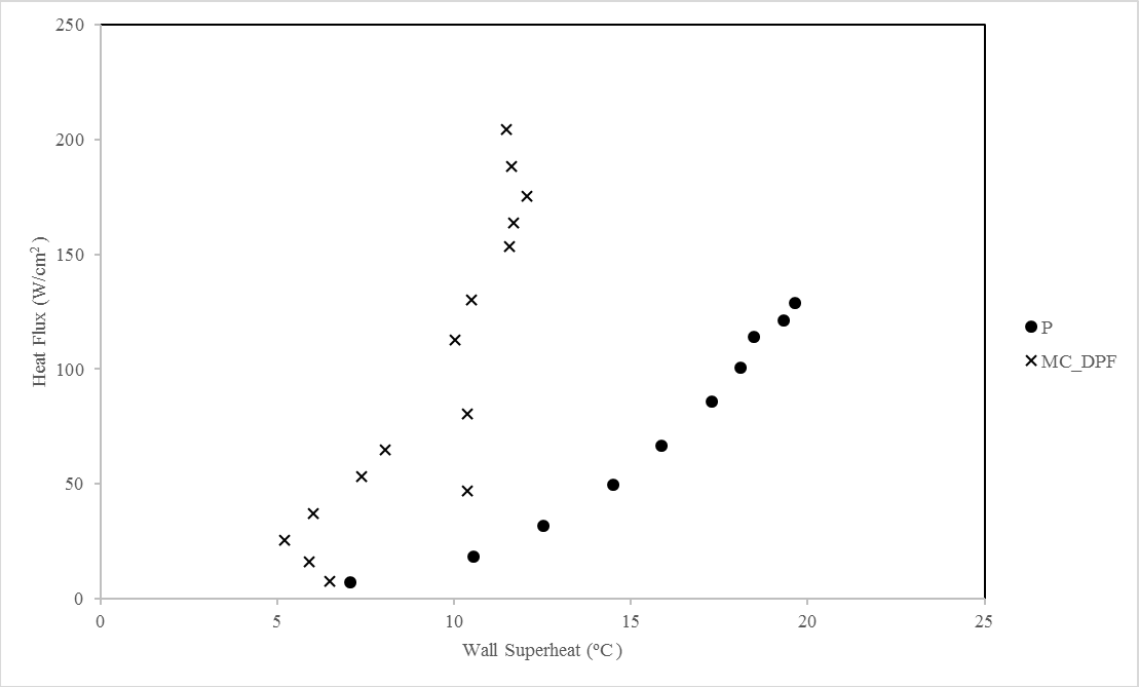

Figure 6.13. Heat flux comparison between plain surface and microchannel with double pin fins

Figure 6.14. shows heat transfer coefficent vs. heat flux comparison between plain surface and microchannel with double pin fins. The HTC reported in this study was 65.514 kW/m^{2o}C for a plain copper test chip. The HTC reported for microchannel with double pin fins was 177.83 kW/m^{2o}C at a heat flux of 204.34 W/cm^2. Microchannel with double pin fins represents an enhancement of %171.44 compared to a plain copper test chip.

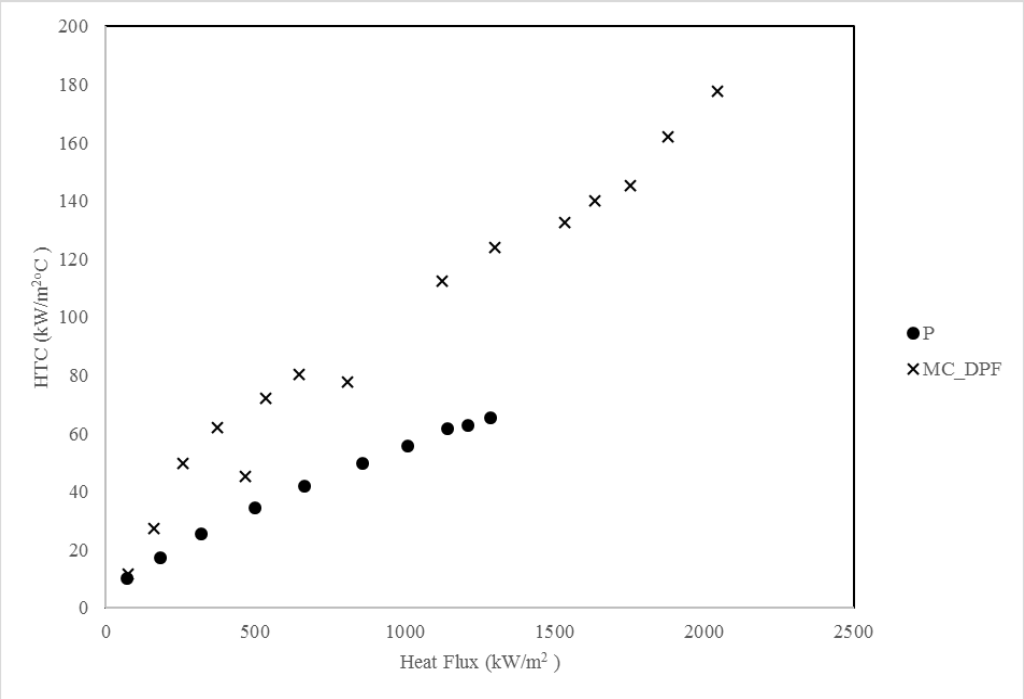

Figure 6.14. Heat transfer coefficent vs. heat flux comparison between plain surface and microchannel with double pin fins

6.10. Test Results Comparison

Figure 6.15. shows the pool boiling curves for the test chips. Heat flux was plotted in units of W/cm^2 which is commonly used in electronic cooling application. The maximum heat flux and the wall temperature were two key parameters which presented. To serve as a baseline for enhancement comparisions, plain copper test chip was tested for its boiling performance. A CHF of 128.71 W/cm^2 at a wall superheat of 19.64 ^{o}C was reached with the plain test chip. The plain with sintered chip reached a CHF of 179.73 W/cm^2 at 13.25 ^{o}C. Microchannel chip reached a CHF of 203.03 W/cm^2 at 15.66 ^{o}C. The pin fins chip reached a CHF of 243.75 W/cm^2 at 15.46 ^{o}C. Microchannel with sintered fin tops reached a CHF of 214.19 W/cm^2 at 14.30 ^{o}C wall superheat. Microchannel with single pin-fins reached a CHF of 220.91 W/cm^2 at 13.78 ^{o}C. Microchannel with double pin-fins reached a CHF of 204.34 W/cm^2 at 11.94 ^{o}C. At lower heat fluxes all copper test chips shows significant enhancement over a plain chip. At higher heat flux, the copper test chips with pin-fins surface performed the best. The highest heat flux reported in this study was 243.75 W/m^2 for pin-fins surface representing an enhancement of %89.37 compared to a plain copper test chip.

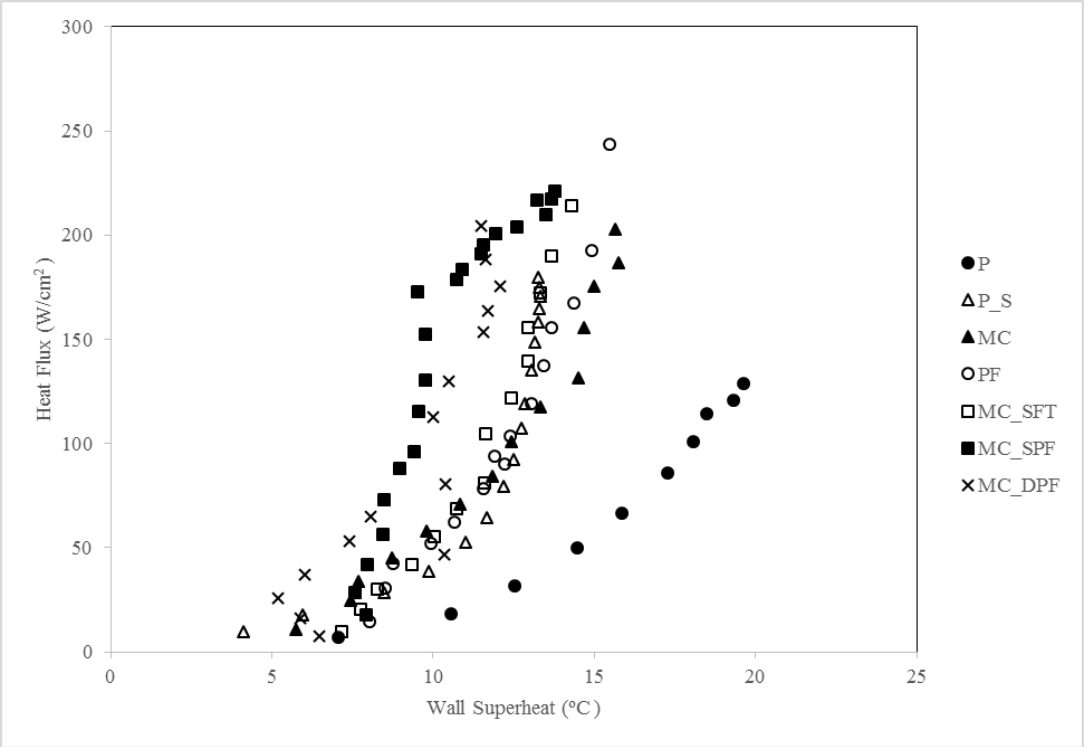

Figure 6.15. Pool boiling curves for the test samples

Using the heat transfer coefficient provides a more quantitative way to compare the heat transfer performance. Figure 6.16. shows the variation of HTC with the heat flux. The general trend indicated that HTC increased with increasing heat fluxes. The lowest HTC reported in this study was 65.514 kW/m^{2o}C for a plain copper test chip. The highest HTC reported in this study was 181.03 kW/m^{2o}C at a heat flux of 172.61 W/m^2 for microchannel with single pin-fins representing an enhancement of %176.32 compared to a plain copper test chip. It can be concluded that pin-fins and sintered surface over microchannels had a significant role to play in enhancing the boiling performance by providing additional heat transfer surface area and also acting as liquid feed conduits to the nucleation sites.

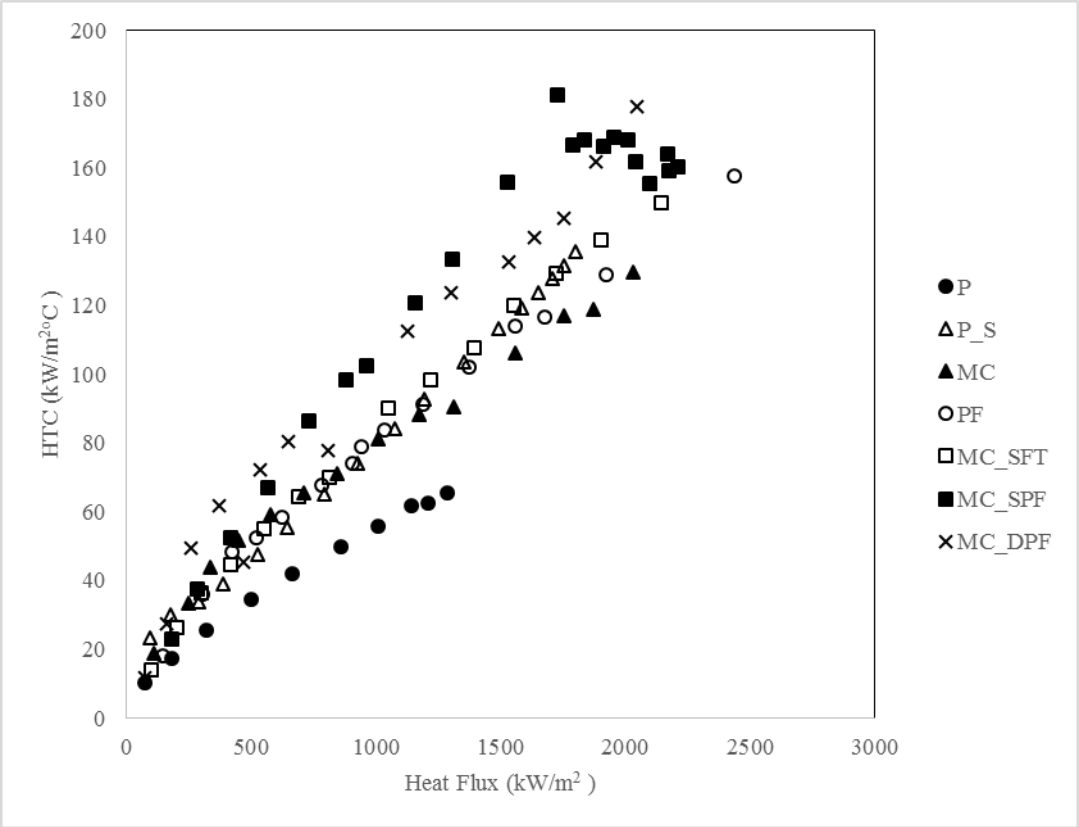

Figure 6.16. Heat transfer performance of the samples

Table 6.1. shows the enhancement summary compared to a plain test chip. It was from Table 6.1. that the highest heat flux enhancement was reached with pin-fins. On the other hand, the highest heat transfer coefficient was reached with microchannels with single pin-fins because of a low wall superheat.

Table 6.1. The enhancement summary

Test sample	Name	Type of surface	Wall Superheat ΔT_{sat} °C	Heat Flux q'' (W/cm^2)	Heat Transfer Coefficient h (kW/m^2°C)	Enhanced Heat Flux %	Enhanced Heat Transfer Coefficient %
1	P	Plain	19.65	128.72	65.51	Baseline	Baseline
2	P_S	Plain with Sintered	13.25	179.73	135.64	39.63	107.04
3	MC	Microchannel	15.66	203.03	129.61	57.73	97.84
4	MC_SFT	Microchannel with Sintered Fin Tops	14.30	214.19	149.80	66.40	128.65
5	PF	Pin-Fins	15.46	243.75	157.67	89.37	140.67
6	MC_SPF	Microchannel with Single Pin-Fins	13.78	220.91	181.03	71.62	176.32
7	MC_DPF	Microchannel with Double Pin-Fins	11.49	204.34	177.83	58.75	171.44

6.11. Comparison Existing Best Test Result to Literature

The data are compared with the results from other surfaces reported in the literature. Figure 6.17. and Figure 6.18. show the comparison of best performing chip with other enhancements available in the literature. Patil and Kandlikar [41] reported a maximum CHF of 325 W/cm^2 at a wall superheat of 7.3 ^{o}C with fin width= 200 μm, channel width=500 μm and channel depth=400 μm with electrodeposition of microporous surface on fin top. The thickness of deposit is 73.3 μm. Kandlikar [42] used the depth of groove= 200 μm and the corner angle= 60 ^{o}. He reported a record of heat transfer coefficient 629 kW/m^{2o}C at a CHF of 300 W/cm^2 at a wall superheat of 4.8 ^{o}C. Cooke and Kandlikar [21] studied the effect of geometrical parameters of microchannel surfaces. The best performing chip dissipated a heat flux of 233 W/cm^2 at a heat transfer coefficient 269 kW/m^{2}K at wall superheat of 9 ^{o}C with fin width= 230 μm, channel width=375 μm and channel depth=400 μm. Mori and Okuyama [59] used a honeycomb stuctured porous plate. The wall thickness δ_s of the grid, the vapor escape channel width d_v, and the diameter of the honeycomb porous plate are 0.4 mm, 1.3 mm, and 30 mm, respectively. The heat flux was 250 W/cm^2 at a wall superheat of approximately 50 ^{o}C with a honeycomb porous plate for a height of 1.2 mm. Li and Peterson [36] used a sintered wire mesh. The objectives of their investigation were to examine effect of thickness, volumetric porosity, and mesh size of the porous coatings on the boiling performance, characteristics, and the CHF. The CHF was in the range of 325 W/cm^2 but very very high wall superheat in excess of 50 ^{o}C. Jaikumar [64] reported a CHF value of 396 W/cm^2 and a record of heat transfer coefficient 535 kW/m^{2o}C at a wall superheat of 7.4 ^{o}C. The channel width of the test chip was 500 μm with 3 cross-linked microchannels.

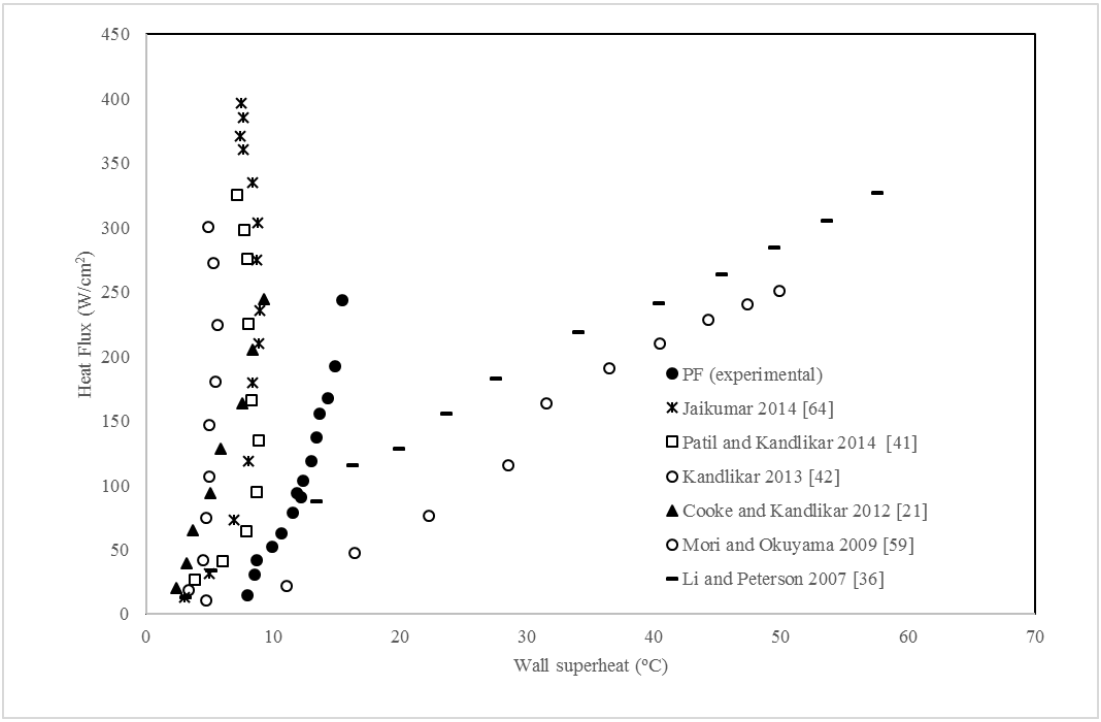

Figure 6.17. Comparison of best performing chip with other enhancements available in the literatüre . . . [21,36,41,42,59,64]

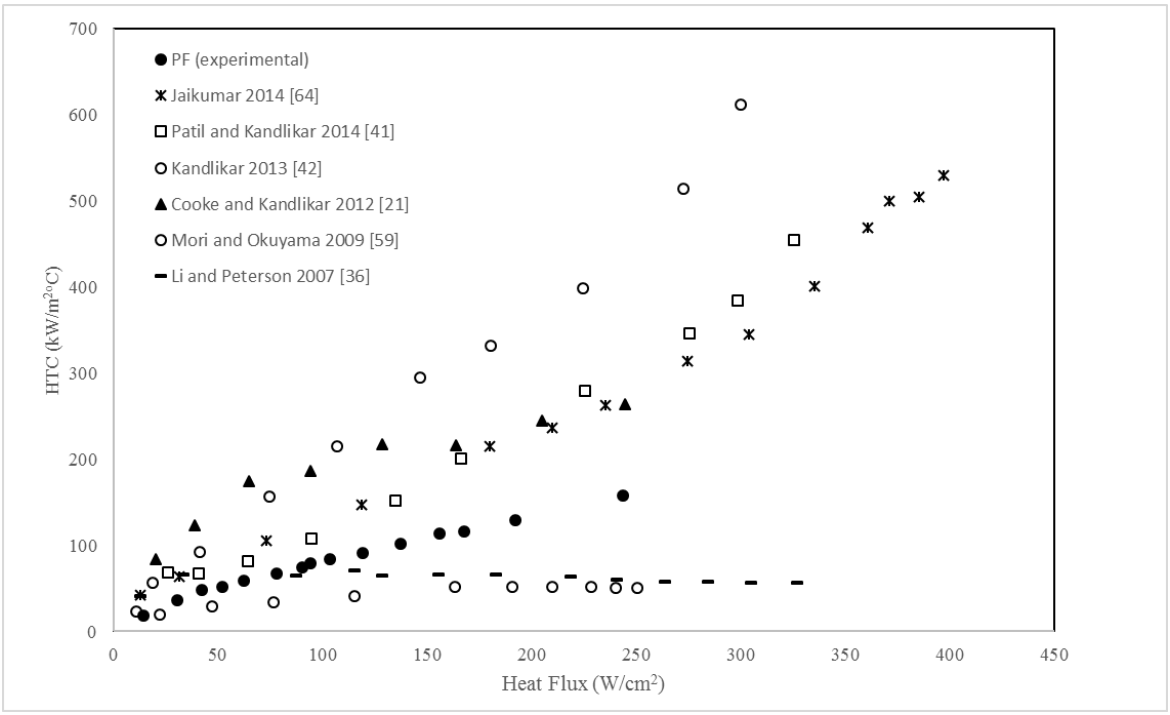

Figure 6.18. Comparison of best performing chip with other enhancements available in the literature [21,36,41, 42,59,64]

CHAPTER 7. CONCLUSION

The fullfillment of the objectives of the experimental investigation manifests itself in a number of ways. A comprehensive literature search was conducted, a new set of experimental data was gathered and published.

Seven different surfaces have been investigated to observe the effect of the surface modifications on boiling heat transfer. These individual surfaces were tested and their boiling characteristics were observed and recorded. In this study, boiling heat transfer by using these surfaces was enhanced but was not utilized to its maximum limits.

Following conclusions are drawn from this study.

1. The pin-fins and microporous surface were investigated with channel width=500 μm, fin width= 200 μm and channel depth= 400 μm. The surface modifications have significantly increased the critical heat heat flux and heat transfer coefficient over a plain copper chip surface. The increased performance for all surfaces can be attributed to area enhancement and availability of additional nucleation sites.

2. It was determined that best performing were pin-fins. The pin-fins were effective in enhancing heat transfer in the nucleate boiling region and increasing CHF.

3. Combining two different enhancement techniques (microchannel with sintered, microchannel with pin-fins) by increasing nucleation activity

through sintered surface coatings and pin-fins in microchannel geometry improved the pool boiling performance.

4. All enhanced surfaces increase the heat transfer compared to a plain copper test chip. All of the enhanced surfaced showed enhancement and when the heat flux was normalized by the surface area of the chip, the pin-fins outperformed the plain chip. This was due to a change in the heat transfer mechanism through bubble and liquid dynamics on the chips, with the channels facilitating liquid supply to the nucleation sites.

5. Additional nucleation sites and bubble pumping mechanism provided by sintered top fins and seperate liquid-vapor pathways provided microchannels to improve the pool boiling performance.

6. High speed images captured at a rate of 4000 frames per second by a high speed camera. It was observed from the high speed camera that nucleation occurred on the top of the microchannels fins. The porous surface provides nucleation sites and the channels acts as water supply.

7. It was seen from the high speed camera that the majority of bubble growth occured fin top of the microchannel but bubbles also nucleated at the bottom of the channel. For microchannels with single pin-fins chips, it was also seen from the high speed camera that the bubble growth occured fin top of pin-fins and nucleate at the bottom of the channel.

8. The best performance was achieved a heat flux of 243.75W/cm^2 at 15.46 ^{o}C at pin-fins chip. This was 1.9 times that of the plain chip for the heat flux.

9. The highest HTC reported in this study was 181.03 kW/m^{2o}C at a heat flux of 172.61 W/m^2 for microchannel with single pin-fins. This was 2.8 times that of the plain for the heat transfer coefficient.

10. Different enhancements such as nanowires, carbon nanotubes (CNTs), etc. could be evaluated for their heat transfer performance over open microchannels.

11. It was conducted experiments on some of the established open microchannel geometries but varied their dimensions to the effect. More importantly, it was identified fins within microchannels and in an open field as a possible enhancement structure. These gave very good results. These can be further embedded with nanoscale features to make them suitable in satellite heat sinks.

CHAPTER 8. RECOMMENDATIONS FOR FUTURE WORK

The present work was done with saturated water as working fluid at atmospheric pressure. Future work needs to be directed at identifying the optimized surfaces with the combination of microchannel, sintered and pin-fins structures. Further investigation can be recommended not only different surface but also different working fluids with compatiable materials and at different pressures. A more in-depth understanding of the underlying microchannel and pin fins are necessary to explain the achieved enhancement. Bubble behavior of all enhanced surfaces should be analyzed to better understand the heat transfer mechanism. While this study explored pool boiling applications, research into the possible enhancements to flow boiling applications would also be recommended.

Using a dielectric fluid or water at reduced pressures with these test chips could show enhancement. All enhanced surfaces can be used as an evaporator section of vapor chamber in order to dissipate the heat flux from the electronic devices which operate a maximum temperature range of 80-85 ^{o}C for space applications.

In order to increase CHF and reduce wall superheat, several studies needs to be focused on the effects of contact angle, thermal properties, dimensions (the channel width, channel depth, fin depth for microchannel; fin height, fin thickness, fin depth for pin-fins), shape, thickness, orientation in space, roughness (surface finish), and microstructure (including shapes, and density of pores that are considered to be vapor bubble generating centers) of the boiling surfaces.

REFERENCES

[1] Lee, H., Park, I., Mudawar, I., Hasan, M.M., Micro-channel evaporator for space applications- 1. experimental pressure drop and heat transfer results for different orientations in earth gravity, International Journal of Heat and Mass Transfer, 77 : 1213-1230, 2014.

[2] Moore, G. E., Cramming more components onto integrated circuits. Electronics 38, 8, 114–117, 1965.

[3] Saenen, T., Modeling a two-phase microchannel electronics cooling system, Dissertation for the degree of Doctor in Engineering, Katholieke Universiteit Leuven, Heverlee, Belgium, January 2013.

[4] Nukiyama, S., The maximum and minimum values of the heat Q transmitted from metal to boiling water under atmospheric pressure, Journal of Japan Society of Mechanical Engineers, 37: p. 367-374, 1934. Transl: Int. J. Heat Mass Transf., vol. 9, no. 12: 1419–1433, Dec. 1966.

[5] Incropera, F.P., Bergman, T.L., Lavine, A.S., And Dewitt, D.P., Fundamentals of heat and mass transfer, John Wiley&Sons, 2011.

[6] Honda, H., Wei, J.J., Enhanced boiling heat transfer from electronic components by use of surface microstructures, Exp. Therm. Fluid Sci., 28 (2-3): 159-169, 2004.

[7] Bergles, A.E., Enhancement of pool boiling. International Journal of Refrigeration, 20(8):545-551, 1997.

[8] Kandlikar, S.G., Grande, W.J., Evolution of microchannel flow passages-thermohydraulic performance and fabrication technology, Heat Transfer Eng., 24 (1): 3-17, 2003.

[9] Kandlikar, S.G., Garimella S., Li D., Colin S., King M.R., Heat transfer and fluid flow minichannels and microchannels, 1st edition, Elsevier Ltd. Oxford, UK, 2006.

[10] Young, T., An essay of the cohesion of fluids, Philosophical Transactions of the Royal Society of London, Vol. 95 (1805): 65-87, 1805.

[11] Feng, X., Jiang, L., Design and creation of superwetting/antiwetting surfaces. Advanced Materials, volume 18, number 23: 3063-3078, 2006.

[12] Good, R.J., Contact angles and the surface free energy of solids, Surface and Colloid Science: 1-29, 1979.

[13] Kandlikar, S.G., Steinke, M.E., Contact angles and ınterface behavior during rapid evapoartion of liquid on a heated surface, International Journal of Heat and Mass Transfer 45: 3771-3780, 2002.

[14] Bergles, A. E., Chyu, M. C., Characteristics of nucleate pool boiling from porous metallic coatings, Adv. Enhanc. Heat Transf.-1981 ASME HTD, 18: 61–71, 1981.

[15] Tuckerman, D.B., Pease, R. F. W., High-performance heat sinking for VLSI, IEEE Electron Device Lett., vol. 2, no. 5: 126–129, 1981.

[16] Baldassari, C., And Marengo, M., Flow boiling in microchannels and microgravity, Progress in Energy and Combustion Science, 39: 1-36, 2013.

[17] Nakayama, W., Daikoku, T., Kuwahara, H., Nakajima, T., Dynamic model of enhanced boiling heat transfer on porous surfaces – part ı: experimental investigation, J. Heat Transfer 102: 445–450, 1980.

[18] Cooke, D., Kandlikar, S. G., Pool boiling heat transfer and bubble dynamics over plain and enhanced microchannels, J. Heat Transfer., 133(5): 052902-1-9, 2011.

[19] Yao, Z., Lu, Y. W., Kandlikar S. G., Effects of nanowires height on pool boiling performance of water on silicon chips, Int. Journal of Thermal Sciences., 1-7**,** 2011.

[20] Yao, Z., Lu, Y.W., Kandlikar, S. G., Direct growth of copper nanowires on a substrate for boling applications, The Institute of Engineering and Technology, Micro & Nano Letters., Vol.6, Iss.7: 563-566, 2011.

[21] Cooke D., Kandlikar S. G., Effect of open microchannel geometry on pool boiling enhancement, Int. Journal of Heat and Mass Transfer., 55: 1004-1013, 2012.

[22] Yao Z., Lu Y. W., Kandlikar, S. G., Fabrication of nanowires on orthogonal surfaces of microchannels and their effect on pool boiling, J.Micromech. Microeng., 22, 115005:1-9, 2012.

[23] Yao, Z., Lu, Y. W., Kandlikar, S. G., Pool boiling heat transfer enhancement through nanostructures on silicon microchanels, Journal of Nanotechnology in Engineering and Medicine., vol.3, 031002-1, 2012.

[24] Patil, C. M., Kandlikar, S. G., Review of the manufacturing techniques for porous surfaces used in enhanced pool boiling, Heat Transfer Engineering., 35(10): 887-902, 2014.

[25] Cooke, D., Experimental study of pool boiling heat transfer enhancement over microchannel surfaces, Thesis, Rochester Institute of Technology, 2011.

[26] Kim, D.E, Yu, D.I, Jerng, D.W, Kim, M.H., Ahn H.S., Review of boiling heat transfer enhancement on micro/nanostructured, Experimental Thermal and Fluid Science 66: 173-196, 2015.

[27] Moita, A.S., Teodori, E., Moreira A.L.N., Influence of surface topography in the boiling mechanisms, International Journal of Heat and Fluid Flow 52: 50-63, 2015

[28] Shojaeian, M., Kosar, A., Pool boiling and flow boiling on micro-and nanostructured surfaces, Experimantal Thermal and Fluid Science 63: 45-73, 2015.

[29] Mudawar, I., Anderson, T.M., Optimization of enhanced surfaces for high flux chip cooling by pool boiling, J. Electron. Packag, vol. 115, no. 1: 89–100, Mar. 1993.

[30] Hübner, P., Künstler, W., Pool boiling heat transfer at finned tubes: influence of surface roughness and shape of the fins, Int. J. Refrig., vol. 20, no. 8: 575–582, Dec. 1997.

[31] Mitrovic, J., Hartmann, F., A new microstructure for pool boiling, Superlattices Microstruct., vol. 35, no. 3–6: 617–628, Mar. 2004.

[32] Honda, H., Wei, J.J., Enhanced boiling heat transfer from electronic components by use of surface microstructures, Exp. Therm. Fluid Sci., vol. 28, no. 2–3: 159–169, Jan.
2004.

[33] Honda, H., Takamatsu, H., Wei, J.J., Enhanced boiling of fc-72 on silicon chips with micro-pin-fins and submicron-scale roughness, Trans. ASME J. Heat Transfer 124: 383–390, 2002.

[34] Honda, H., Takamatsu, H., Wei, J.J., Effect of the size of micro-pin-fin on boiling heat transfer from silicon chips immersed in FC-72, in: Proceedings of 12th International Heat Transfer Conference, Grenoble, France, vol. 4: 75–80, 2002

[35] Guglielmini, G., Misale, M., Schenone, C., Boiling of saturated FC-72 on square pin fin arrays, Int. J. Therm.Sci. 41: 599-608, 2002.

[36] Li, C., Peterson, G. P., Parametric study of pool boiling on horizontal highly conductive microporous coated surfaces, J. Heat Transf.-Trans. Asme, 129(11): 1465–1475, 2007.

[37] Webb, R. L., Nucleate boiling on porous coated surfaces, Heat Transf. Eng., 4(3-4): 71–82, 1981.

[38] Li, C. H., Li, T., Hodgins, P., Hunter, C. N., Voevodin, A. A., Jones, J. G., Peterson, G. P., Comparison study of liquid replenishing impacts on critical heat flux and heat transfer coefficient of nucleate pool boiling on multiscale modulated porous structures, Int. J. Heat Mass Transf., 54(15–16): 3146–3155, 2011.

[39] Cooke, D., Kandlikar, S. G., Effect of open microchannel geometry on pool boiling enhancement, Int. J. Heat Mass Transf., 55(4): 1004–1013, 2012.

[40] Jaikumar, A., Kandlikar, S. G., Ultra-high pool boiling performance and effect of channel width with selectively coated open microchannels, Int. J. Heat Mass Transf., 95: 795–805, 2016.

[41] Patil, C.M., Kandlikar, S.G., Pool boiling enhancement through microporous coatings selectively electrodeposited on fin tops open microchannels, International Journal of Heat and Mass Transfer 79: 816-828, 2014.

[42] Kandlikar, S.G., Controlling bubble motion over heated surface through evaporation momentum force to enhance pool boiling heat transfer, Applied Physics Letter 102: 051611, 2013.

[43] Betz, A. R., Xu, J., Qiu, H., Attinger, D., Do surfaces with mixed hydrophilic and hydrophobic areas enhance pool boiling?, Appl. Phys. Lett., 97(14): 141909, 2010.

[44] Mahamudur Rahman, M., Pollack, J., Mccarthy, M., Increasing boiling heat transfer using low conductivity materials, Sci. Rep., 5: 13145, 2015.

[45] Chu, K.-H., Soo Joung, Y., Enright, R., Buie, C. R., Wang, E. N., Hierarchically structured surfaces for boiling critical heat flux enhancement, Appl. Phys. Lett., 102(15): 151602-151602–4, 2013.

[46] Rohsenow W., A method of correlating heat transfer data for surface boiling of liquids," Trans of the ASME, 74(6), p.969-975, 1952.

[47] Drew, T.B., Mueller, C., Boiling, AIChE; Vol.33: 449-473, 1937.

[48] Kutateladze, S.S., On the transition to film boiling under natural convection, Kotloturbostroenie, vol. 3: 1-10, 1948.

[49] Zuber, N., Hydrodynamic aspects of boiling heat transfer, Ph.D. thesis, Research Laboratory, Los Angeles and Ramo-Wooldridge Corporation, 1959.

[50] Kandlikar, S.G.., A Theoretical Model to Predict Pool Boiling CHF Incorporating Effects of Contact Angle and Orientation, Paper presented in the session on Fundamentals of Critical Heat Flux in Pool and Flow Boiling, in: ASME National Heat Transfer Conference, Pittsburgh, August 2000, ASME J. Heat Transfer 123: 1071– 1079, 2001.

[51] Lienhard, J.H., Dhir, V.K., Hydrodynamic prediction of peak pool boiling heat fluxes from finite bodies, Journal of Heat Transfer, vol. 95, no. 2: 152-158, 1973.

[52] Kutateladze, S. S., A hydrodynamic theory of changes in a boiling process under free convection, Izvestia Akademia Nauk, S.S.S.R., Otdelenie Tekhnicheski Nauk, No. 4: 529, 1951.

[53] Kirishenko, Yu. A., Cherniakov, P. S., Determination of the first critical thermal heat flux on flat heaters, J. Eng. Phys., 20: 699–702, 1973.

[54] Diesselhorst, T., Grigull, U., Hahne, E., Hydrodynamic and surface effects on the peak heat flux in pool boiling, in heat transfer in boiling, E. Hahne, and U. Grigull, eds., Hemisphere Publishing Corporation, Washington, 1977.

[55] Kandlikar, S. G., Steinke, M. E., Contact angle of droplets during spread and recoil after ımpinging on a heated surface, Trans IChemE, 79, Part A: 491–498, 2001.

[56] Das, A. K., Das, P. K., Saha, P., Nucleate boiling of water from plain and structured surfaces, Experimental Thermal and Fluid Science, 31(8): 967-977, 2007.

[57] Takata, Y., Hidaka, S., Cao, J. M., Nakamura, T., Yamamoto, H., Masuda, M., Ito, T., Effect of surface wettability on boiling and evaporation, 30: 209-220, 2005.

[58] Yang, Y., Ji, X., Xu, J., Pool boiling heat transfer on copper foam covers with water as working fluid, International Journal of Thermal Sciences, 49(7): 1227- 1237, 2010.

[60] Li, C., Peterson, G. P., Parametric study of pool boiling on horizontal highly conductive microporous coated surfaces, Journal of Heat Transfer, 129(Compendex): 1465-1475, 2007.

[61] Kathiravan, R., Kumar, R., Gupta A., Chandra R., Preparation and pool boiling characteristics of copper nanofluids over a flat plate heater, International Journal of Heat and Mass Transfer 53: 1673-1681, 2010.

[62] Kwark, S.M., Moreno, G., Kumar, R., Moon, H., You, S.M., Nanocoating characterization in pool boiling heat transfer of pure water, International Journal of Heat and mass Transfer 53: 4579-4587, 2010.

[63] Kim, J.H., Enhancement of pool boiling heat transfer using thermally-conductive microporous coating techniques, PhD, The University of Texas at Arlington, Dec.2006.

[64] Jaıkumar, A., Pool boiling enhancement through improved liquid supply pathways over open microchannels, Thesis, Rochester Institute of Technology, November 2014.

ANNEX

1. Thermocouple Calibration

K-type thermocouples were calibrated over range of operating temperature (25-200 ^{o}C at intervals of 25 ^{o}C) using an Omega CL950 hot point$^{(R)}$ Dry Block Calibrator. All the thermocouples used in the experiment operated in the set range. The below figure shows the calibration curve for one thermocouple. Similar calibration curves were obtained for all thermocouples which used in the experiment. A linear curve fit was applied to the collected points to determine the equation for the thermocouple. The calibration is displayed with R^2 value. This calibration equation values were inputted in the LabVIEW block diagram for temperature measurement.

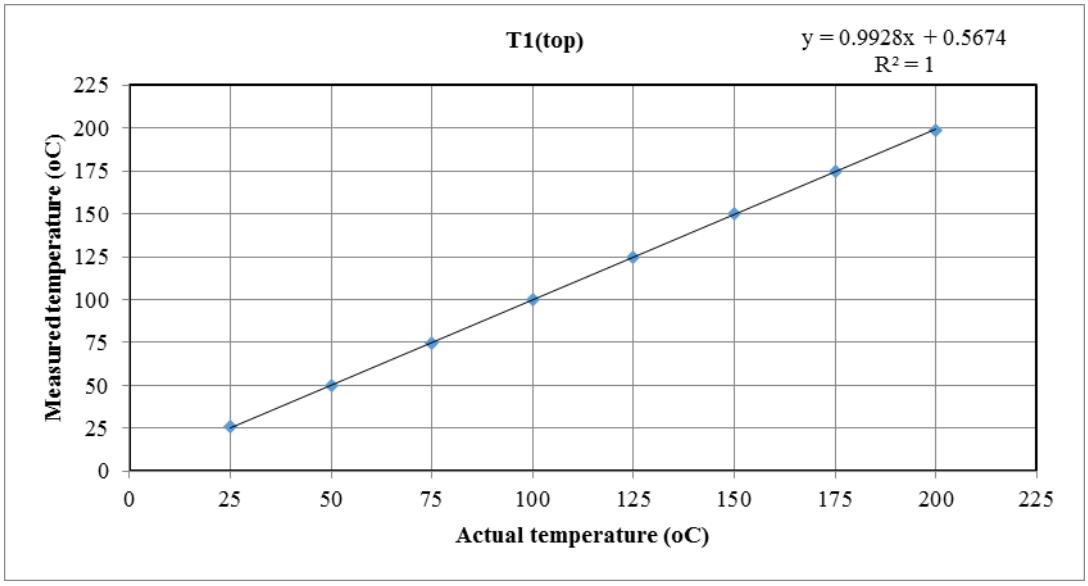

Similar procedure was followed for all thermocouples used. Standard deviation for each thermcouple was also calculated and used in the uncertainty analysis.

2.Uncertainty Calculations

The temperature change along the z-axis is calculated using a 3 point backward Taylor Series approximation as follows.

$$\frac{dT}{dx} = \frac{3T_T - 4T_M + T_B}{2x_1}$$

$$\frac{U_{\frac{dT}{dx}}}{\frac{dT}{dx}} = \sqrt{\frac{\left(\frac{\partial\left(\frac{dT}{dx}\right)}{\partial T_T}\right)^2 * U_{T_T}^2 + \left(\frac{\partial\left(\frac{dT}{dx}\right)}{\partial T_M}\right)^2 * U_{T_M}^2 + \left(\frac{\partial\left(\frac{dT}{dx}\right)}{\partial T_B}\right)^2 * U_{T_B}^2 + \left(\frac{\left(\frac{dT}{dx}\right)}{\partial x_1}\right)^2 * U_{x_1}^2}{\left(\frac{dT}{dx}\right)^2}}$$

$$\frac{\partial\left(\frac{dT}{dx}\right)}{\partial T_T} = \frac{-3}{2x_1} = \frac{3\frac{dT}{dx}}{3T_T - 4T_M + T_B}$$

$$\frac{\partial\left(\frac{dT}{dx}\right)}{\partial T_M} = \frac{-4}{2x_1} = \frac{-4\frac{dT}{dx}}{3T_T - 4T_M + T_B}$$

$$\frac{\partial\left(\frac{dT}{dx}\right)}{\partial T_B} = \frac{1}{2x_1} = \frac{\frac{dT}{dx}}{3T_T - 4T_M + T_B}$$

$$\frac{\partial\left(\frac{dT}{dx}\right)}{\partial x_1} = -\frac{3T_T - 4T_M + T_B}{2x_1^2} = -\frac{\frac{dT}{dx}}{x_1}$$

$$\frac{U_{\frac{dT}{dx}}}{\frac{dT}{dx}}=\sqrt{\frac{\left(\frac{3\frac{dT}{dx}}{3T_T-4T_M+T_B}\right)^2*U_{T_T}^2+\left(\frac{-4\frac{dT}{dx}}{3T_T-4T_M+T_B}\right)^2*U_{T_M}^2+\left(\frac{\frac{dT}{dx}}{3T_T-4T_M+T_B}\right)^2*U_{T_B}^2+\left(-\frac{\frac{dT}{dx}}{x_1}\right)^2*U_{x_1}^2}{\left(\frac{dT}{dx}\right)^2}}$$

$$\frac{U_{\frac{dT}{dx}}}{\frac{dT}{dx}}=\sqrt{\frac{\left(\frac{3\frac{dT}{dx}}{3T_T-4T_M+T_B}\right)^2*U_{T_T}^2+\left(\frac{-4\frac{dT}{dx}}{3T_T-4T_M+T_B}\right)^2*U_{T_M}^2+\left(\frac{\frac{dT}{dx}}{3T_T-4T_M+T_B}\right)^2*U_{T_B}^2+\left(-\frac{\frac{dT}{dx}}{x_1}\right)^2*U_{x_1}^2}{\left(\frac{dT}{dx}\right)^2}}$$

$$\frac{U_{\frac{dT}{dx}}}{\frac{dT}{dx}}=\sqrt{\left(\frac{\left(3*U_{T_T}\right)^2+\left(-4*U_{T_M}\right)^2+\left(U_{T_B}\right)^2}{\left(3T_T-4T_M+T_B\right)^2}\right)+\left(-\frac{U_{x_1}}{x_1}\right)^2}$$

The heat flux is calculated as follows.

$$q''=-k_{Cu}\frac{dT}{dx}$$

$$\frac{U_{q''}}{q''}=\sqrt{\frac{\left(\frac{\partial q''}{\partial k_{Cu}}\right)^2*U_{k_{Cu}}^2+\left(\frac{\partial q''}{\partial\frac{dT}{dx}}\right)^2*U_{\frac{dT}{dx}}^2}{\left(q''\right)^2}}$$

$$\frac{\partial q''}{\partial k_{Cu}}=-\frac{dT}{dx}=\frac{q''}{k_{Cu}}$$

$$\frac{\partial q''}{\partial\frac{dT}{dx}}=-k_{Cu}=\frac{q''}{\frac{dT}{dx}}$$

$$\frac{U_{q''}}{q''}=\sqrt{\frac{\left(\frac{q''}{k_{Cu}}\right)^2*U_{k_{Cu}}^2+\left(\frac{q''}{\frac{dT}{dx}}\right)^2*U_{\frac{dT}{dx}}^2}{\left(q''\right)^2}}$$

$$\frac{U_{q^{"}}}{q^{"}} = \sqrt{\left(\frac{U_{k_{Cu}}}{k_{Cu}}\right)^2 + \left(\frac{U_{\frac{dT}{dx}}}{\frac{dT}{dx}}\right)^2}$$

The chip's wall temperature is calculated as follows.

$$T_w = T_T - q^{"}\frac{x_2}{k_{Cu}}$$

$$\frac{U_{T_w}}{T_w} = \sqrt{\frac{\left(\frac{\partial T_w}{\partial T_T}\right)^2 * U_{T_T}^2 + \left(\frac{\partial T_w}{\partial q^{"}}\right)^2 * U_{q^{"}}^2 + \left(\frac{\partial T_w}{\partial x_2}\right)^2 * U_{x_2}^2 + \left(\frac{\partial T_w}{\partial k_{Cu}}\right)^2 * U_{k_{Cu}}^2}{(T_w)^2}}$$

$$\frac{\partial T_w}{\partial T_T} = 1 = \frac{T_w}{T_w}$$

$$\frac{\partial T_w}{\partial q^{"}} = -\frac{x_2}{k_{Cu}} = -\frac{T_w}{T_w}\frac{x_2}{k_{Cu}}$$

$$\frac{\partial T_w}{\partial x_2} = -\frac{q^{"}}{k_{Cu}} = -\frac{T_w}{T_w}\frac{q^{"}}{k_{Cu}}$$

$$\frac{\partial T_w}{\partial k_{Cu}} = -q^{"}\frac{x_2}{{k_{Cu}}^2} = -\frac{T_w}{T_w}q^{"}\frac{x_2}{{k_{Cu}}^2}$$

$$\frac{U_{T_w}}{T_w} = \sqrt{\frac{\left(\frac{T_w}{T_T}\right)^2 * U_{T_T}^2 + \left(\frac{T_w}{T_w}\frac{x_2}{k_{Cu}}\right)^2 * U_{q^{"}}^2 + \left(\frac{T_w}{T_w}\frac{q^{"}}{k_{Cu}}\right)^2 * U_{x_2}^2 + \left(-\frac{T_w}{T_w}q^{"}\frac{x_2}{k_{Cu}^2}\right)^2 * U_{k_{Cu}}^2}{(T_w)^2}}$$

$$\frac{U_{T_w}}{T_w} = \sqrt{\left(\frac{U_{T_T}}{T_w}\right)^2 + \left(-\frac{U_{q^{"}}}{T_w}\frac{x_2}{k_{Cu}}\right)^2 + \left(-\frac{U_{x_2}}{T_w}\frac{q^{"}}{k_{Cu}}\right)^2 + \left(-\frac{U_{k_{Cu}}}{T_w}\frac{q^{"}x_2}{k_{Cu}^2}\right)^2}$$

The wall superheat is calculated as follows.

$$\Delta T_{sat} = T_w - T_{sat}$$

$$\frac{U_{\Delta T_{sat}}}{\Delta T_{sat}} = \sqrt{\frac{\left(\frac{\partial \Delta T_{sat}}{\partial T_w}\right)^2 * U_{T_w}^2 + \left(\frac{\partial \Delta T_{sat}}{\partial T_{sat}}\right)^2 * U_{T_{sat}}^2}{\left(\Delta T_{sat}\right)^2}}$$

$$\frac{U_{\Delta T_{sat}}}{\Delta T_w} = 1 = \frac{\Delta T_{sat}}{\Delta T_{sat}}$$

$$\frac{U_{\Delta T_{sat}}}{\Delta T_{sat}} = -1 = -\frac{\Delta T_{sat}}{\Delta T_{sat}}$$

$$\frac{U_{\Delta T_{sat}}}{\Delta T_{sat}} = \sqrt{\frac{\left(\frac{\Delta T_{sat}}{T_{sat}}\right)^2 * U_{T_w}^2 + \left(-\frac{\Delta T_{sat}}{\Delta T_{sat}}\right)^2 * U_{T_{sat}}^2}{\left(\Delta T_{sat}\right)^2}}$$

$$\frac{U_{\Delta T_{sat}}}{\Delta T_{sat}} = \sqrt{\left(\frac{U_{T_w}}{\Delta T_{sat}}\right)^2 + \left(-\frac{U_{T_{sat}}}{\Delta T_{sat}}\right)^2}$$

The heat transfer coefficient is calculated as follows.

$$h = \frac{q''}{\Delta T_{sat}}$$

$$\frac{U_h}{h} = \sqrt{\frac{\left(\frac{\partial h}{\partial q''}\right)^2 * U_{q''}^2 + \left(\frac{\partial h}{\partial \Delta T_{sat}}\right)^2 * U_{\Delta T_{sat}}^2}{\left(h\right)^2}}$$

$$\frac{\partial h}{\partial q''} = \frac{1}{\Delta T_{sat}} = \frac{h}{q''}$$

$$\frac{\partial h}{\partial \Delta T_{sat}} = -\frac{q''}{\Delta T_{sat}^{\ 2}} = -\frac{h}{\Delta T_{sat}}$$

$$\frac{U_h}{h} = \sqrt{\frac{\left(\frac{h}{q''}\right)^2 * U_{q''}^2 + \left(-\frac{h}{\Delta T_{sat}}\right)^2 * U_{\Delta T_{sat}}^2}{\left(h\right)^2}}$$

$$\frac{U_h}{h} = \sqrt{\left(\frac{U_{q''}}{q''}\right) + \left(-\frac{U_{\Delta T_{sat}}}{\Delta T_{sat}}\right)}$$

3. The letter

R·I·T

Rochester Institute of Technology
Department of Mechanical Engineering
James E. Gleason Building
76 Lomb Memorial Drive
Rochester, New York 14623-5604
v/tty. 585-475-5181 fax 585-475-7710

Satish G. Kandlikar
Gleason Professor of Mechanical Engineering
E-mail : sgkeme@rit.edu URL http://www.rit.edu/mechanical/taleme

November 25, 2016

To:
Dissertation Committee Members for Murat Bulut

Dear Dissertation Committee members,

I am currently the Gleason Professor of Mechanical Engineering at Rochester Institute of Technology in Rochester, NY, USA and I am writing this letter to strongly recommend Murat Bulut at his request. Murat served as a visiting research scholar in my lab. I have known him since 1996. I was his advisor while he was pursuing his master of science degree at mechanical engineering department at RIT. He worked in my lab between 1996 and 1998.

He first approached me in July 2014 about the possibility of work in my laboratory for his PhD study. After receiving the scholarship from TUBITAK, he came to work in my lab from December 2015 to October 2016. He studied on Enhanced Microchannel Evaporator with Integrated Nanostructures in Space Application in my lab. During his time working on his PhD, he learned the operation of various laboratory instruments. He demonstrated the ability to work independently with great creativity and ethusiasm. He also put in many long hours. He worked as hard as one of my best graduate students.
Overall, I stongly give him my highest recommendation.

Sincerely,

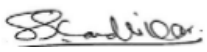

RESUME

Murat Bulut was born in Osmaniye in 1972. He started the elementary school in Ercis, Van and he completed the elementary school in Fatsa, Ordu. He started the middle school in Fatsa, Ordu and completed it in Manisa. He received the high school diploma from Manisa Industrial and Technical High School in Electronic in Manisa. He holds a Bachelor of Science degree in Mechanical Engineering from Selcuk University in Konya, TURKEY and a Master of Science degree in Mechanical Engineering from Rochester Institute of Technology (RIT) in Rochester, NY, USA. His masters thesis involved Experimental Investigation of Flow Boiling Heat Transfer with Ethylene Glycol/Water, under the supervision of Prof. Dr. S.G. Kandlikar. He has been Ph.D candidate since 2012 in Mechanical Engineering Department in Sakarya University. He has been a visiting scholar since December 2015 at RIT, under the supervision of Prof. Dr. S.G. Kandlikar. He joined TURKSAT A.S in 2006 as Satellite Thermal Engineer and worked for Thales Alenia Space between 2006-2007 and 2010-2013 in Cannes, France. Before joining TURKSAT A.S., he worked for Carrier Corporation at Large Rooftop Products as an application and development engineer in Syracuse, NewYork and McMinnville, Tennessee, USA. His major interest of study is Heat Transfer, HVAC, Spacecraft Thermal Control and Termal Vacuum applications. He published over 40 papers in national and international journals and conferences.